Copy No. _____

Guide for Mechanistic-Empirical Design
OF NEW AND REHABILITATED PAVEMENT STRUCTURES

FINAL DOCUMENT

APPENDIX QQ:
STRUCTURAL RESPONSE MODELS FOR RIGID PAVEMENTS

NCHRP

Prepared for
National Cooperative Highway Research Program
Transportation Research Board
National Research Council

Submitted by
ARA, Inc., ERES Division
505 West University Avenue
Champaign, Illinois 61820

July 2003

Acknowledgment of Sponsorship

This work was sponsored by the American Association of State Highway and Transportation Officials (AASHTO) in cooperation with the Federal Highway Administration and was conducted in the National Cooperative Highway Research Program which is administered by the Transportation Research Board of the National Research Council.

Acknowledgements

The research team for NCHRP Project 1-37A: Development of the 2002 Guide for the Design of New and Rehabilitated Pavement Structures consisted of Applied Research Associates, Inc., ERES Consultants Division (ARA-ERES) as the prime contractor with Arizona State University (ASU) as the primary subcontractor. Fugro-BRE, Inc., the University of Maryland, and Advanced Asphalt Technologies, LLC served as subcontractors to either ARA-ERES or ASU along with several independent consultants.

Research into the subject area covered in this Appendix was conducted at ARA-ERES. The author of this Appendix QQ is Dr. Lev Khazanovich with assistance from Mr. Thomas Yu, Dr. Chetana Rao, and Dr. Olga Selezneva. Dr. Michael Darter provided technical and managerial coordination of the rigid pavement design team, monitored progress, set schedules and deadlines, and provided periodic technical review of research results as they became available. Mr. Alex Gotlif assisted with all the intensive development of the neural networks.

Foreword

This appendix is a supporting reference to the design of JPCP and CRCP presented in PART 3, Chapters 4 and 7 of the Design Guide. Of particular interest is the selection of the finite element program for structure model development, selection of an analytical subgrade model for rigid pavement analysis, finite element model development for determining critical jointed plain concrete pavement (JPCP) bottom surface stresses, and finite element model development for determining critical continuously reinforced concrete pavement (CRCP) stresses.

APPENDIX QQ
STRUCTURAL RESPONSE MODELING OF RIGID PAVEMENTS

This appendix addresses the following issues:

- Selection of the finite element program for structure model development
- Selection of an analytical subgrade model for rigid pavement analysis
- Finite element model development for determining critical jointed plain concrete pavement (JPCP) stresses
- Finite element model development for determining critical continuously reinforced concrete pavement (CRCP) stresses

CHAPTER 1. FINITE ELEMENT PROGRAM SELECTION

INTRODUCTION

The performance of rigid pavements depends on the stresses and deflections imposed by repeated traffic and environmental loadings. For example, transverse cracking in JPCP is governed by the maximum tensile stresses at the bottom of the concrete slab, whereas crack deterioration in CRCP can be related to the shear stresses in the reinforcement and at the crack surface. Therefore, reliable predictions of pavement responses are essential for a mechanistic-empirical design procedure. The structural model used for those predictions should satisfy the following requirements:

- The model should adequately describe the pavement structure (constructed layers and subgrade).
- The model should account for discontinuities in the pavement structures (cracks and joints).
- The model should be able to analyze multi-wheel loading with nonuniform tire print distribution.
- The model should be able to analyze environmental loading (such as temperature curling and moisture warping).

Finite element methods permit the development of structural models that satisfy all these requirements. A variety of finite element programs are available to a pavement engineer today. These programs can be divided into general-purpose finite element programs and finite element codes developed specifically for analysis of pavement systems.

The programs from the first group, such as ABAQUS, ANSYS, and DYNA3D, are more powerful and capable, since they can conduct three-dimensional nonlinear dynamic analysis. These programs have been used successfully for pavement analysis in several research studies, and a number of finite element models built using these products are available today (Mallela et al. 1993, Darter et al. 1995, Kennedy 1998). However, these programs usually demand considerable computational resources, as well as time for developing a structural model for each problem.

The programs developed specially for analysis of concrete pavement systems include:

- ILLI-SLAB (Tabatabie and Barenberg 1980)
- WESLIQID (Chou 1981)
- J-SLAB (Tayabji and Colley 1983)
- FEACONS-IV (Choubane and Tia 1995)
- KENSLAB (Huang 1993)
- KOLA (Kok 1990)
- EVERFE (Davids, Turkiyyah, and Mahoney 1998)

Most of these programs can analyze multi-wheel loading of one- or two-layered medium thick plates resting on a Winkler foundation or an elastic solid (ILLI-SLAB, WESLIQID, KENSLAB). The latest enhancements to ILLI-SLAB include ILSL2, developed at the University of Illinois, and a revised version of ILSL2 developed by ERES Consultants (Khazanovich 1994, Khazanovich and Yu 1998). These two programs contain many advanced features that distinguish them from other pavement programs that are based on plate theory. EVERFE can analyze multi-layered pavement systems using a 3D-continuum brick element for the portland cement concrete (PCC) and base layers.

Evaluation Criteria

Selection of an appropriate analysis method for the Design Guide was based upon a clear set of defensible criteria. The selection procedure must first focus on the appropriate analysis approach, defined here as the underlying theories, assumptions, approximations, and algorithms. Once a short list of appropriate analysis approaches has been identified, specific computer implementations/programs can then be evaluated. Program details such as maximum number of layers/nodes/elements/material types should be deferred until an appropriate analysis approach has been selected. These details usually have no theoretical basis and are merely the features/ limitations of each program.

Evaluation criteria can be divided into two categories:

- Technical – the ability to predict the correct answer.
- Operational – the ability to implement the method in a practical design environment.

Within each category, the criteria can be subdivided into those that are of high importance and those that are of comparatively less importance.

Table 1.1 summarizes the technical evaluation criteria for the analysis methods and their relevant importance for rigid pavement criteria. The “moderate” designation means either that the criterion is moderately important under all conditions or that it is very important in some cases (e.g., some rehabilitation scenarios) and less important in others (e.g., new construction). Operational evaluation criteria are summarized in table 1.2. The same operational criteria were used for flexible and rigid pavements.

Table 1.1. Technical evaluation criteria and their relative importance for rigid pavements.

Criterion	Rigid Pavements
Ability to calculate/predict critical pavement response parameters accurately	High
Material behavior	
- Stress dependence	Low/None
- Tension/shear failure (unbound materials)	Low
- Temperature sensitivity of material properties	Low[1]
- Moisture sensitivity of material properties	High[2]
- Rate sensitivity	Low/None
- Aging	Moderate
- Interface slip	Moderate[3]
Geometry	
- Semi-infinite vs. finite boundaries	High
- Contact/gap interfaces	High
- Many (i.e., more than 3) layers	Moderate
Loading	
- User-defined axle/wheel configurations	High
- Nonuniform tire contact pressures	High
- Horizontal loading	Low
- Thermal loading	High
- Moisture-induced deformations (non-freeze/thaw)	High
- Freeze/thaw effects	High
Special Requirements	
- Fracture analysis (e.g., specialized crack tip elements, J-integral calculations)	Low[4]
Algorithm robustness	High

[1]Temperature-induced curling is covered under the "loading" category.
[2]Important primarily for unbound layers and subgrade.
[3]For some rehabilitation scenarios.
[4]May be more important if selected distress transfer function requires explicit calculation of crack tip response.

Initial Selection Process

In the first step of the analytical tool selection, the most promising program from each group of programs was selected. ABAQUS was selected as the most promising tool among general-purpose finite element packages, and ILSL2 and ISLAB2000 were selected among the plate theory-based pavement programs. Since these programs represent an extension of ILLI-SLAB, they may be referred as ILLI-SLAB in some portions of this document. EVERFE was selected as a 3D-pavement program specifically developed for rigid pavement analysis.

Table 1.2. Operational evaluation criteria and their level of importance.

Criterion	High Importance	Moderate Importance	Low Importance
Computational efficiency/time	X		
Ability to modify program (e.g., source code availability)		X[1]	
Licensing/proprietary restrictions		X	
Documentation			X[2]
User support			X[3]
Verification, validation, and acceptance with the profession	X		
Ability of agencies, contractors, etc. to use the analysis method	X		
Cost (initial acquisition, modification, annual licensing)		X[4]	
Platform (e.g., Windows 95/NT PC vs. UNIX workstation)	X		
Pre- and post-processing capabilities			X
Provides migration path for future technical advances		X	

[1]It is assumed that any selected analysis program will require some modification.
[2]Necessary primarily for the project team to be able to use and modify the program effectively. New end user documentation will be provided as part of the 2002 Design Guide.
[3]End user support will be provided as part of the overall 2002 Design Guide software support and not by the analysis program author/vendor.
[4]Assumes that any initial acquisition and modification costs will be spread over a large number of copies of the 2002 Design Guide software.

ABAQUS

ABAQUS is a very powerful and reliable general-purpose, production-oriented, finite-3D, dynamic, nonlinear finite element code designed to address structural and heat transfer problems. ABAQUS incorporates implicit (ABAQUS/STANDARD) and explicit (ABAQUS/EXPLICIT) dynamic solvers to allow analysis of a wide range of linear and nonlinear applications. The ABAQUS solvers are well integrated, allowing a single analysis to switch between solvers as needed.

ABAQUS is a modular code consisting of a library of over 300 different element types, a comprehensive material model library, and a library procedure with different procedures (static, heat transfer, dynamic). This makes ABAQUS the most powerful general-purpose code available.

Selecting ABAQUS is further justified by the fact that the majority of 3D finite element rigid pavement models were developed using it. Zaghloul and White (1993) developed a nonlinear, dynamic model of rigid pavements. Mallela and George (1994) developed a three-dimensional finite element model for load-deflection analysis of concrete pavement when subject to a falling weight deflectometer type raid loading. Darter et al. (1995) used ABAQUS to investigate the effect of foundation support and base layers on pavement responses. Hammons (1997) used

ABAQUS for a comprehensive analysis of joints in JPCP pavements. Several other researchers have over time used ABAQUS to model joints, voids, aircraft loads, etc.

ILSL2 and ISLAB2000

ILSL2 and ISLAB2000 were selected from the group of the programs specifically developed for rigid pavement analysis. ILSL2 (Khazanovich 1994) is the latest public domain revision of the finite element program ILLI-SLAB, and ISLAB2000 is a proprietary revision of ILSL2, developed by ERES Consultants in cooperation with Michigan and Minnesota Departments of Transportation, Michigan Technical University, University of Michigan, Michigan State University, and University of Minnesota. These two programs will be generically referred to as ILLI-SLAB in this document.

Selection of these two programs was driven by their technical superiority compared to the programs from their group. Currently, most finite element programs, including J-SLAB, FEACONS, and KOLA, can analyze only a single layer slab when a temperature gradient is introduced. WESLIQID and KENSLAB can analyze a two-layered slab, but only if the temperature gradient is linear and both layers are subjected to the same temperature gradient. The features of ILLI-SLAB that distinguish it from all other programs are as follows (Khazanovich 1994, Khazanovich and Yu 1998):

- A wide selection of subgrade models, including Winkler, elastic solid, Pasternak, Kerr-Vlasov, and Zhemochkin-Sinitsyn-Shtaerman.
- An ability to analyze the effect of the independent actions of two pavement layers.
- An ability to analyze the effect of linear and nonlinear temperature distribution throughout the pavement thickness.
- An ability to analyze partial-depth cracks.

Some of these features are discussed below.

Advanced Subgrade Models

ILLI-SLAB incorporates a number of subgrade models that promise to provide realistic characterization of PCC slab support, such as:

- Winkler or dense liquid (DL) model.
- Elastic sold (ES) model
- Two Parametric (TP) model.
- Zhemochkin-Sinitsyn Shtaerman (ZSS) model.
- Kerr-Vlasov (KV) model.

The advantages and limitations of some of these models are discussed in chapter 2. Although Winkler model is recommended for the 2002 Design Guide, availability of other models is important for future improvements and upgrade of the Guide.

Totsky Model

ILLI-SLAB represents a significant improvement in the analysis of curling of two unbonded pavement layers. Curling of unbonded PCC overlays or PCC slabs constructed on a stabilized base is a difficult phenomenon to analyze because curling can cause the upper pavement slab to lift off the underlying pavement or stabilized base. Many finite element programs for PCC pavements allow analysis of two-layered systems. However, in almost all cases, this is accomplished by converting the two-layer system to a structurally equivalent single-layer system. This conversion is feasible only if one of the following can be assumed:

- The two layers are fully bonded.
- The two layers are fully unbonded and they assume the same deflection profile.

Because the two pavement layers are not actually modeled as two separate layers, most finite element programs, including ILLI-SLAB, cannot analyze the independent actions of the two layers. Until recently, the separation between the slab and the base could only be modeled using 3D finite element programs. ILSL2 incorporates a new approach to analyzing the layer separation problem, developed by Totsky (Totsky 1981). This approach models the multi-layered pavement system resting on subgrade as a series of springs and plates. The plate elements model the bending, whereas the springs accommodate the direct compression occurring in such a system.

Implementation of Totsky's approach in a finite element code required the introduction of a special 8-noded (24-degree-of-freedom) element (see figure 1.1). The first four nodes are placed at the neutral axis of the upper plate, while the other four nodes are placed at the neutral axis of the lower plate. The stiffness matrix for this element is:

$$[K] = \begin{bmatrix} [K_{PL1}] + [K_{DLI}] & -[K_{DLI}] \\ -[K_{DLI}] & [K_{DLI}] + [K_{PL2}] + [K_{DLS}] \end{bmatrix} \quad (1)$$

where:
$[K_{PL1}]$ and $[K_{PL2}]$ are the stiffness matrices of the upper and lower plates, respectively.
$[K_{DLI}]$ is the stiffness matrix of the interlayer springs.
$[K_{DLS}]$ is the stiffness matrix of the subgrade.

In view of the potential for separation during temperature analysis, it is assumed for simplicity that the stiffness matrices for both the spring interlayer and subgrade are dependent only on nodal displacements, and not on nodal rotations. The stiffness of the interlayer spring may be specified by the user, or the program will calculate it from the plate parameters using recommendations developed by Khazanovich and Ioannides (1998).

Figure 1.1. 8-noded finite element setup for Totsky Model.

The curling problem in the Totsky model is solved iteratively. The analysis begins with all of the interface springs in compression (compression due to the self-weight of the slab). The pavement layers are then allowed to curl. If any of the springs are in tension at the end of the first iteration, those springs are removed and the system reanalyzed. The iteration continues until an equilibrium condition has been reached. The interface springs that have been removed during the solution process represent the layer separation. The use of the Totsky model in ILSL2 allows very accurate modeling of the curling problem.

Effect of Non-Linear Temperature Gradient

The nonlinearity in the temperature distribution through a concrete slab was theoretically predicted by Thomlinson (1940) and was subsequently proven by experimental data presented by numerous investigators (Mirabell 1990, Dempsey 1969, Jansen 1987). Janssen (1987) concluded from the results of field testing, laboratory testing, and computer modeling that significant drying in concrete pavement slabs usually occurs only at rather shallow depth top 25-50 mm). This causes shrinkage that is nonlinear throughout the slab thickness and affects concrete pavement in a manner similar to a nonlinear temperature distribution. Armaghani et al. (1987) and Choubane and Tia (1992) analyzed numerous field test data obtained by Florida Department of Transportation personnel and concluded that a quadratic function can often adequately describe in situ temperature distributions. They stated that replacing an actual distribution by a linear approximation determined based on the temperatures at the top and bottom of the slab leads to the overestimation of maximum stresses for daytime conditions. This also leads to the underestimation of maximum stresses in the slab for nighttime conditions. The same conclusion was also reached independently by Mirambell (1990).

Korenev and Chernigovskaya (1962) proposed splitting any arbitrary temperature distribution throughout the slab thickness into three components: one causing only slab expansion or contraction, another causing curling (i.e., slab bending), and a third tending to cause distortion of the cross-section, thereby giving rise to self-equilibrating stresses resisting this distortion. This four-step approach was implemented into ILSL2 (Khazanovich 1994):

1 Split the nonlinear temperature distribution into its three components:
- The part that causes constant strain throughout-the-slab-thickness strain,
- The part that causes strain linear throughout-the-slab-thickness strain, and
- The part that causes nonlinear strain.

2 Using available finite element formulations, determine the deflection profile and bending stress distribution due to the applied traffic loads and the linear strain-causing component of the original nonlinear temperature distribution.
3 Using a closed-form analytical solution, evaluate the normal components of the self-equilibrating thermal stress distribution due to the nonlinear strain-causing component of the temperature distribution.
4 Superimpose the bending stresses from step 2 and the self-equilibrating thermal stresses from step 3 to obtain the resultant stress distribution.

A detailed description of each step and examples of application of this procedure can be found elsewhere (Khazanovich and Ioannides 1994).

An advantage of this formulation is that an increase in the degree of nonlinearity of temperature distributions does not lead to an increase in the number of nodes used in the finite element model. Therefore, there is no significant increase in computation cost. At the same time, modeling of nonlinear temperature in ABAQUS and EVERFE requires the addition of nodes if the available model does not provide enough flexibility in temperature distribution assignment.

ILSL2 vs. ISLAB2000

Due to its ability to account for different subgrade models, separation between constructed layer, nonlinear temperature gradient throughout-the-pavement depth, and the effect of partial-depth cracks, ILSL2 is a very powerful analytical tool and attractive alternative to the general-purpose 3D finite element packages. Nevertheless, ILSL2 has several limitations. Being an extension of an old-generation engineering program, ILSL2 is cumbersome to use; however, more seriously, there are problems associated with the core of the ILLI-SLAB code, which were inherited by ILSL2. Throughout its development history, the task of maintaining a clean and efficient code was not a high priority for ILLI-SLAB. Consequently, the current code contains numerous inefficiencies and redundancies.

ERES Consultants, in cooperation with Michigan and Minnesota Departments of Transportation, Michigan Technical University, University of Michigan, Michigan State University, and University of Minnesota, developed a new finite element code that retains all positive features of ILSL2 but will be more computational efficient and provide a user-friendly interface. The maximum allowable number of nodes is significantly increased. An unnecessary limitation requiring all pavement joints in one direction to have the same properties will be eliminated. ISLAB2000 also permits modeling of several layers of the pavement system (versus only two layers in ILSL2).

The increased analysis capacity is a very important improvement to enable more accurate analysis of many common problems, especially when significant slab curling is involved. Although ISLAB2000 is a proprietary product, a limited version of the program required for structural response analysis for the 2002 Design Guide will be provided by ERES Consultants.

EVERFE

EVERFE is a rigid pavement 3D finite element analysis tool developed at the University of Washington in cooperation with Washington Department of Transportation. At the present time, EVERFE is the most sophisticated and user-friendly 3D finite element program specifically developed for rigid pavement analysis. The program employs an intuitive graphical user interface that greatly simplifies model generation, and result interpretation is demonstrated via a sample problem. EVERFE incorporates a novel technique for modeling aggregate interlock joint shear transfer and rationally incorporates nonlinearities, as well as a new method for modeling dowel joint shear transfer. An advanced solution strategy employed by EVERFE that allows realistic 3D models to be simulated on desktop computers.

Nevertheless, EVERFE has significant limitations.

1. The computation time of the program is still substantial – about an hour for a single run with a fine mesh on a PC with a Pentium III 450 MHz processor.
2. If a stabilized base is present, it is modeled as a continuous layer under transverse PCC joints. This may cause significant overestimation of the load transfer efficiency at the joints if a crack is developed throughout the base layer.

Comparison of ILSL2 and ISLAB2000

Since ISLAB2000 is an extension of ILLI-SLAB, it is not a surprise that ILLI-SLAB results can be reproduced using ISLAB2000. Figures 1.2 and 1.3 present comparisons of maximum deflections and maximum stresses obtained from these two codes from 120 finite element problems representing a variety of rigid pavement design and loading conditions. As expected, an excellent correlation is observed. It should be noted, however, that not every analysis from ISLAB2000 can be repeated using ILSL2, since ISLAB2000 capabilities are much greater than those of ILSL2.

Comparison of ISLAB2000 and PLITA

PLITA is a finite element program for analysis of slab-on-grade. Although this program cannot be used directly for pavement analysis, it was found to be an excellent source for ILSL2 and ISLAB2000 verification. Several factorials of finite element runs were performed to compare maximum deflections predicted in the slab for various slab thickness and subgrade models (Winkler and Pasternak). Figures 1.4 and 1.5 presents comparisons of maximum deflections for interior and edge loading.

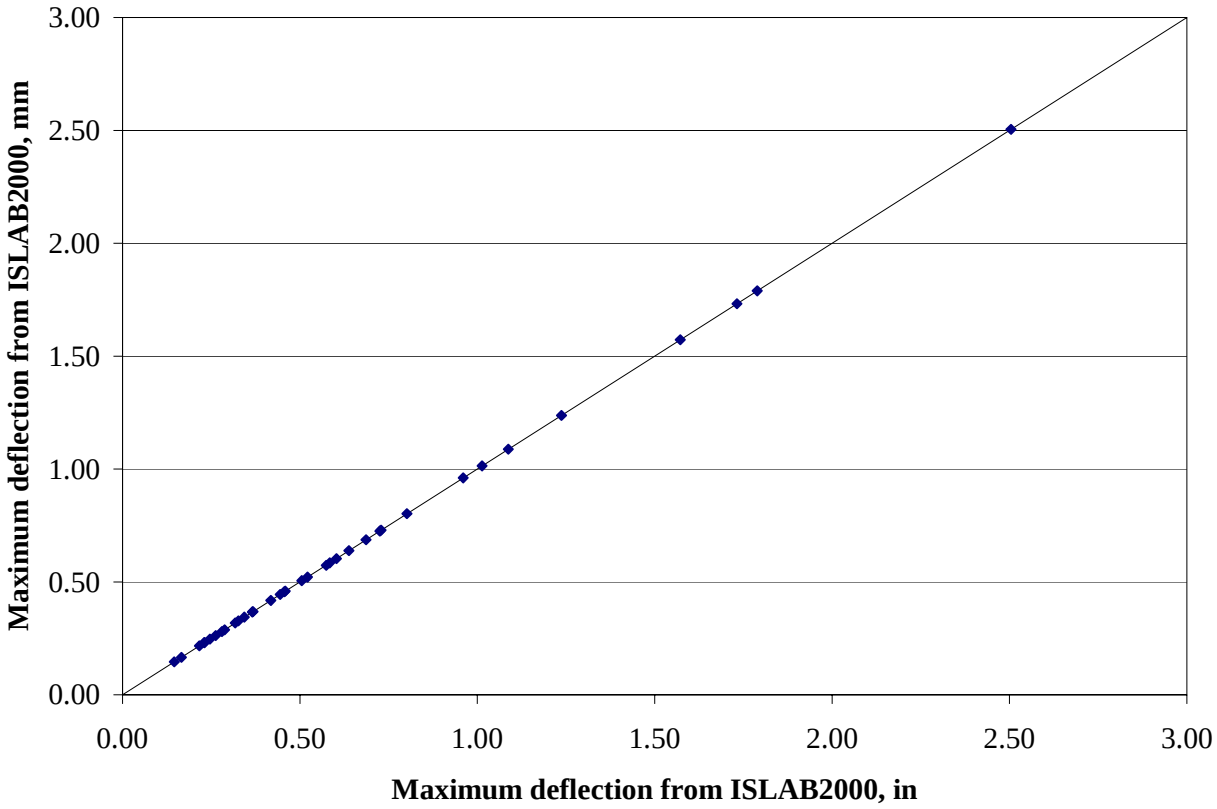

Figure 1.2. Comparison of maximum deflections from ILSL2 and ISLAB2000.

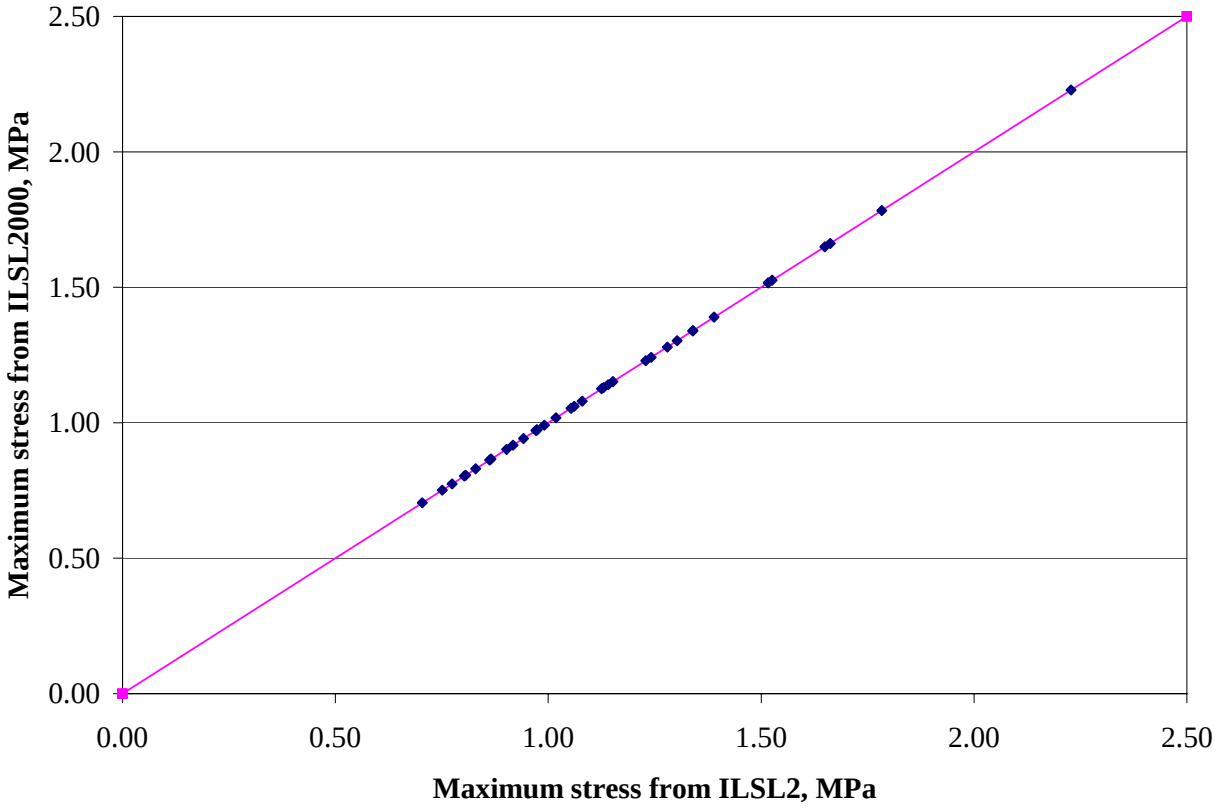

Figure 1.3. Comparison of maximum stresses from ILSL2 and ISLAB2000.

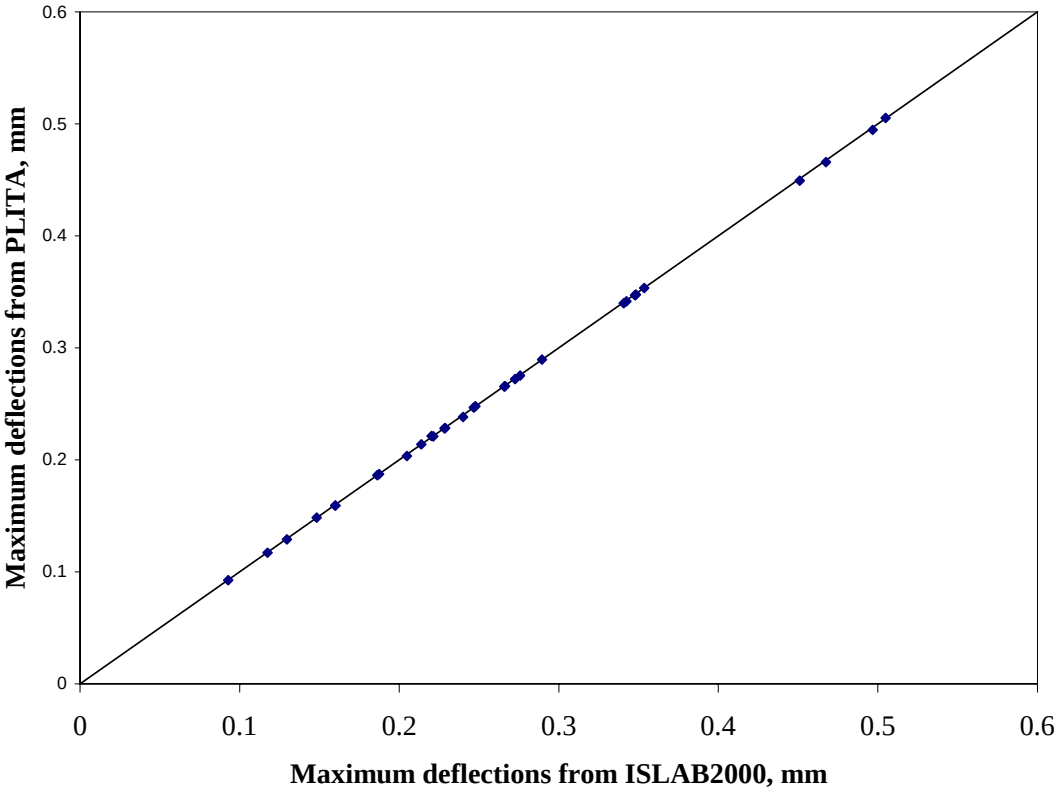

Figure 1.4. Comparison of maximum deflection from ISLAB2000 and PLITA, interior loading.

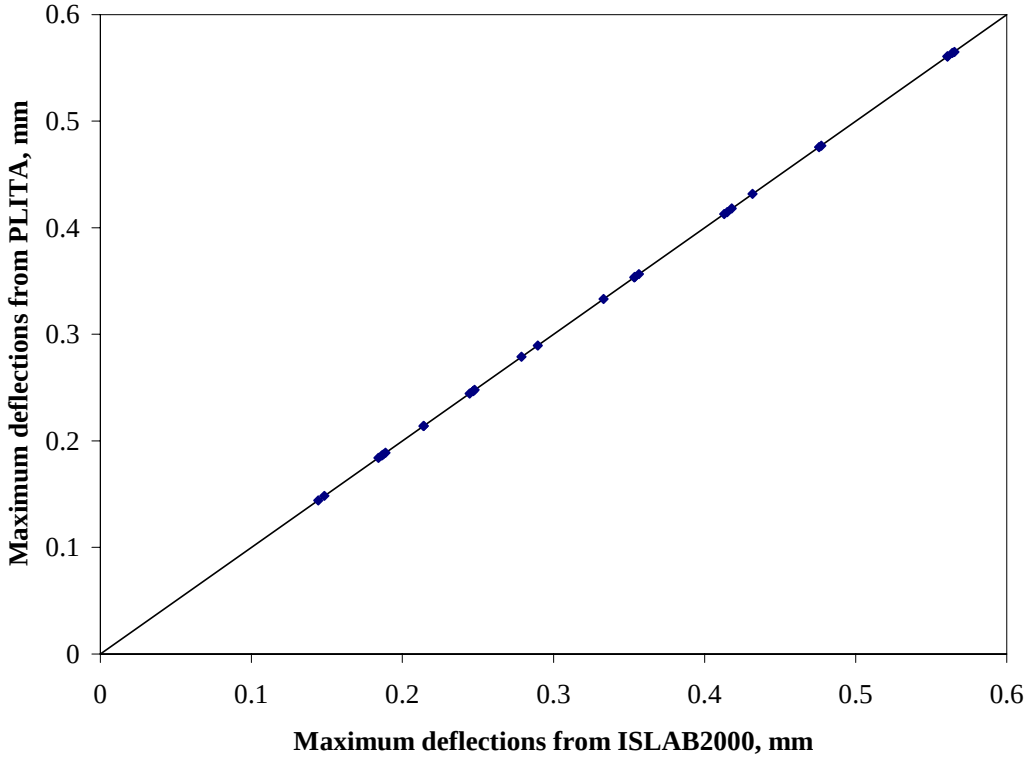

Figure 1.5. Comparison of maximum deflection from ILSL2 and PLITA, edge loading.

Comparison of ABAQUS and ISLAB2000

Hammons (1997) conducted a comprehensive comparison of ABAQUS and ILLI-SLAB. He considered several cases of a single slab resting on the Winkler foundation and loaded by a single load at its interior or at the edge. A variety of elements from ABAQUS's element library were used to analyze these problems (several types of brick elements and several types of shell elements). The results of the analysis were compared among themselves and with the results from ILLI-SLAB, and the following conclusions were made:

1. The results from ILLI-SLAB closely match the results from ABAQUS if a shell element S8R is employed in the ABAQUS model and the transverse shear stiffness G_z of S8R is assigned to be equal to 100 times the default G_z. The latter models infinite shear modulus assumed by the medium plate theory. Excellent correspondence in the predicted stresses and deflections for both interior and edge loading verifies robustness of the ILLI-SLAB finite element code.
2. A very good correlation was found between the ILLI-SLAB and ABAQUS for the maximum bending stresses when an interior loading condition was considered. It should be noted that higher order elements had to be employed in the ABAQUS model, and substantially higher computational time was required by the ABAQUS model to achieve ILLI-SLAB's level of accuracy. At the same time, the models built using ABAQUS's C3D8 and C3D8R brick elements, being much more computationally demanding than ILLI-SLAB, failed to produce reasonable level of accuracy (see figures 1.6 and 1.7 and table 1.3).
3. The maximum deflections predicted by ILLI-SLAB were consistently 1 to 2 percent lower than those predicted by ABAQUS (when an acceptable level of accuracy is achieved in ABAQUS).
4. The greatest discrepancy was found for maximum bending edge stresses. Whereas ILLI-SLAB predicts the location of the maximum edge stresses right at the slab edge, results from comprehensive 3D ABAQUS models show that the maximum edge stress occurs within 0.1 radii of relative stiffness form the slab edge and is approximately 10 percent less than predicted by ILLI-SLAB (see figure 1.8). Two observations, however, can be made:

    a. Hammons found that this difference is consistent and should not affect performance prediction since a consistent discrepancy can be accounted for in the fatigue model calibration.
    b. Hammons's analysis considered only single wheel loading, and no curling effect was considered. Modeling of a full axle loading acting along with a temperature gradient throughout the slab thickness may reduce the effect of localized loading and make 3D stress predictions closer to ILLI-SLAB predictions.
    c. Even an analysis of a simple structure (single slab, no curling) required substantial computational resources (minutes and hours of CRAY CPU time). At the same time, an ILLI-SLAB analysis requires only a few seconds of Pentium PC time.

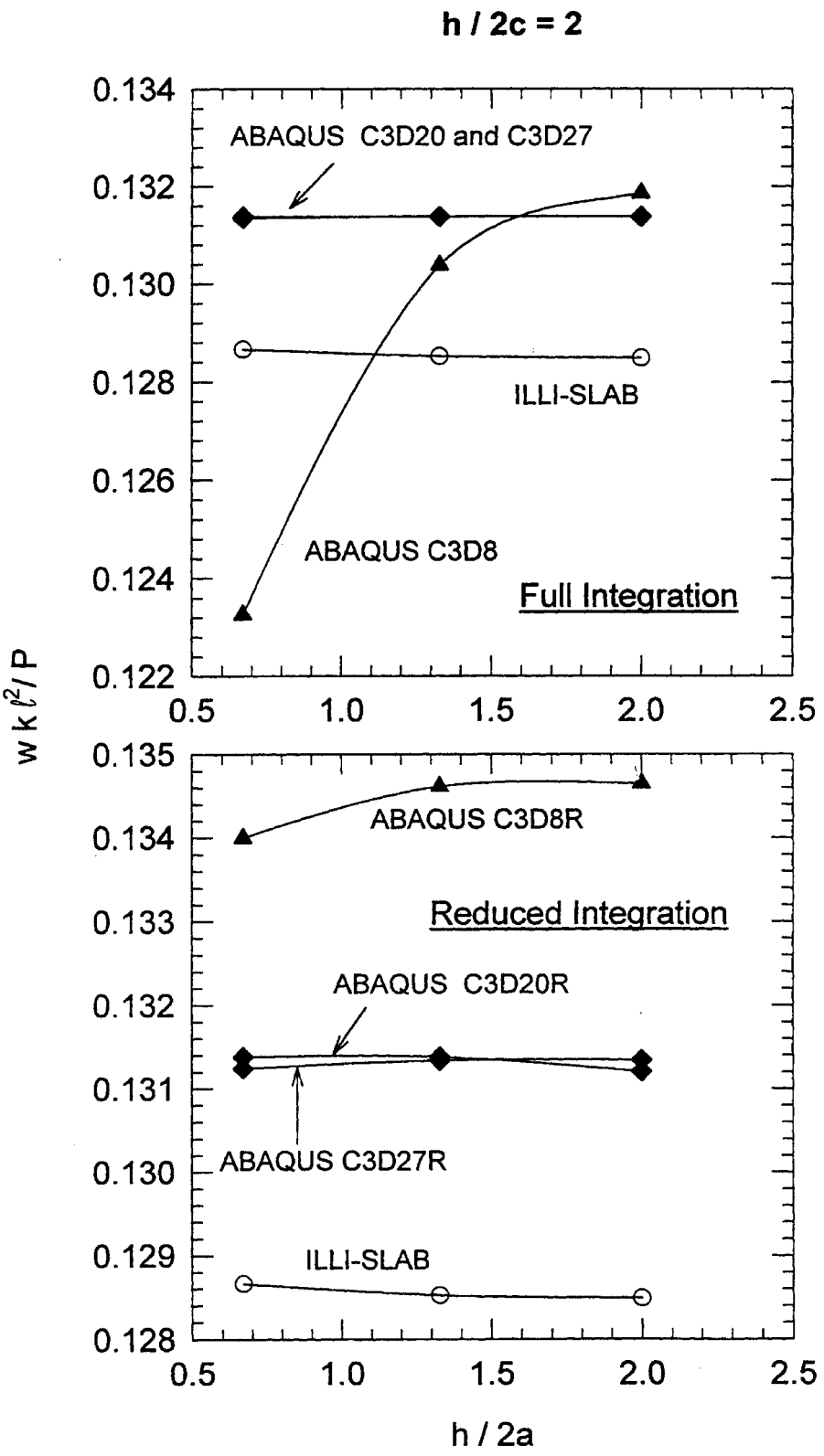

Figure 1.6. Comparison of ILLI-SLAB and ABAQUS center slab deflections (Hammons 1997).

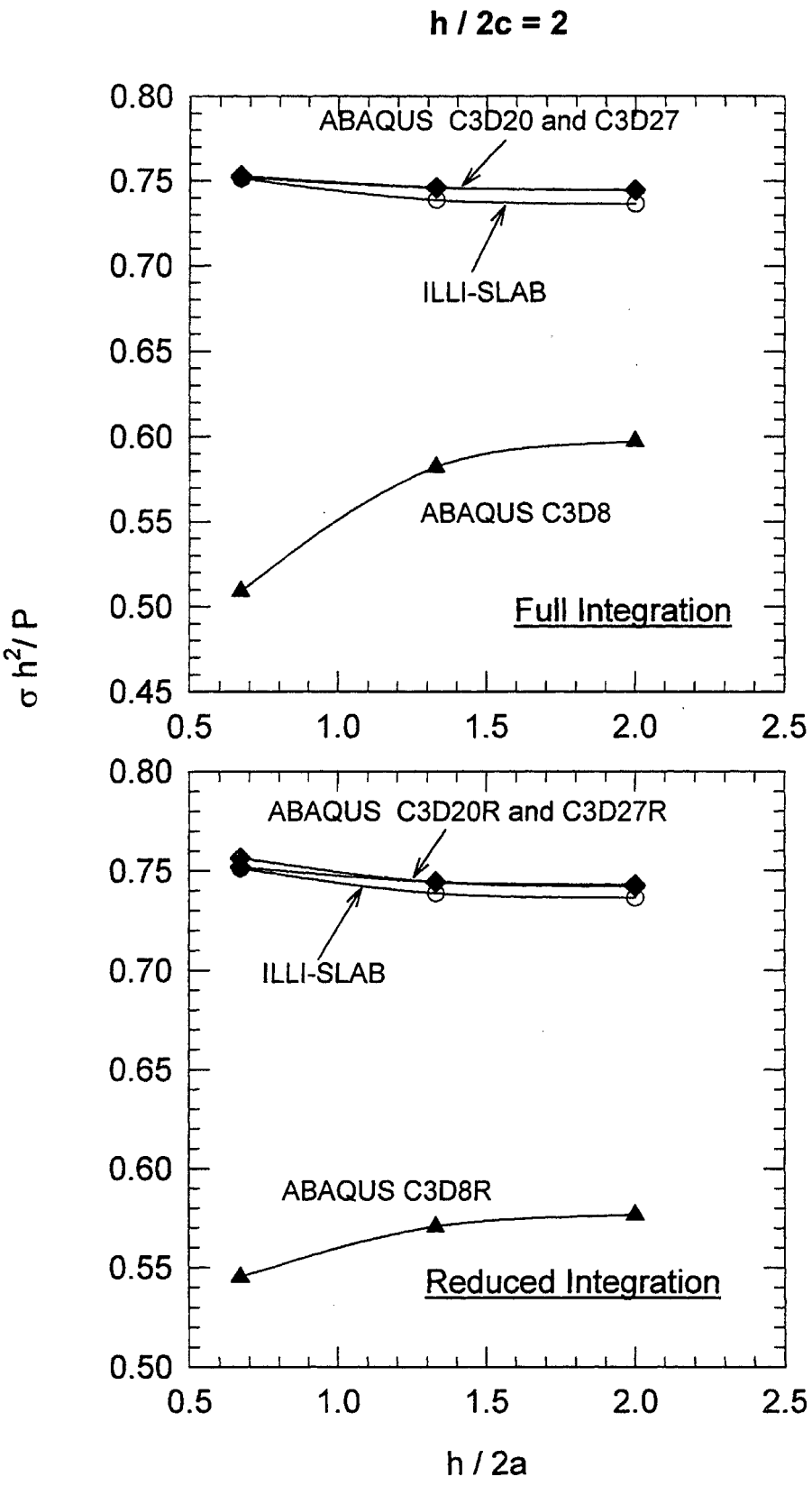

Figure 1.7. Comparison of ILLI-SLAB and ABAQUS center slab bending stresses (Hammons 1997).

Table 1.3. Results of convergence study using ILLI-SLAB and ABAQUS (Hammons 1997).

h/2a	**ILLI SLAB (2D)**	*h/2c*	**ABAQUS**					
			C3D8	**C3D8R**	**C3D20**	**C3D20R**	**C3D27**	**C3D27R**
Dimensionless Stress at Center of Loaded Area ($\sigma h^2/p$)								
0.67	0.751	1.0	0.414	0.431	0.754	0.751	0.753	0.750
		1.5	0.476	0.505	0.754	0.755	0.752	0.751
		2.0	0.509	0.545	0.753	0.757	0.752	0.752
Dimensionless Deflection at Center of Loaded Area ($wk\ell^2/p$)								
0.67	0.129	1.0	0.128	0.146	0.131	0.131	0.131	0.131
		1.5	0.124	0.137	0.131	0.131	0.131	0.131
		2.0	0.123	0.134	0.131	0.131	0.131	0.131
CPU Time on CRAY Y-MP Computer, sec								
0.67	--	1.0	8.6	7.4	25.1	20.9	28.4	32.6
		1.5	12.8	11.0	38.3	32.1	57.3	50.4
		2.0	17.0	14.7	52.7	44.2	81.2	54.0

Table entries of "—" indicate that this computation was not performed or is not applicable.

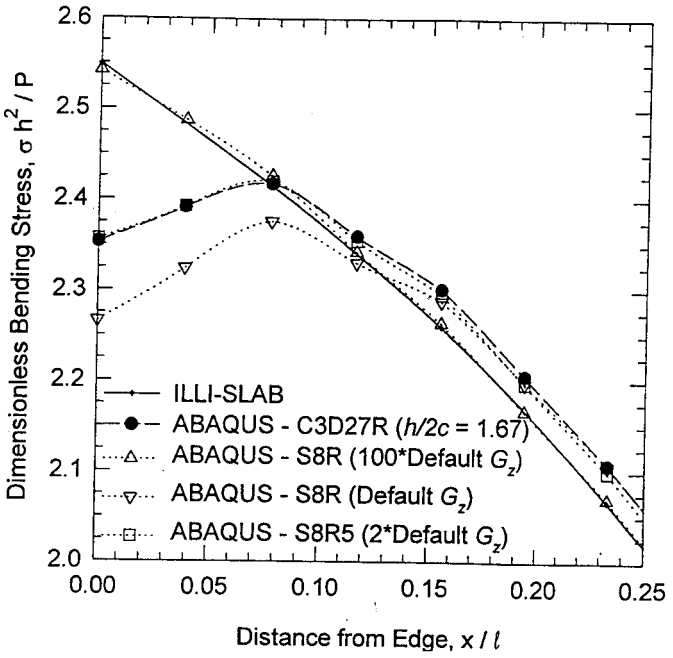

Figure 1.8. Comparison of ILLI-SLAB and ABAQUS edge bending stresses (Hammons 1997).

Hammons also examined the joint model used in ILLI-SLAB. Based on analysis of field test data and on comparison with the ABAQUS model, he concluded that the ILLI-SLAB model provides sufficient accuracy for a gross analysis of pavement systems. Although explicit modeling of the dowel in the 3D model is perhaps useful for research purposes, it is unnecessarily complicated for practical purposes.

Bases on the results of Hammons's analysis, as well as the observation that the discrepancy between ILLI-SLAB and ABAQUS does not exceed the discrepancy that would be caused by uncertainties in the input parameter values, it can be concluded that ILLI-SLAB is a reliable tool for a simplified analysis of rigid pavement systems.

Field Verification of ISLAB2000 and ILSL2

A comparison between ISLAB2000 and AASHO Road Test measurements was conducted in this study. The measured responses from the main loop were simulated. The main loop was set up to measure the edge deflections and strains at the slab edge under moving truck loads. The configuration of the main loop is shown in figure 1.9.

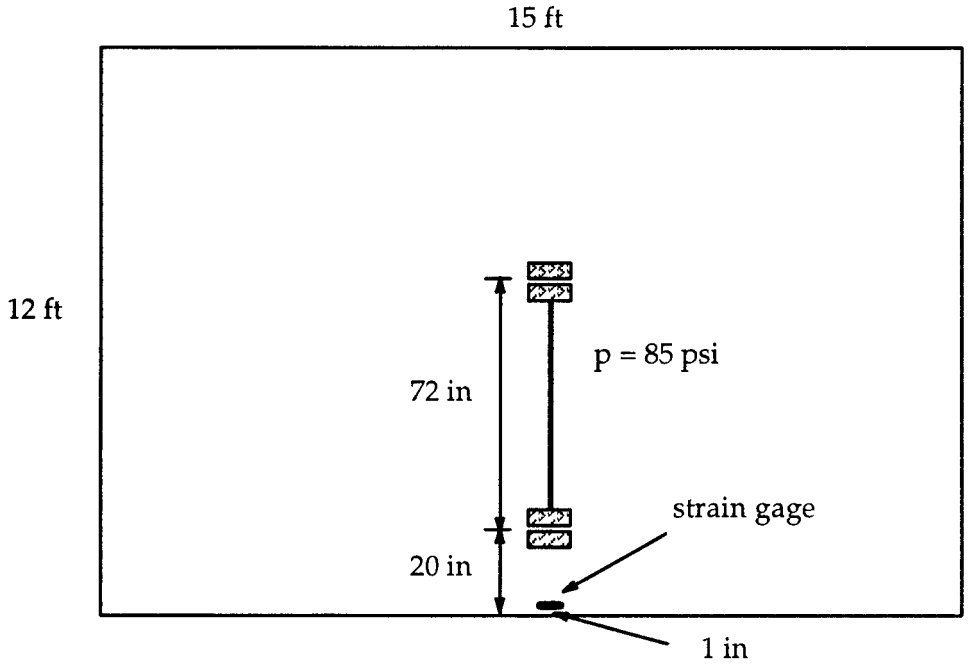

Figure 1.9. Configuration of main loop test set up at AASHO Road Test.

A factorial of finite element runs for different combinations of axle loads and PCC slab thicknesses was performed. A flat slab condition was assumed for all cases. The coefficient of subgrade reaction was selected equal to 46 kPa/mm, as recommended by Darter et al. (1995). Three slabs were considered in the longitudinal direction, and one slab was considered in the transverse direction. The deflection load transfer efficiency at the joints was assumed to be 70 percent. The constant pressure and the tire width were kept the same for all cases.
The longitudinal bending stresses at the bottom of the PCC slab are located at midslab at 125.4 mm from the slab edge. These stresses were compared with stresses calculated from measured strains. The results of those comparisons are shown in figure 1.10. The ISLAB2000 finite element matches the measured stresses very closely.

Final Model Selection

The ability to calculate/predict the critical pavement response parameters is clearly the overriding criterion that must be satisfied by any analysis method. In addition to accuracy of prediction, the selection of an analysis method depends primarily on whether the analysis can be completed in a "reasonable" amount of time (i.e., computational practicality). Based on these two criteria, the computer program ISLAB2000 was selected.

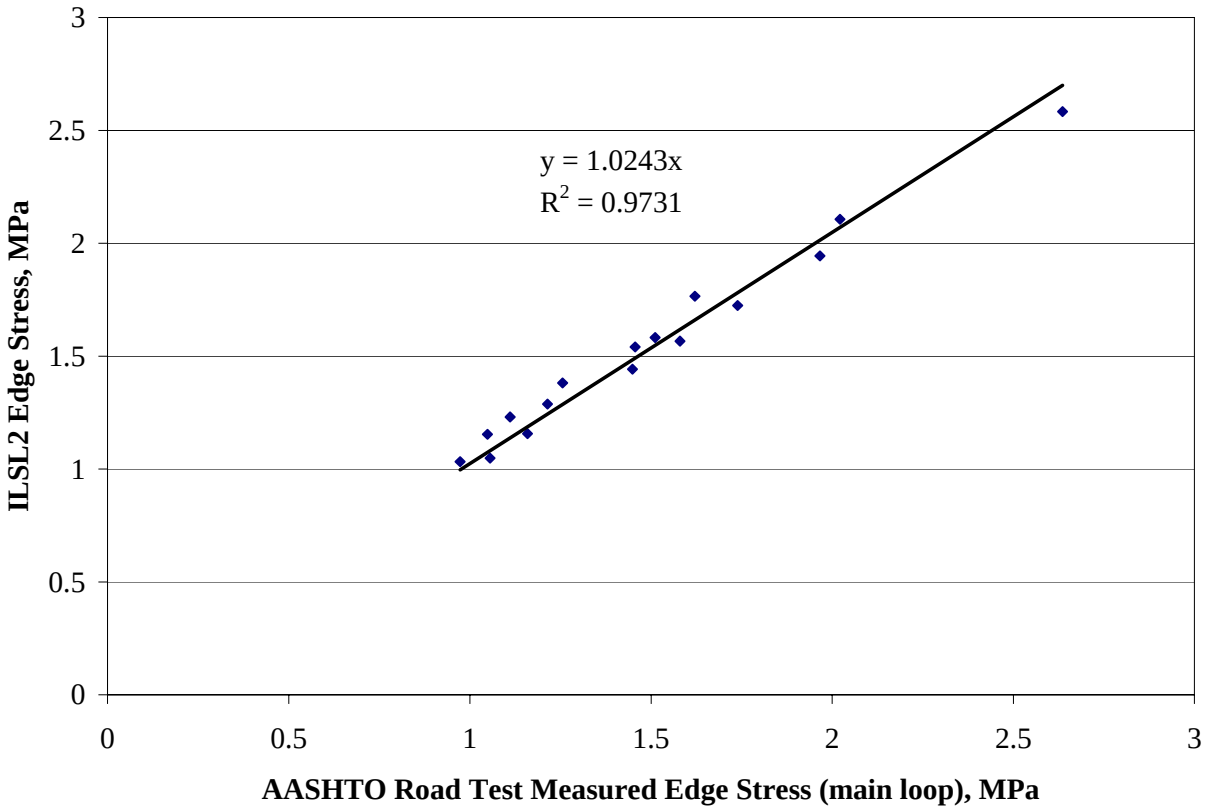

Figure 1.10. ISLAB2000 calculated stress versus AASHO Road Test measured stress.

The following considerations were taken into account:

1. The computer program ISLAB2000 is a revision of the finite element program ILLI-SLAB that has been successfully used in rigid pavement analysis for many years. ISLAB2000 contains all positive features of ILLI-SLAB (including the features of ILSL2) but is free from several unnecessary limitations.
2. ISLAB2000 is able to model all of the important features of the pavement systems (multiple slabs in both directions, multiple layers, mismatched joints, multiple loads, temperature curling).
3. The comparison of ABAQUS and ISLAB2000 (ILLI-SLAB) models showed that the ILLI-SLAB model, being significantly more computationally efficient, does not introduce significant error in the predicted structural responses.
4. Comparisons of the stresses predicted by ISLAB2000 with the measured stresses from the AASHO Road test show good correspondence.
5. Tens of thousand of cases will need to be analyzed for a single design trial, and the development of rapid solutions will require millions of finite element runs. The computation time for all these runs makes it impractical to use a 3D finite element model as a basic analytical tool.

REFERENCES

The AASHO Road Test, Proceedings of the Conference Held May 16-18, 1962, St. Louis, Mo., Highway Research Board Special Report 73.

Armaghani, J.M., T.J. Larsen, and L.L. Smith. (1987). Temperature Response of Concrete Pavements. *Transportation Research Record 1121*. Washington, DC: Transportation Research Board.

Chou, Y.T. (1981). *Structural Analysis Computer Programs for Rigid Multicomponent Pavement Structures with Discontinuities- WESLIQID and WESLAYER; Report 1: Program Development and Numerical Presentations; Report 2: Manual for the WESLIQID Finite Element Program; Report 3: Manual for the WESLAYER Finite Element Program*. Technical Report GL-81-6, U.S. Army Engineer Waterways Experiment Station, May.

Choubane, B., and M. Tia. (1992). Nonlinear Temperature Gradient Effect on Maximum Warping Stresses in Rigid Pavements. *Transportation Research Record No. 1370*, Transportation Research Board, National Research Council, Washington DC, pp. 11-19.

Darter, M.I., K.T. Hall, and C. Kuo. (1995). *Support Under Portland Cement Concrete Pavements*. NCHRP Report 372. Washington, DC: National Cooperative Highway Research Program.

Davids, W.G., Turkiyyah, G.M., and J. Mahoney. (1998) EverFE -- a New Rigid Pavement Finite Element Analysis Tool, *Transportation Research Record No*, National Research Council, Washington, DC, pp. 69-78

Dempsey, B.J. (1969). A Heat-Transfer Model for Evaluating Frost Action and Temperature Related Effects in Multilayered Pavements Systems. Thesis presented to the University of Illinois, at Urbana, IL, in partial fulfillment of the requirements for the degree of Doctor of Philosophy.

Hammons M.I. (1997). Development of an Analysis System for Discontinuities in Rigid Airfield Pavements. FAA, Technical Report GL-97-3.

Hibbitt, Karlsson, and Sorensen, Inc. (1989*). ABAQUS, Finite Element Computer Program. Version 4.9*.

Huang, Y.H. (1993). *Pavement Analysis and Design*. Prentice Hall, Englewood Cliffs, NJ.

Janssen, D.J. Moisture in Portland Cement Concrete.(1987). *Transportation Research Record 1121*, Transportation Research Board, National Research Council, Washington, DC, pp. 40-44.

Kennedy J.C. (1998). Material Nonlinear and Time-Dependent Effects on Pavement Design for Heavyweight, Multi-Wheel Vehicles, *Proceedings of the First International symposium on 3D Finite Element For Pavement Analysis and Design*.

Khazanovich L. and A.M. Ioannides. (1994). Structural Analysis of Unbonded Concrete Overlays under Wheel and Environmental Loading. *Transportation Research Record No* 1449, Washington, DC: Transportation Research Board.

Khazanovich, L. (1994). *Structural Analysis of Multi-Layered Concrete Pavement Systems*. Ph.D. Thesis, University of Illinois, Urbana, IL.

Khazanovich, L. and T. Yu (1998). ILSL2- A Finite Element Program for Analysis of Concrete Pavements and Overlays, *Proceedings*, Fifth International Conference on Bearing Capacity of Roads and Airfields, Trondheim, Norway.

Kohnke, P.C. (1989). *ANSYS Engineering Analysis System-Theoretical Manual*. Swanson Analysis Systems, Inc. Houston, PA.

Kok, A.W.M. (1990). A PC Program for the Analysis of Rectangular Pavements Structures. *Proceedings,* Second International Workshop on the Design and Rehabilitation of Concrete Pavements, Sigüenza, Spain, October, pp. 113-120.

Korenev, B.G., and E.I. Chernigovskaya. (1962). *Analysis of Plates on Elastic Foundation*. Gosstroiizdat, Moscow, (in Russian).

Livermore Software Technology Corporation (1997). *LS-DYNA, A Nonlinear, Explicit, Three Dimensional Finite Element Code for Soil and Structural Mechanics.* Version 940.

Mallela, J., and K.P. George (1994). "Three-Dimensional Dynamic Response Model for Rigid Pavements," In *Transportation Research Record 1448*, Transportation Research Board, Washington, D.C., 1994.

Mirambell, E. (1990). Temperature and Stress Distributions in Plain Concrete Pavements Under Thermal and Mechanical Loads. *Proceedings,* Second International Workshop on the Design and Rehabilitation of Concrete Pavements, Sigüenza, Spain.

Tabatabie, A.M., and E.J. Barenberg. (1980). Structural Analysis of Concrete Pavement Systems. ASCE*, Transportation Engineering Journal*. Vol. 106, No. 5, pp. 493-506.

Tayabji, S.D., and B.E. Colley. (1983). Improved Pavement Joints. *Transportation Research Record 930*, Transportation Research Board, National Research Council, Washington, DC, pp. 69-78.

Thomlinson, J. (1940). Temperature Variations and Consequent Stresses Produced by Daily and Seasonal Temperature Cycles in Concrete Slabs. *Concrete Constructional Engineering*, Vol. 36, No. 6, pp. 298-307; No. 7, pp. 352-360.

Totsky, O.N. (1981). *Behavior of Multi-Layered Plates on Winkler Foundation*. Stroitel'naya Mekhanika I Raschet Sooruzhenii, No. 6, Moscow, pp.54-58, (in Russian).

Zaghloul, S. and T. White (1993). Nonlinear Dynamic Analysis of Concrete Pavements, Proceedings, Fifth International Conference on Concrete Pavement Design and Rehabilitation, Vol 1., West Lafayette, IN: Purdue University, pp. 277-292.

CHAPTER 2. SUBGRADE SOIL CHARACTERIZATION

Mechanistic modeling of subgrade support for rigid pavement is an important step toward improvement of current pavement design and rehabilitation procedures. Input parameters for such a model should be easy to determine, and the associated analysis process should ideally be inexpensive. However, development of this model is not simple because a real soil is a nonuniform foundation that can, under certain conditions, exhibit non-linear visco-elastic-plastic behavior. Nevertheless, experience in rigid pavement analysis and design has shown that subgrade may be modeled as linear elastic.

The most widely adopted mechanistic idealization for analysis concrete pavements is that of a plate on a dense liquid (DL) foundation (Westergaard 1948), usually implemented in a finite element program, such as ILLI-SLAB (Tabatabaie and Barenberg 1980), WESLIQID (Chou 1981), J-SLAB (Tayabji and Colley 1986), FEACONS III (Tia et al. 1987), or KENSLABS (Huang 1993). The advantage of this approach is that it allows consideration of the critical load transfer phenomena, occurring at the PCC slab joints, and the concomitant development of major distress types, such as faulting, pumping and corner breaking. The DL foundation (Winkler, 1864) is the simplest foundation model and requires only one parameter, the modulus of subgrade reaction, k, which is the proportionality constant between the applied pressure and the load plate deflection. Subgrade deformations are local in character, that is, they develop only beneath the load plate. Furthermore, they are elastic or recoverable upon load removal.

The elastic solid (ES) half-space or Boussinesq subgrade idealization is often considered a more realistic representation of real soils. Deformations in the ES model are global in character, that is, they develop not only under the load plate but also beyond it. All deformations are linearly elastic. In treating slab-on-grade problems, this model can also be considered single-parametric since the only parameter required is the coefficient C, defined as:

$$C = \frac{E_s}{1 - \mu_s^2}, , , , , , (2.1)$$

in which
E_s = the elastic modulus of the subgrade
μ_s = Poisson's ratio.

ES models, however, are more computationally demanding.

The discussion of improved subgrade models begins with the realization that neither the DL nor the ES idealization is entirely adequate when applied to real soils, and that the predictions from both exhibit discrepancies with observed in situ behavior. The DL model assumes no shear interaction at all between adjacent spring elements and results in a foundation parameter, k, which is sensitive to the size of the plate used in its determination. On the other hand, the ES model ascribes to the foundation a higher degree of shear interaction than is occurred in real soils, resulting in infinite stress predictions under the edges and corners of a plate resting on it. Furthermore, the DL foundation assumes zero deflections beyond the edge of the load plate, whereas the ES model assumes a gradual decrease in deflection beyond the edges of the load plate. The deflection responses of real soils beyond the edge of the load plate are between the DL and ES model predictions.

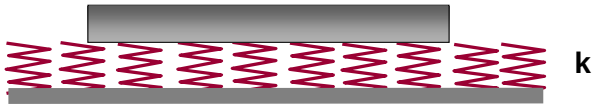

p = k w

Figure 2.1. Winkler model.

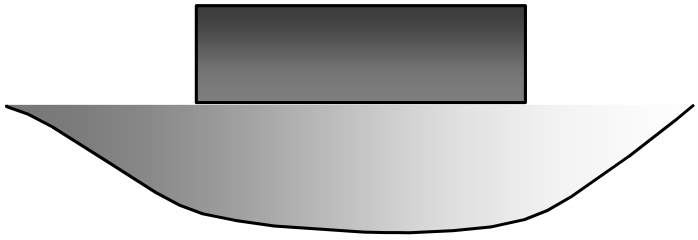

Figure 2.2. ES model.

In an attempt to find a physically close and mathematically simple representation for the subgrade response, two approaches were utilized (Kerr 1993):

- Start with ES and introduce modifications, such as assumptions with respect to expected displacements and/or stresses. This was done, for example, by Reissner (1958, 1967) and Vlasov (1960).
- Start with a Winkler foundation and, in order to bring it closer to actual soil behavior with respect to transfer of shear, assume some kind of interaction between the adjacent springs. That was done by Pasternak (1954), and Kerr (1964) and is illustrated in figure 2.3.

Both of these two alternatives produced the Two-Parameter foundation model (TP). The TP, often referred to as the Pasternak or Vlasov subgrade, offers an attractive alternative to the ES continuum in providing a degree of shear interaction between adjacent soil elements. Accordingly, subgrade reaction pressure, q, is related to surface deflection, w, through:

$$q = k\,w - G\,\nabla^2 w \quad , , , , , , \quad (2.2)$$

where
k is a vertical spring stiffness (as for DL)
G is a coefficient describing the interaction between adjacent springs
∇^2 is the Laplace operator.

In the last several years, this model has been investigated by several researchers (Korenev and Chernigovskaya 1962, Ioannides, Barenberg, and Thompson 1985, Khazanovich and Ioannides 1993, Kerr 1993, Pronk 1993 and 1997). An analytical solution for TP similar to Westergaard's DL interior loading formulae has been presented by Korenev and Chernigovskaya (1962). Additional solutions may be obtained by finite element (FE) analysis, which for TP is much less

tedious than for ES since the subgrade stiffness matrix for TP is banded. Several finite element programs developed for analysis of rigid pavement, such as ILLISLAB (Ioannides 1985, Khazanovich 1994) and KOLA (Kok 1993), permit analysis using TP models. A backcalculation procedure for Pasternak model parameters was developed by Stet et al. (1998). In the recommendations of the 4th International Symposium on Theoretical Modeling of Concrete Pavements to the 8th International Symposium on Concrete Roads, the Pasternak model was named the preferable option for subgrade modeling.

Comparisons between DL and TP presented by Pronk (1993) suggest that the latter can be considered a logical improvement of DL. The deflection profile predicted by TP vanishes much faster than the corresponding ES basin and may be a better approximation of the deflections observed in a real foundation of finite depth. If the shear modulus, G, is set to be equal to 0, then the TP model is reduced to the Winkler model. On the other hand, for a specific slab width and length, the shear modulus, G, can be selected to closely match critical responses of the same slab resting on ES foundation.

To illustrate this principle, consider a 200-mm thick, 3.5-m wide, and 4.5-m long PCC slab resting on the ES foundation with the modulus of elasticity and Poisson's ratio equal to 70 MPa and 0.45, respectively. If the slab is loaded by an interior load distributed by square with a side equal to 266 mm, then the DL model with the k-value equal to 75 kPa/mm and the TP model with k-value and G-modulus equal to 16.5 kPa/mm and 15600 N/mm, respectively, closely match the maximum deflection of the slab on ES foundation. However, if the same load is applied at the slab edge and the slab thickness is varied from 150 mm to 300 mm, then the predictions of these models differ.

Figure 2.4 shows that the ratios between the maximum slab bending stresses from TP or DL models to the corresponding maximum stress from ES for different slab thickness. While the DL model overestimates maximum bending stresses from 10 to 30 percent, the TP model closely matches ES maximum bending stresses. Therefore, the significantly less computationally demanding TP model can be used in place of the ES model in routine analysis. However, considering that the ES model significantly overestimates subgrade shear resistance, it might be not the best application of the TP model.

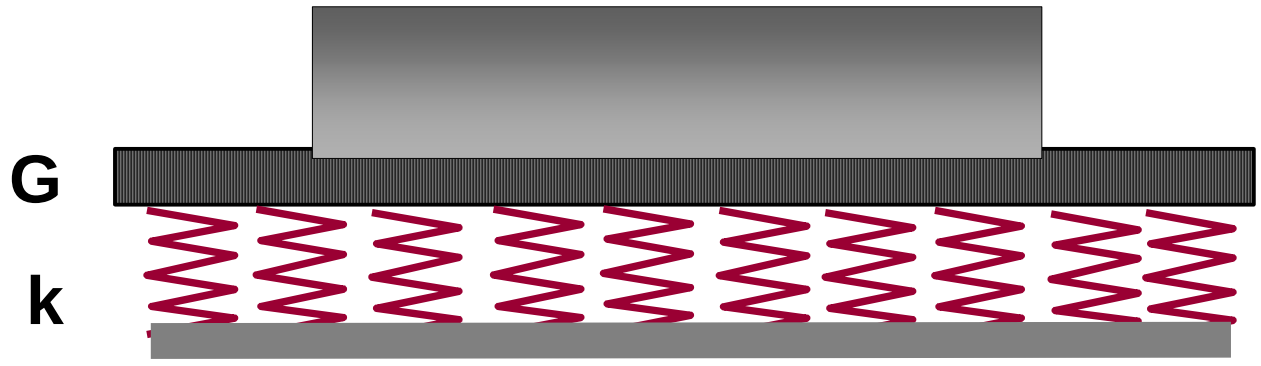

Figure 2.3. Pasternak model.

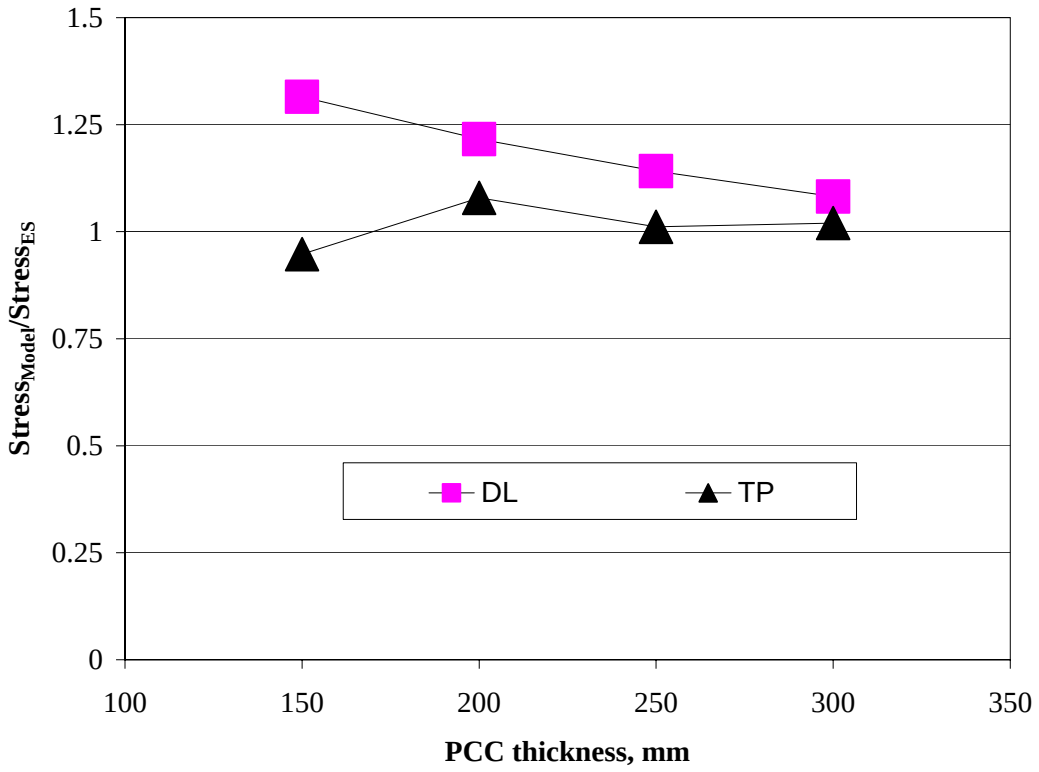

Figure 2.4. Comparison of maximum bending edge stresses.

Selection of Subgrade Model Based on FWD Test Results

In the past, the plate load test was recognized as the primary source of information concerning the numerical values to be assigned to the constants describing the Winkler model. This test, however, is expensive and difficult to conduct. Moreover, although Westergaard's original recommendation was to estimate k-value using measured slab deflections, this test is traditionally performed directly on the subgrade and rarely used for subgrade characterization in rehabilitation design. For the latter, the Falling Weight Deflectometer (FWD) test is the most common source of information for subgrade characterization. In this study, FWD deflections were simulated using the finite element program ILLI-SLAB and compared with field measurements from the LTPP database.

To investigate the effect of subgrade shear resistance on the results of FWD test conducted at the center of the slab, a factorial of 432 ILLI-SLAB runs was performed. The PCC slab was assumed to be in full contact with the foundation. The PCC thickness was varied from 152 mm to 356 mm. The coefficient of subgrade reaction, k-value, was varied from 13.5 to 135 kPa/mm. The shear coefficient, G, was varied from 0 (Winkler model) to 6.1 kN/mm. To evaluate the effect of shear coefficient on the shape of the deflection bowl, a ratio between the maximum deflection and the deflection 1524 mm apart was plotted against the radius of relative stiffness, ℓ , defined as follows:

$$\ell = \sqrt[4]{\frac{E h^3}{12(1-\mu^2)k}} \quad , , , , , \quad (2.3)$$

where

E = slab modulus of elasticity
μ = slab Poisson's ratio
h = slab thickness
k = k-value

For the range of values of the radius of relative stiffness that are typically observed for highway pavements (from 800 to 1200 mm), the ratio between the maximum and outermost sensor deflections depends only on the radius of relative stiffness and does not depend on G. As shown in figure 2.5, within this range the scatter due to the effect of G is negligible. On the other hand, no unique relationship exists between the maximum deflection and the radius of relative stiffness (see figure 2.6), which means that the magnitude of the maximum deflection depends on both G and k for the entire range of radius of relative stiffness.

Analysis of figures 2.5 and 2.6 shows that G cannot be backcalculated from the interior loading FWD deflections and should be derived from another test or assumption. It is important to note, however, that selection of G affects not only backcalculated k-value but also backcalculated slab modulus of elasticity. Regardless of subgrade shear capacity, backcalculation will result in the same value for the radius of relative stiffness, ℓ. If the DL model is assumed (G=0), then a coefficient of subgrade reaction, k_0, can be determined from the measured maximum deflection and radius of relative stiffness. However, if a higher G is assumed, then the corresponding backcalculated k-value, k_G, is less than k_0. Backcalculated slab modulus of elasticity, E, should satisfy the following equation:

$$E = \frac{12\ell^4 k(1-\mu^2)}{h^3} \quad , , , , , (2.4)$$

Therefore, backcalculated slab modulus of elasticity from the DL model, E0, can be expected to be greater than the corresponding slab modulus of elasticity from the TP model, EG. Therefore, neglecting subgrade shear capacity leads to overestimating slab modulus of elasticity.

Results of backcalculation of deflection data from the LTPP database support this conclusion. Figure 2.7 presents a comparison of backcalculated PCC moduli of elasticity for GPS sections determined using DL and ES models. A very good correlation between these two sets of moduli is observed. A linear regression analysis resulted in the following relationships:

$$E_{PCC,DL} = 1.3195\ E_{PCC,ES} \quad , , , , , (2.5)$$

R^2 = 97%
N = 350
SEE = 1.8 GPa

where

$E_{PCC,ES}$ = PCC modulus of elasticity backcalculated using ES model, GPa
$E_{PCC\ DL}$ = PCC modulus of elasticity backcalculated using DL model, GPa

Therefore, although subgrade shear resistance cannot be determined from the interior loading deflection basin, it may significantly affect the results of backcalculation.

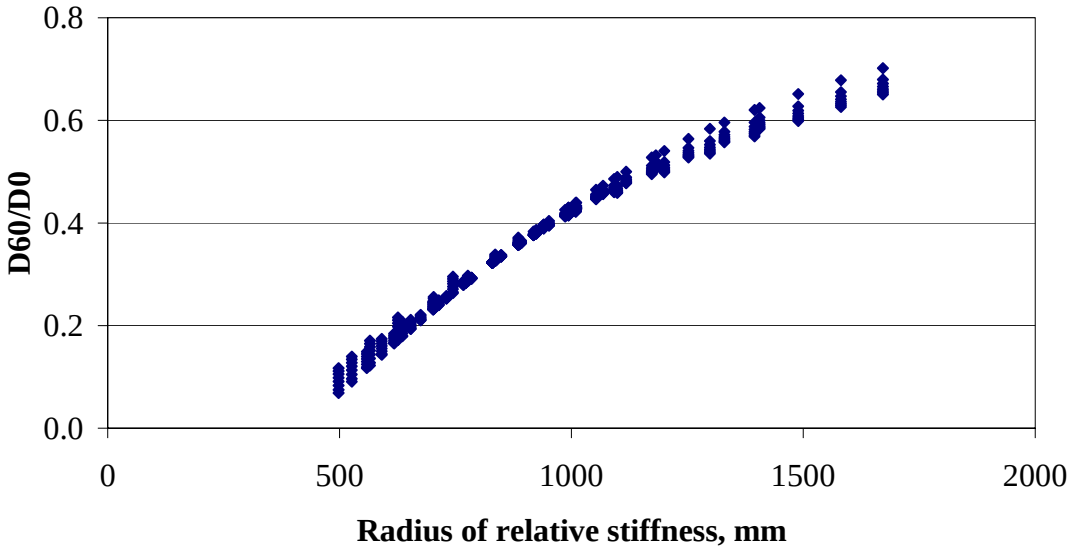

Figure 2.5. Effect of radius of relative stiffness on deflection bowl shape characterizing parameter $D_{60}/D_{0.}$

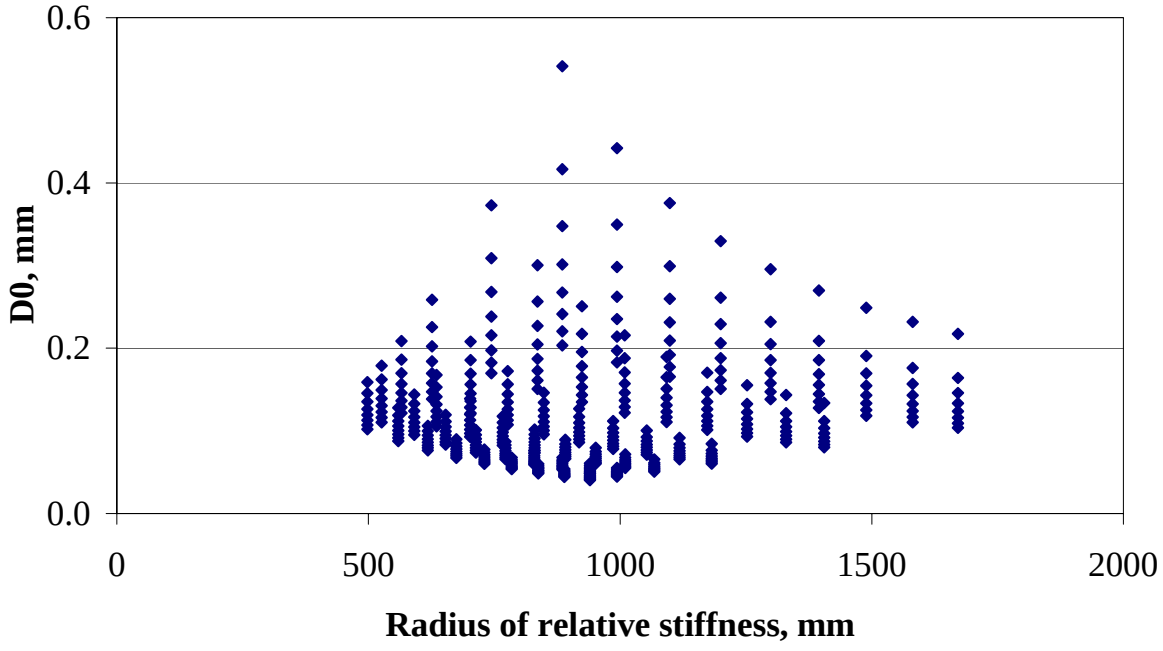

Figure 2.6. Effect of radius of relative stiffness on maximum deflection.

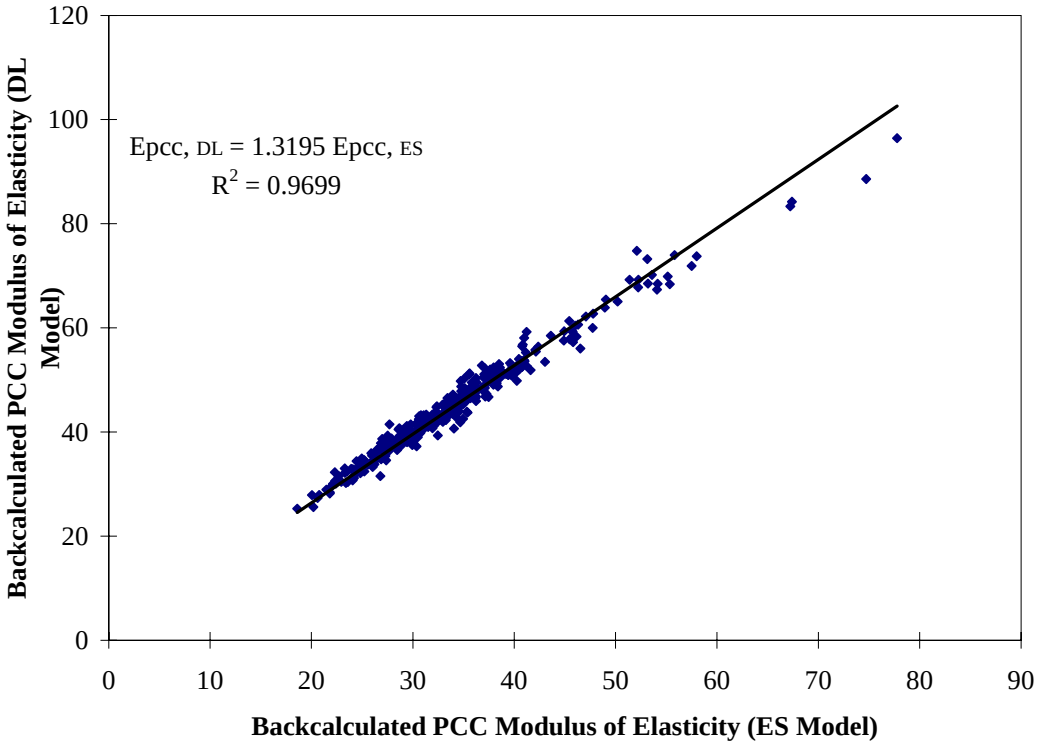

Figure 2.7. Backcalculated PCC modulus of elasticity (ES model) versus backcalculated PCC modulus of elasticity (DL model).

The following conclusions can be made based on these observations:

1. Subgrade shear resistance does not significantly affect the shape of the deflection bowl for the interior loading condition.
2. The FWD center-slab loading test cannot be used to determine what subgrade model better represents subgrade properties.
3. If the slab modulus is not known, the FWD center-slab test cannot be used to determine more than one subgrade parameter. For Pasternak model, either the results of another test are required or additional assumptions should be made.
4. Backcalculated slab modulus of elasticity is affected by the assumed subgrade shear modulus.

Edge Loading

The inability to quantify subgrade shear resistance from the interior loading test calls for an additional test which can provide necessary information. One of the options is to use results of FWD testing conducted near the slab edge. In this study, FWD deflections were simulated for the edge loading condition. The obtained maximum deflections were compared with the maximum deflection for the interior loading. The results are shown in figure 2.8.

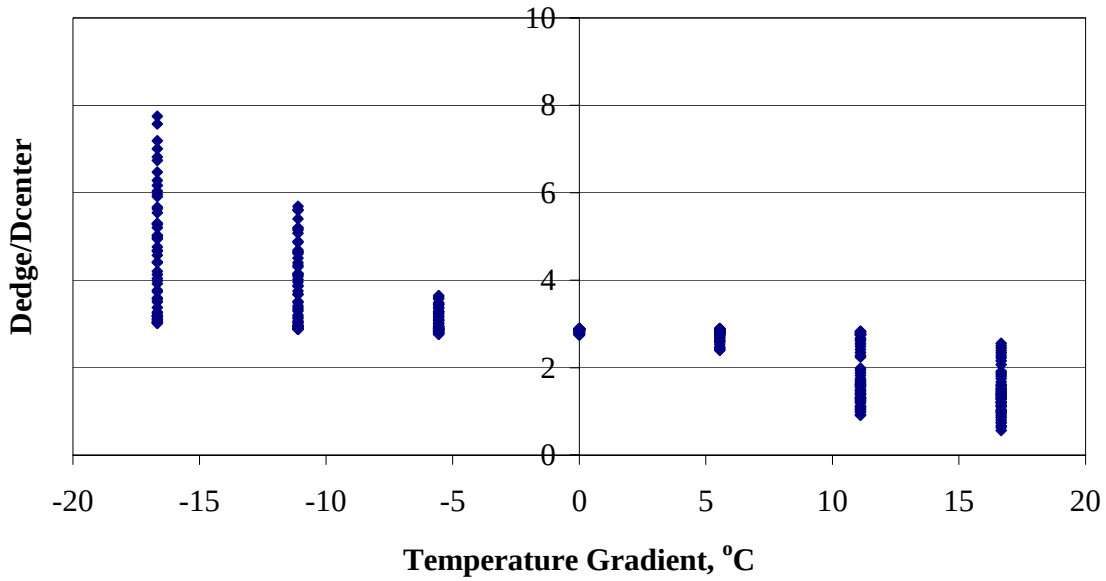

Figure 2.8. Effect of temperature curling and moisture warping on ratio between interior and edge deflections.

If the Winkler model (shear modulus equal to zero) adequately describes subgrade properties, then the ratio between the interior and edge deflections should be from 2.8 to 2.9. In this study, the LTPP database was used to find in situ edge-to-center slab deflection ratios. Table 2.1 presents average ratios calculated for four LTPP sections.

Table 2.1. Ratios of interior to edge deflections for four LTPP database sections.

State ID	Section ID	Test Date	Average Dcenter/Dedge
55	3019	22-Aug-90	1.86
20	4016	08-Sep-89	2.14
55	3012	20-Aug-90	2.07
55	3012	30-Jun-93	1.98
29	5483	19-Jul-91	1.60

All four sections exhibited edge-to-center deflection ratios significantly lower than the 2.8 predicted by the Winkler model if full contact between the slab and the foundation is assumed. To investigate the effect of slab curling/warping on edge-to-center deflection ratios, a factorial of ILLI-SLAB runs was performed. The Winkler foundation model was used for subgrade modeling. The PCC thickness was varied from 152 mm to 356 mm. The coefficient of subgrade reaction, k-value, was varied from 13.5 to 135 kPa/mm. The combined effect of slab temperature curling, moisture warping, and shrinkage was modeled by the effective temperature difference between the top and bottom slab surfaces, which varied from -16.7 to 16.7 oC. Figure 2.9 presents ratios between maximum deflections at the slab edge and at the slab interior due to corresponding FWD loads (deflections due to slab curling without any FWD loads were subtracted). Figure 2.9 presents those ratios for PCC slab thickness equal to 203 and 305 mm and k-value equal to 54 kPa/mm.

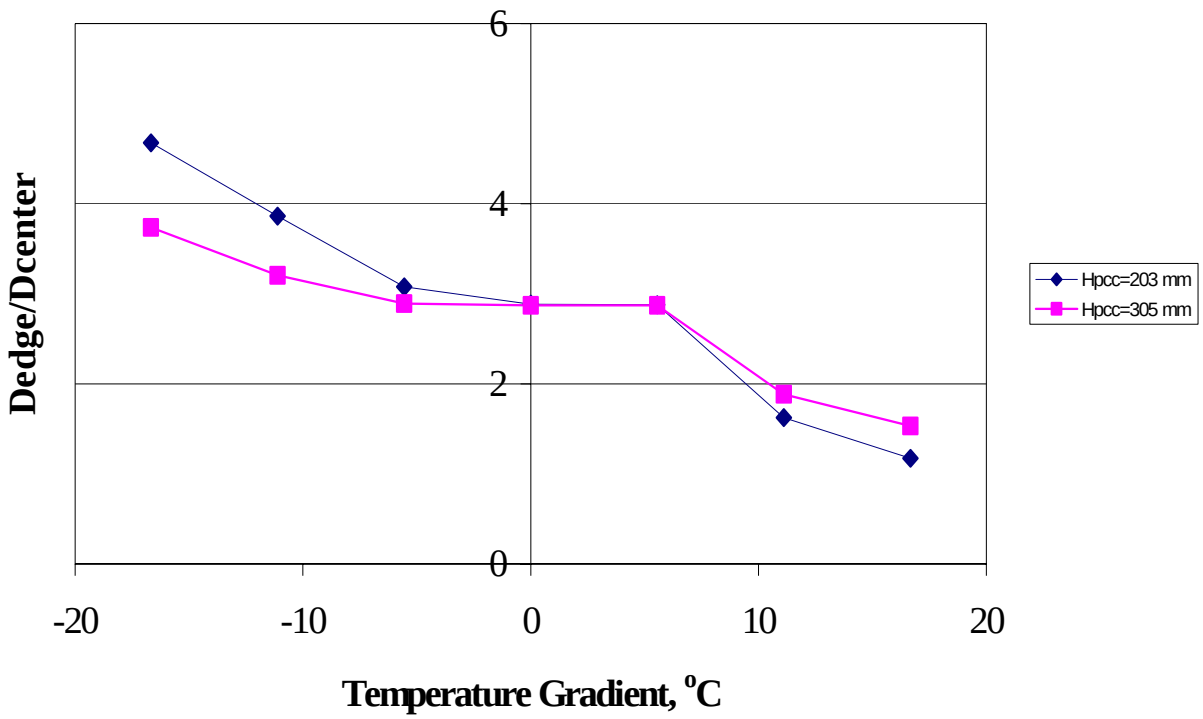

Figure 2.9. Effect of temperature curling and moisture warping on ratio between interior and edge deflections; k=54 kPa/mm; h=203 and 305 mm.

Analysis of figures 2.8 and 2.9 shows that if the temperature difference between the top and bottom slab surfaces is between –5 and 5 ^{o}C (-9 and 9 ^{o}F), then the ratio between the maximum edge and center deflections is similar to that determined for a flat slab condition and approximately 2.8-3.0 for a wide range of slab and subgrade parameters. Usually, the effective temperature gradient lies within these limits if the FWD testing is conducted in the morning. Therefore, one can assume that the difference between observed and predicted values is not due to thermal gradient but due to not accounting for load shear transfer. On the other hand, since temperature curling has a significant effect on edge deflections, this test could not be reliably used for shear modulus determination. The effect of extended beyond the slab edge bases and presence of shoulder may make this test even less applicable.

Accounting for Additional Edge Support Using Extended Base

In the traditional analysis of rigid pavement, it is usually assumed that the base layer has the same width as the PCC surface layer. Therefore, if the DL subgrade model is used, the effect of additional support from the subgrade beyond the slab edge is ignored. In reality, the base layer may be extended from 0.6 to 3.6 m beyond the slab edge in the longitudinal direction. Even if the subgrade is modeled as a DL foundation, the extended part of a base can mobilize additional support reaction from the subgrade.

In this study, a 225-mm-thick PCC slab with a shoulder resting on a 150-mm granular base layer was analyzed (see figure 2.10). The shoulder width was assumed equal to 300 mm. The shoulder was intentionally modeled very short to minimize any effect of support provided by the shoulder and to highlight the effect of additional support provided by the base layer and subgrade. The moduli of elasticity of PCC and base layers were assumed equal to 27.6 GPa and 276 MPa, respectively. The PCC and base layers were 3.6 and 6.6 m wide, respectively. To model more realistically the base behavior under the slab edge, it was assumed that the base is cracked and only shear forces can be transmitted across the crack. It was also assumed that no forces could be transmitted from the PCC slab directly to the shoulder. A single axle 80-kN load was applied at the slab edge.

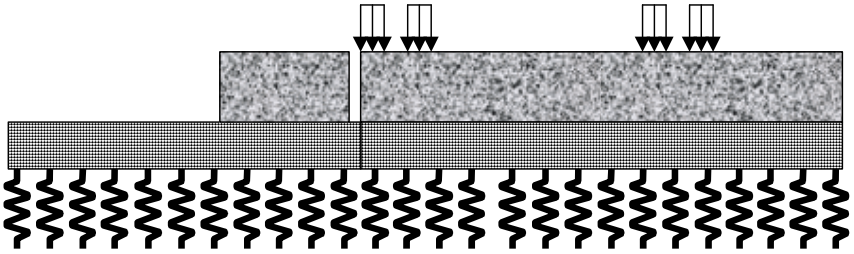

Figure 2.10. Extended base layer.

Figures 2.11 and 2.12 show the effect of crack shear resistance on slab maximum edge deflections and stresses with no temperature curling and a positive temperature gradient of 16.6 ^{o}C, respectively. If shear resistance of the crack is low, then maximum slab responses are close to the maximum responses in the slab with no shoulder and extended base. However, an increase in crack shear resistance, AGG, leads to a significant decrease in the slab maximum responses if no curling is considered. A similar trend is observed in the case of combined traffic and temperature loading, although in this case the effect of additional subgrade support is less pronounced.

The advantage of this approach is that the effect of additional support from the subgrade beyond the slab edge is modeled using a more traditional technique than the TP model. The same k-value that was used in the traditional analysis can be used in this model. The base layer parameters can be determined from laboratory testing or can be backcalculated. The base crack shear resistance can be estimated from the deflection load transfer efficiency between the slab and PCC shoulder, which is typically from 20 to 50 percent.

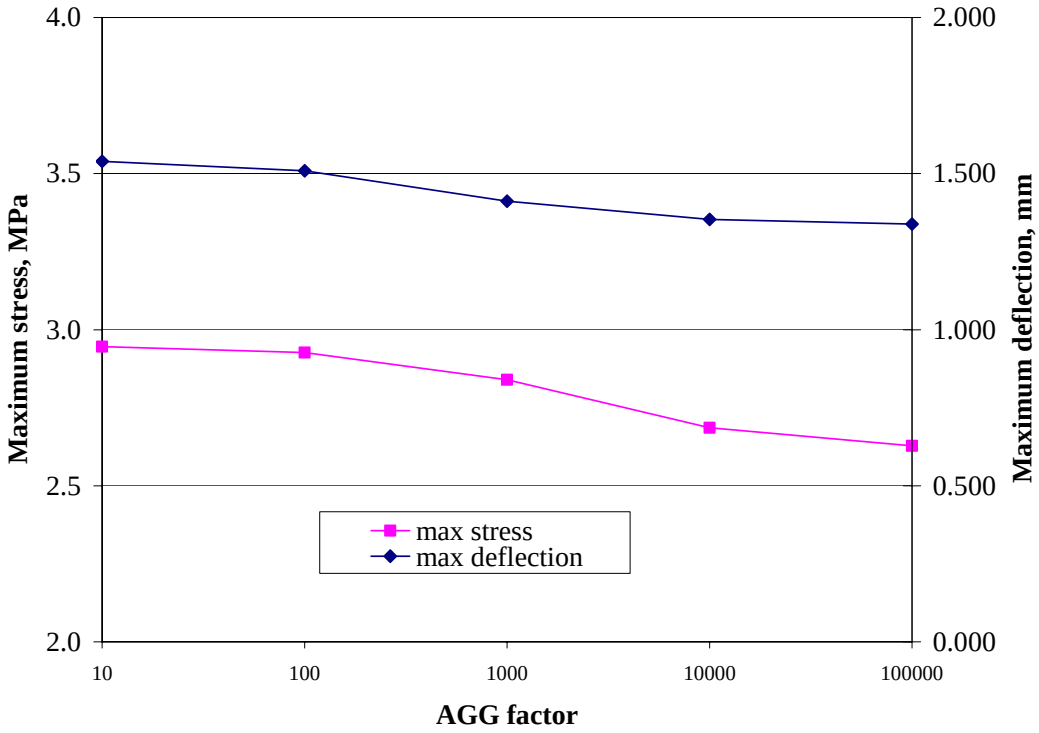

Figure 2.11. Effect of base crack shear resistance on PCC slab responses (no curling).

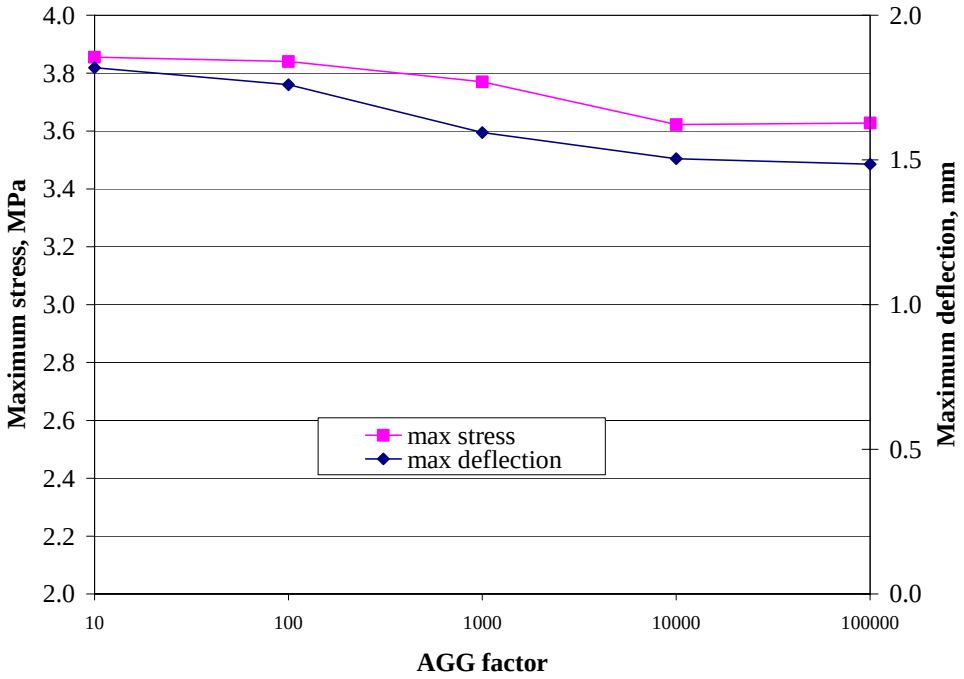

Figure 2.12. Effect of base crack shear resistance on PCC slab responses (with curling).

Computation of Effective Dynamic k-Value

The effective dynamic k-value is obtained by first determining the deflection profile of the PCC surface using an elastic layer program (JULEA), modeling all layers specified for the design. The subgrade resilient modulus is adjusted to reflect the lower deviator stresses that typically exist under a concrete slab and base course as compared to the deviator stress used in laboratory resilient modulus testing. Next, the computed deflection profile is used to backcalculate the effective dynamic k-value. Thus, the effective dynamic k-value is a computed value, not a direct input to the design procedure (except in rehabilitation).

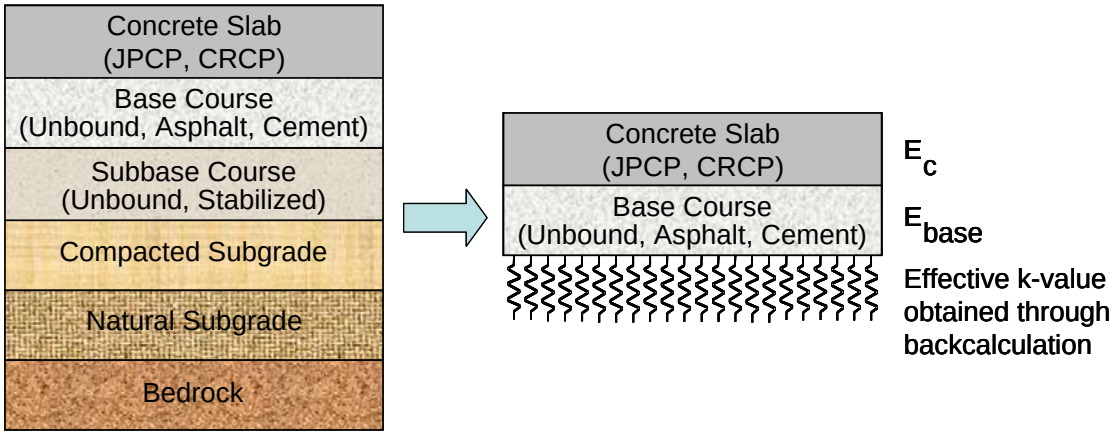

Figure 2.13. Structural model for rigid pavement structural response computations.

The effective k-value used in this Guide is a dynamic k-value, which should be distinguished from the traditional static k-values used in previous design procedures. The procedure to obtain the effective dynamic k-value for each time increment (month) is outlined in the following steps:

1. Assign layer parameters (E and Poisson's ratio) in a manner consistent with flexible pavement design (PART 3, Chapter 3).
2. Using the elastic layer program JULEA, simulate a 9,000-lb Falling Weight Deflectometer (FWD) load with the plate radius 5.9 in and compute PCC surface deflections at 0, 8, 12, 18, 24, 36, and 60 in from the center of the load plate.
3. Adjust the subgrade resilient modulus to account for the lowered deviator stress level beneath a PCC slab and base.
4. Using the elastic layer program JULEA, again simulate a 9,000-lb FWD load with the plate radius equal to 5.9 in, and with the recalculated subgrade resilient modulus and subbase moduli.
5. Calculate PCC surface deflections at 0, 8, 12, 18, 24, 36, and 60 in from the center of the load plate.
6. Use the Best Fit method (*12)* to compute the dynamic modulus of subgrade reaction using the PCC surface deflections.

The "effective" dynamic k-value represents the compressibility of all layers beneath the PCC slab. For example, if the pavement is constructed in a region with bedrock close to the surface (less than 10 ft), then the bedrock is entered as a stiff layer (high elastic modulus) beneath the subgrade soil layer. The PCC surface deflections calculated using JULEA reflects the presence of the

bedrock layer; consequently, the presence of the bedrock layer is reflected in the calculated effective dynamic k-value.

The effective dynamic k-value of the subgrade is calculated for each month of the year and utilized directly to compute critical stresses and deflections in the incremental damage accumulation over the design life of the pavement. Factors such as water table depth, depth to bedrock, and frost penetration depth (frozen material) can significantly affect effective dynamic k-value. All of these factors are considered in the EICM.

Conclusions

The results of this study showed that the TP model offers more realistic subgrade modeling than the DL model. Much less computationally demanding than the ES model, it permits close matching of slab critical responses with the ES model. As shown by several research studies over the past 30 years, the TP model has great potential as a powerful tool in subgrade characterization. Nevertheless, for the following reasons, **the research team does not recommend this model for inclusion in the 2002 Design Guide:**

1. Although the model is well known to researchers, it is not well known by practitioners.
2. At the present time, there are no established and field-verified guidelines for the selection of TP model parameters, G and k. Moreover, since TP k-value is different from DL k-value, it may create confusion for practicing engineers.
3. The majority of the research related to the TP model focuses on the analysis of a single slab subjected to traffic loading only (no curling effect). Although the latest version of ILLISLAB permits curling analysis with the TP model, this is a relatively new technology, and extensive field testing and calibration could be required.
4. Almost all available performance prediction models for rigid pavement use the DL subgrade model. Therefore, switching to the TP model may cause difficulties in recalibration of those models.

The research team concluded that, at the present time, in spite of its limitations, the DL model is the best model for use in a mechanistic-empirical design procedure. Indeed:

- The DL-based structural models are well established and tested.
- The guidelines for the DL model k-value are well established based on the results of several major studies, including NCHRP 1-30.
- Use of the DL model and extended base allows the engineer to mitigate the main drawback of the DL model lack of accounting for support of the subgrade resting beyond the slab edge. This approach utilizes more traditional techniques and does not introduce new subgrade parameters.

Therefore, the research team recommends **use of the DL model in the 2002 Design Guide** and, at the same time, encourages research in the TP model for inclusion in future design procedures.

References

Chou, Y.T. *Structural Analysis Computer Programs for Rigid Multicomponent Pavement Structures with Discontinuities- WESLIQID and WESLAYER*. Technical Report GL-81-6, U.S. Army Engineer Waterways Experiment Station, May 1981.

Choubane, B., and M. Tia. Nonlinear Temperature Gradient Effect on Maximum Warping Stresses in Rigid Pavements. *Transportation Research Record No. 1370*, 1992.

Huang, Y.H. *Pavement Analysis and Design*. Prentice Hall, 1993.

Ioannides, A.M. et al. A Finite Element Analysis of Slabs-on-Grade Using a Variety of Support Models. *Proceedings,* Third International conference on Concrete Pavement Design and Rehabilitation, Purdue University, 1985.

Kerr, A.D. Elastic and Viscoelastic Foundation Models. *Journal of Applied Mechanics, Transactions*, ASME, Vol. 31, No. 3, pp. 491-498, 1964.

Kerr, A.D. Mathematical Modeling of Airport Pavements. *Proceedings*, ASCE Specialty Conference "Airport Pavement Innovations Theory to Practice," 1993.

Khazanovich, L., and A.M. Ioannides. A Finite Element Analysis of Slabs-on-Grade Using Improved Subgrade Soil Models. *Proceedings*, ASCE Specialty Conference "Airport Pavement Innovations Theory to Practice," 1993.

Kok, A.W.M. PC Program for the Analysis of Rectangular Pavements Structures. *Proceedings,* Second International Workshop on the Design and Rehabilitation of Concrete Pavements, Sigüenza, Spain, 1990.

Korenev, B.G., and E.I. Chernigovskaya. *Analysis of Plates on Elastic Foundation*. Gosstroiizdat, Moscow, 1962 (in Russian).

Pasternak, P.L. (1954), "Fundamentals of a New Method of Analysis of Structures on Elastic Foundation by Means of Two Subgrade Coefficients," Gosudarstvennoe Izdatel'stvo Literatury po Stroitel'stvu i Arkhitekture, Moscow (in Russian).

Pronk, A.C. The Pasternak Foundation: An Attractive Alternative for the Winkler Foundation. *Proceedings,* Fifth International Conference on Concrete Pavement Design and Rehabilitation, 1993.

Reissner, E. Note on the Formulation of the Problem of the Plates on an Elastic Foundation. *Journal of Applied Mechanics*, 1967

Reissner, E. A Note on Deflections of Plates on a Viscoelastic Foundation. *Acta Mechanics*, 1967

Tabatabie, A.M., and E.J. Barenberg. Structural Analysis of Concrete Pavement Systems. ASCE*, Transportation Engineering Journal*. Vol. 106, No. 5, 1980.

Tayabji, S.D., and B.E. Colley. Improved Pavement Joints. *TRR 930*, 1983.

Vlasov, V.Z., and N.N. Leont'ev. Beams, Plates and Shells on Elastic Foundations. NASA-NSF, NASA TT F-357, TT 65-50135, Israel Program for Scientific Translations, 1960 (translation date: 1966)

Westergaard, H.M. (1948). New Formulas for Stresses in Concrete Pavements of Airfields. *Transactions.* American Society of Civil Engineers, Volume 113.

Winkler, E. (1864), "Die Lehre von der Elastizitt und Festigkeit" (Theory of Elasticity and Strength), H. Dominicus, Prague (in German).

CHAPTER 3. DETERMINATION OF CRITICAL BENDING STRESSES AT THE BOTTOM SURFACE OF JPCP

INTRODUCTION

The maximum bending stress from edge loading at the midslab location of a JPCP is the critical response that leads to bottom-up fatigue cracking. Therefore, the first requirement for the development of a model for calculating transverse cracking of JPCP is to develop an improved model for calculating the edge stress. Of interest was the maximum combined edge stress from traffic loading and temperature curling that leads to fatigue damage.

The structural model used for prediction of JPCP responses should adequately describe JPCP behavior under a variety of combinations of traffic and climatic loading, as well as account for joint spacing and joint transfer effects. It would be extremely difficult, if not impossible, to develop a closed form analytical solution capable of accounting for all these effects. Over the past 30 years, the finite element method (FEM) has been proven to be a flexible and accurate tool for predicting pavement response. However, FEM is quite inefficient for analyzing damage accumulation in the JPCP, which may require the prediction of PCC tensile stresses for a large number of loading and site condition combinations.

In previous studies by Smith et al. (1990) and Yu et al. (1996), stresses for edge loading conditions were determined using regression equations developed as part of NCHRP Project 1-26 (Barenberg and Thompson 1992). These equations are based on the results obtained from the finite element program ILLI-SLAB and provide an accurate and efficient means of determining the combined stress due to single 80-kN axle loads and slab curling for edge loading conditions. The regression equations made it feasible to analyze a large number of cases to adequately address the effects of temperature gradients on fatigue damage for several projects. However, these regression equations are not suitable for this study because of their inability to analyze the effect of tandem and tridem axle configurations on the stresses in the PCC slab. Improvement of these regressions is a complex and time-consuming process. This prompted the research team researchers to investigate alternative tools for development of rapid solutions.

In the last decade, artificial neural networks (NN) gained substantial popularity for solution of computationally efficient problems in pavement analysis, design, and evaluation (Meier and Rix 1994). Several NN models were proposed for predicting responses in airfield jointed concrete pavements (Haussmann et al. 1997; Ceylan et al. 1998, 1999, 2000). The most recent model can almost instantaneously predict responses for a variety of combinations of design and loading parameters. In spite of some limitations (single slab size and an inability to analyze the effect of the base layer), the model eliminates the need to use ILLI-SLAB for the most typical airport pavement analysis scenarios.

This chapter describes the development of NN for predicting critical tensile bending stresses at the bottom of JPCP, which lead to bottom-up transverse cracking. The development of the finite element model is presented first. Then, the equivalency concepts are introduced. These concepts are used to reduce the number of independent input variables required for training the NN. Finally, this chapter presents information about the training and testing of the NN, as well as a sensitivity study.

FACTORS AFFECTING JPCP STRESSES

Past research has shown that bottom-up cracks in JPCP are a result of accumulated fatigue damage caused by longitudinal stresses at the bottom surface of the slab (Darter 1977). The higher the stresses induced by traffic and environmental loading, the more likely that cracks develop. The magnitude of these stresses depends on a variety of factors, including the following:

- PCC slab and base layer parameters (thickness, modulus of elasticity, coefficient of thermal expansion, and unit weight).
- Interface condition between the PCC slab and base layers.
- JPCP joint spacing.
- Lane width and load transfer efficiency between the lanes.
- Shoulder type.
- Subgrade properties (stiffness and presence of voids).
- Temperature distribution throughout the JPCP slabs thickness.
- Axle type, weight, and position (distance from the slab edge).

Any finite element model used for analysis of stresses in JPCP should accurately account for all these factors.

Slab Geometry

To obtain a realistic estimation of PCC bottom surface stresses, it is important for a finite element model to be as close to the real pavement system as possible. On the other hand, it is desirable not to model unimportant feature and elements of the system to make the model more computationally efficient and to avoid unnecessary error accumulation. One of the most important decisions to be made in pavement modeling is to assign the number of slabs in the transverse and longitudinal directions that need to be modeled.

Transverse Direction

Only one traffic lane may be modeled in transverse direction. Slabs from the passing lane can be ignored in the analysis. To verify this recommendation, two factorials of finite element runs were performed. The PCC thickness was varied from 200 to 300 mm. 80-kN single axle loads were applied at the slab edge at the midslab location. The difference between the top and bottom slab temperatures was assumed to be 11.1 ^{o}C. The coefficient of subgrade reaction was varied from 27 to 54 kPa/mm. The first model considered two slabs in the transverse direction: a truck lane and a passing lane (see figure 3.1). The second model considered only the traffic lane (see figure 3.2). An AC shoulder was ignored in both cases.

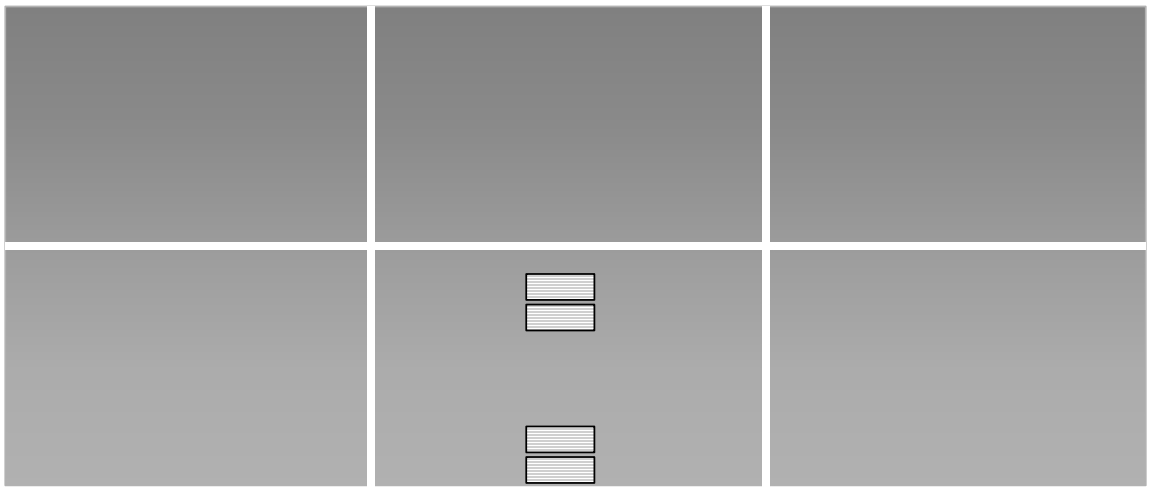

Figure 3.1. Modeling two traffic lanes.

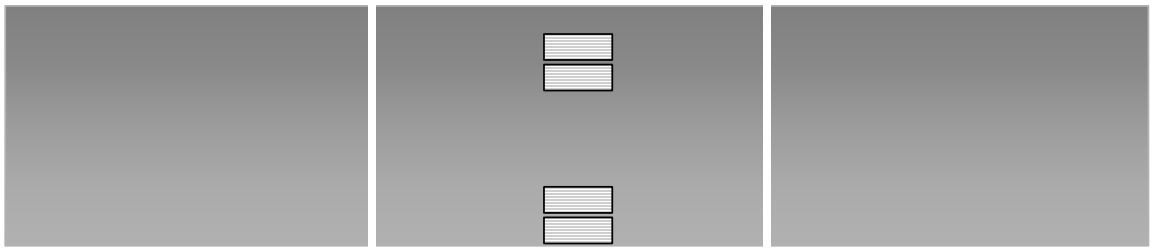

Figure 3.2. Modeling one traffic lane.

Figure 3.3 presents a comparison of the PCC slab maximum bottom surface bending stresses obtained from these two models. One can observe that, for PCC thicknesses and subgrade parameters, the effect of modeling the passing lane is negligible. On the other hand, ignoring this slab in the analysis permits either speed up the analysis or, if necessary, refine the mesh for the rest of the model.

The approach for accounting for a shoulder is discussed in the section “Shoulder Modeling.”

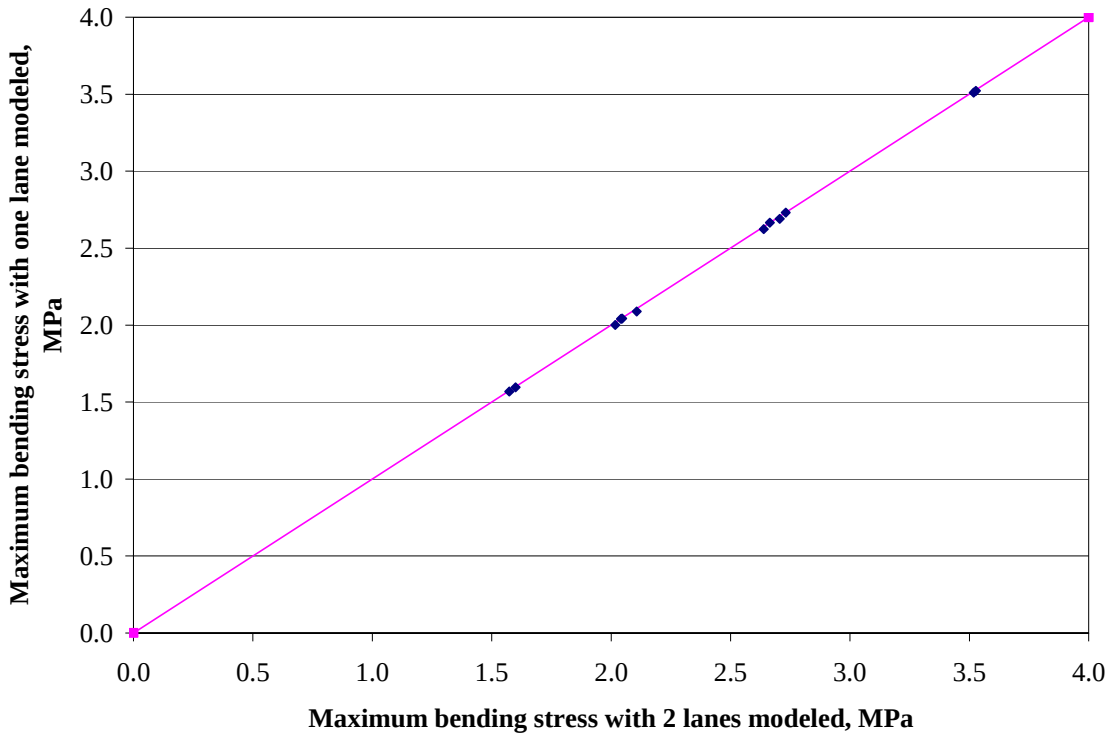

Figure 3.3. Effect of number of slabs in transverse direction on predicted maximum bottom surface bending stresses for different axle locations.

Longitudinal Direction

At least three slabs in longitudinal directions should be modeled in the finite element model. The following example justifies this recommendation. Consider a PCC pavement the joint spacing equal to 4.5 m. An 80-kN single axle load is applied at the slab edge. The difference between the top and bottom PCC slab temperatures was assumed to be equal to 11.1^{o}C. Only one slab was modeled in the transverse direction, but the number of slabs in the longitudinal direction was varied from 1 to 5, as shown in figure 3.4. Figures 3.5 and 3.6 presents the effect of the number of slabs in the model on predicted maximum bottom surface PCC bending stresses for different PCC slab thicknesses. One can observe modeling only one slab in the longitudinal direction may introduce some error in the analysis, particularly with thicker slabs, while no practical difference was observed after increasing the number of slabs from 3 to 5. Analysis of several cases with different pavement design parameters and axle configurations led to the same conclusion.

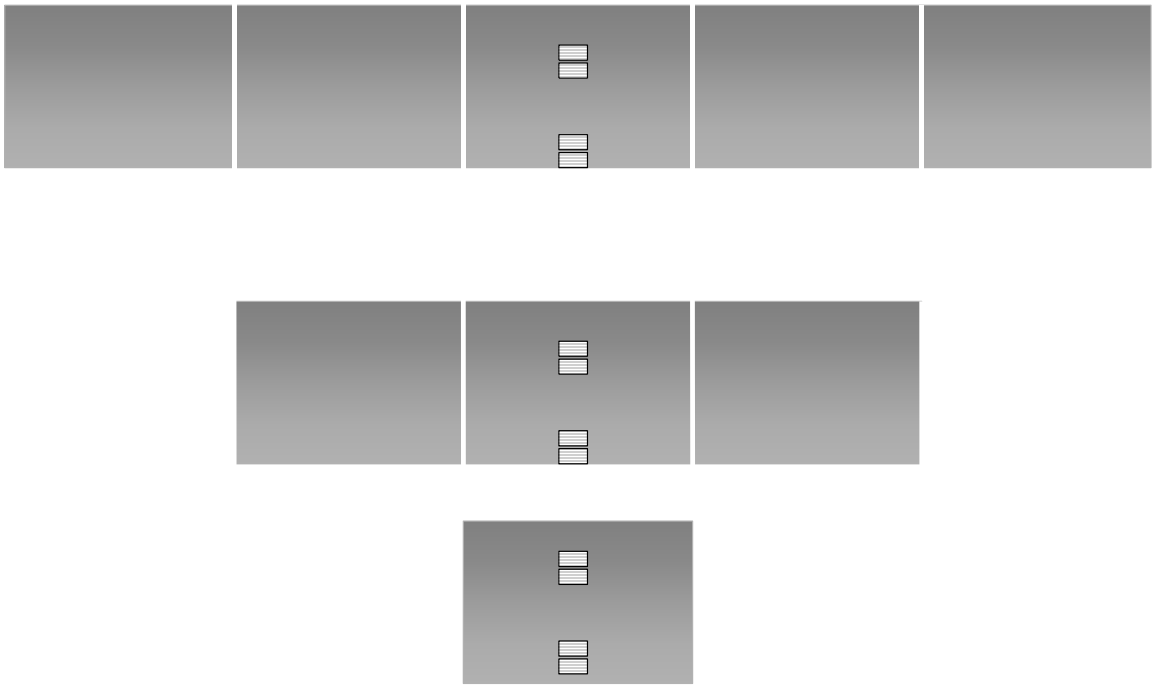

Figure 3.4. Modeling of JPCP with different number of slabs in longitudinal direction.

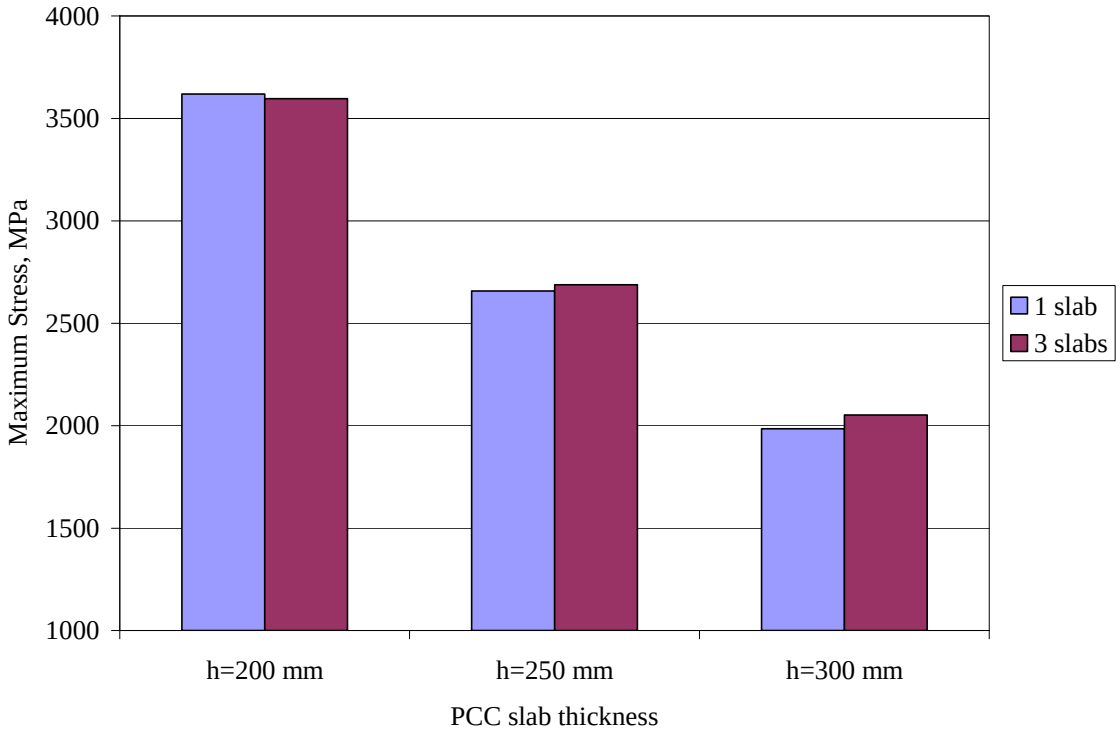

Figure 3.5. Effect of number of slabs in longitudinal direction on predicted critical stresses at the bottom PCC surface (single slabs vs. three slabs).

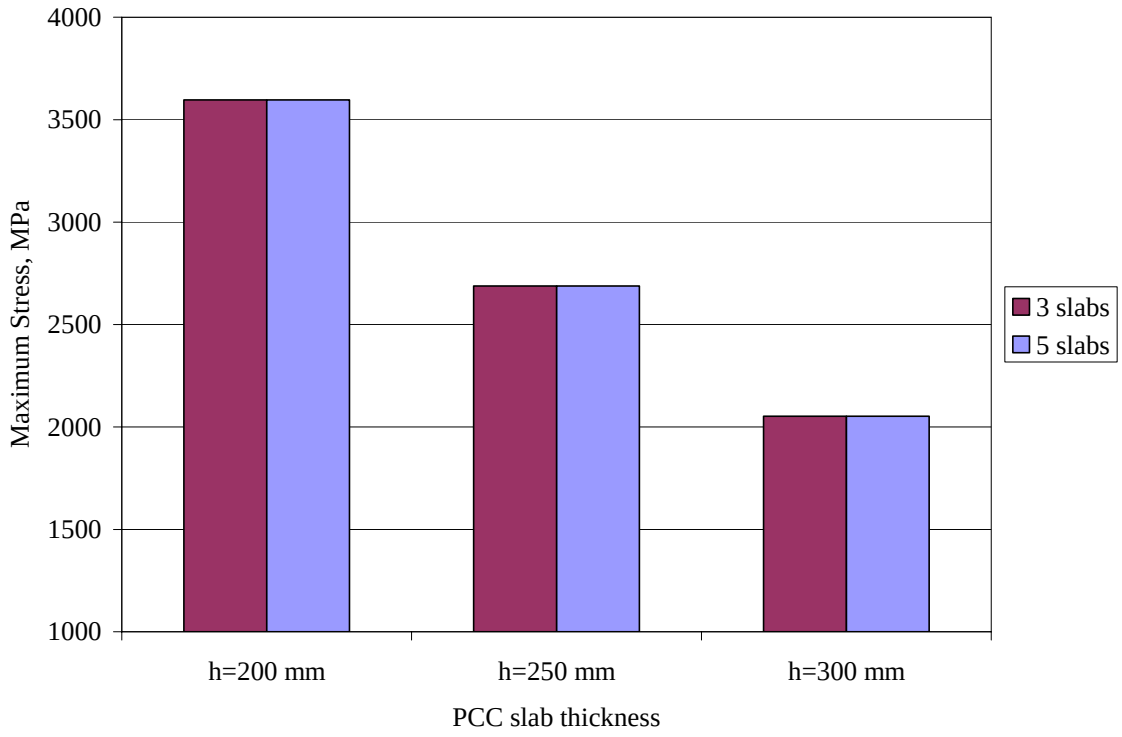

Figure 3.6. Effect of number of slabs in longitudinal direction on predicted critical stresses at the bottom PCC surface (three slabs vs. five slabs).

Modeling of Joints

Load transfer efficiency (LTE) at the transverse joints has only a limited effect on the resulting critical PCC bottom surface stresses. In finite element analyses, the joints can be modeled using vertical shear spring elements. The equivalent stiffness of the spring element (the AGG-factor) should be selected to provide appropriate deflection LTE. Maximum PCC bottom surface tensile stresses are not sensitive to the level of the deflection LTE at the transverse joints if the latter is assigned in a reasonable range. To illustrate this effect, consider a system of three 250-mm-thick PCC slabs resting on a Winkler foundation with the coefficient of subgrade reaction equal to 54.3 kPa/mm. An 80-kN tandem axle load is applied near slab edge at the midslab location of the center slab (see figure 3.7). The difference between the top and bottom slab temperatures is assumed to be 11.1 ^{o}C. The joint spacing is assumed to be 4.5 m, and the deflection joint load transfer efficiency is varied from 2 to 98 percent. The results of the finite element analysis for this system are shown in table 3.1. One can observe that change in LTE from 50 to 98 percent caused only a slight change in the predicted maximum tensile stresses. Therefore, it is recommended to use the same (average) joint stiffness in the maximum bending stresses in the analysis.

Table 3.1. Effect of LTE on maximum bending stresses.

Deflection Load Transfer Efficiency at Transverse Joints, percent	Maximum Bending Stress, MPa
1.83	1.99
11.66	2.00
48.25	2.03
86.82	2.05
97.90	2.05

Loading Positions

Numerous studies have shown that maximum bending stresses at the bottom surface of the PCC slab occur at the slab edge, between two transverse joints, and that these stresses occur when an axle wheel is directly above this location (see figures 3.7 through 3.9).

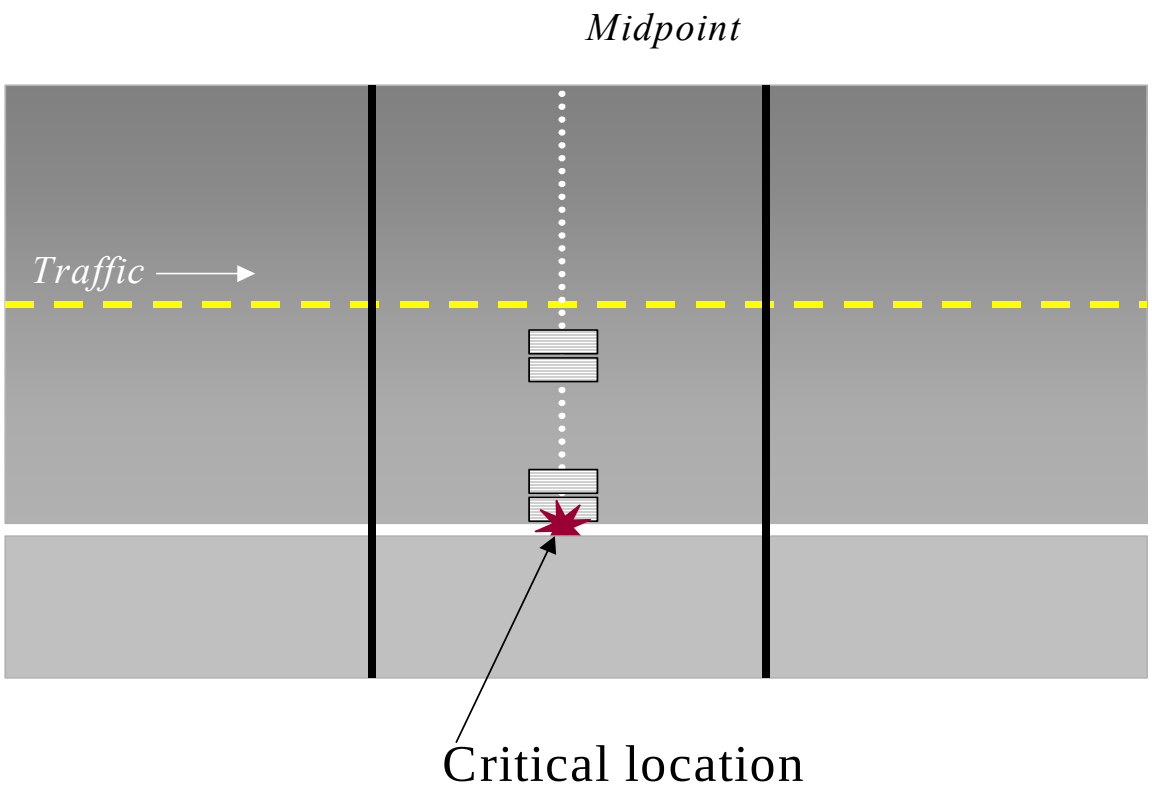

Figure 3.7. Critical single axle position for bottom-to-top cracking.

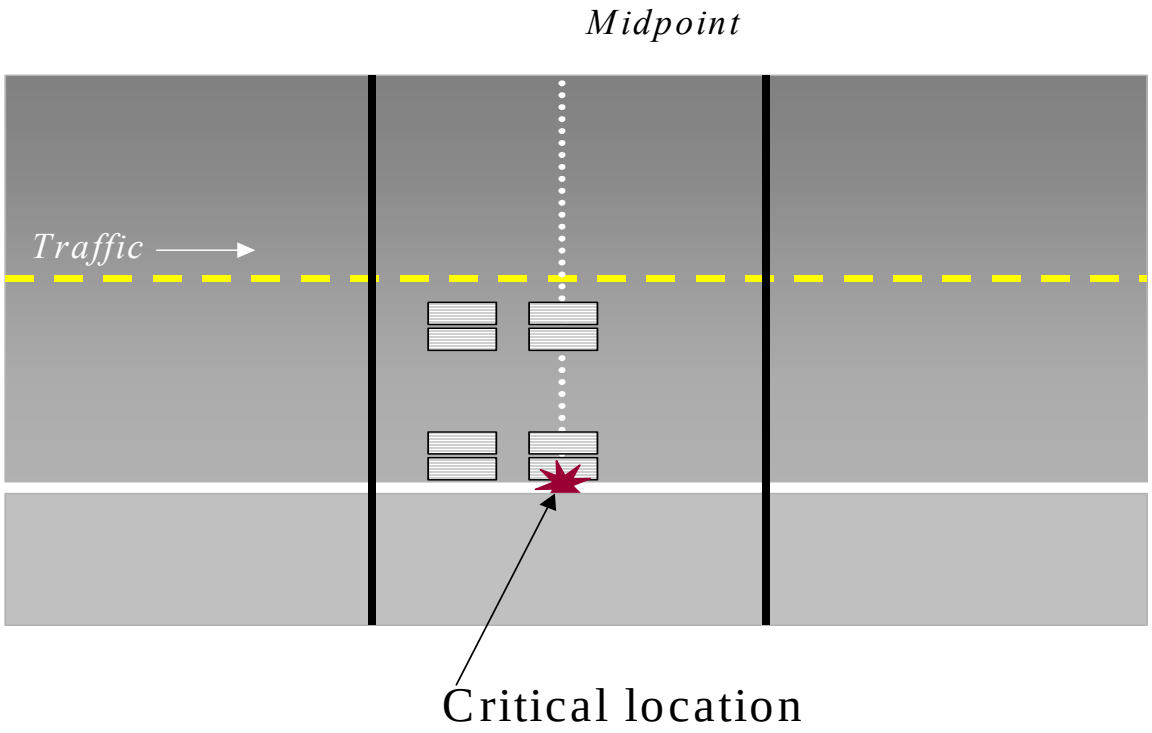

Figure 3.8. Critical tandem axle position for bottom-to-top cracking.

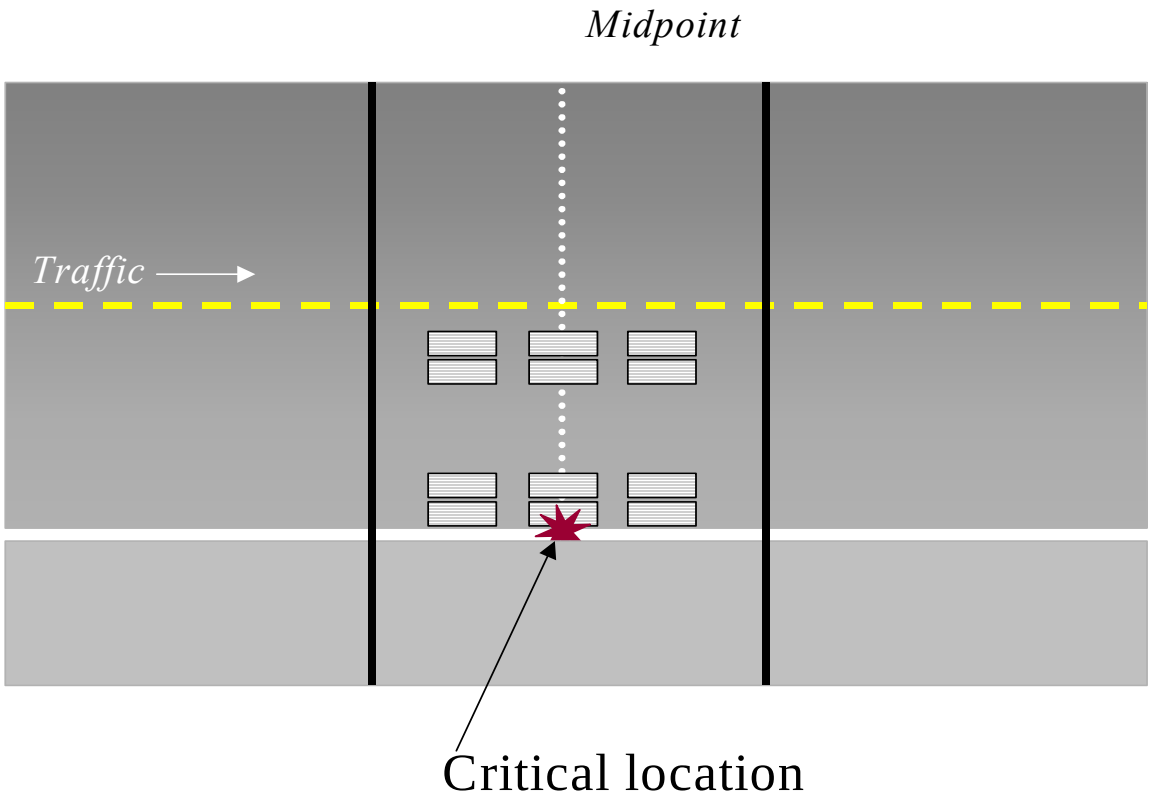

Figure 3.9. Critical tridem axle position for bottom-to-top cracking.

Modeling of Shoulders

The presence of a shoulder reduces traffic loading induced stresses at the bottom surface of a PCC slab. In finite element analyses, the joints can be modeled using vertical shear spring elements. The equivalent stiffness of the spring element (the AGG-factor) should be selected to provide appropriate LTE. If no other information is available, the following LTE should be assumed:

Joint type	LTE_{sh}, percent
Monolithically constructed tied PCC shoulder	50 to 70
Separately constructed tied PCC shoulder	30 to 50
AC shoulder	10-20

Crovetti's (1994) relationship between nondimensional joint stiffness and LTE can be used to determine the appropriate AGG-factor:

$$LTE = \frac{100\%}{1+1.2*\left(\frac{AGG_{tot}}{k\,\ell}\right)^{-0.849}} \quad (3.1)$$

where

AGG_{tot} is the total stiffness.
ℓ is the PCC slab radius of relative stiffness.
k is a coefficient of subgrade reaction (k-value).

Modeling of Base Layer

The base layer should be modeled as fully bonded or fully unbonded (frictionless) with the PCC slab. If the layer is unbonded, then it can be assumed that the PCC slab and the base layer have the same deflection basins (no separation is required to model). Although this assumption may produce a discrepancy in deflection shape prediction, it does not significantly affect predicted maximum PCC bottom surface stresses.

To verify this hypothesis, a two-layered system (200-mm-thick PCC slab over 200-mm-thick base layer) was considered to be loaded by an 80-kN single axle load. The difference between the top and bottom slab temperatures is assumed to be 11.1 ^{o}C. The modulus of elasticity of the PCC slab was assumed to be 27.6 GPa. Two cases of base stiffness were considered (2.76 GPa and 276 MPa). For each case, the base was analyzed as unbonded with and without possible separation from the PCC slab. Table 3.2 presents the resulting maximum PCC bottom surface tensile stresses for each case. Forcing full contact between the PCC slab and the base does not significantly alter the predicted maximum PCC bottom surface stresses. However, the analysis of the full contact case is much less computationally demanding than when possible separation is considered. Therefore, analysis of possible separation of the PCC slab from the base is not recommended.

Table 3.2. Effect of separation of PCC slab from base layer on maximum PCC bottom surface stresses.

Base modulus of elasticity, MPa	**Maximum bending stress, MPa**	
	with separation	**without separation**
276	3.23	3.18
2760	3.11	3.11

If the pavement structure employs more than one stabilized base layer, these layers can be combined into a single layer with an equivalent thickness (Ioannides et al. 1992). Regardless of the base type (granular or stabilized), joints should be placed in the base layer at the locations of the joints in the PCC layers.

Axle Loading

It is common to consider only half of an axle in the analysis of critical bending stresses in JPCP (Salsilli et al. 1993, Ioannides 1990). Although this approach does not introduce significant errors in an analysis of critical bending stresses at the bottom surface of PCC slabs, the computed stresses will be more accurate if the entire axle is modeled. Two different loading positions are shown in figure 3.10. Figure 3.11 shows comparison of the maximum PCC bottom surface stresses obtained from a combined effect of 11.1 temperature differential between the top and bottom PCC surfaces and 80-kN single axle load with the stresses obtained from a combined effect of 11.1 temperature differential between the top and bottom PCC surfaces and 40-kN half single axle load. The PCC thickness was varied from 200 to 300 mm. One can observe that, for all cases considered, ignoring of a half of an axle decreases predicted stresses by approximately 5 percent. Therefore, the entire axle should be modeled.

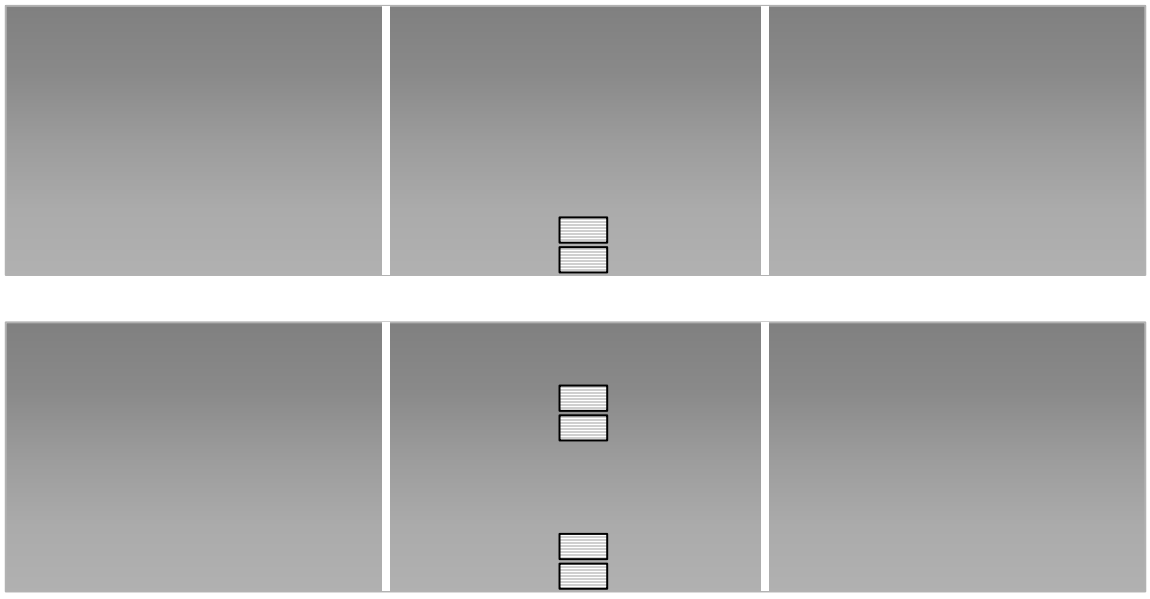

Figure 3.10. Modeling of truck loading using different numbers of wheel loads.

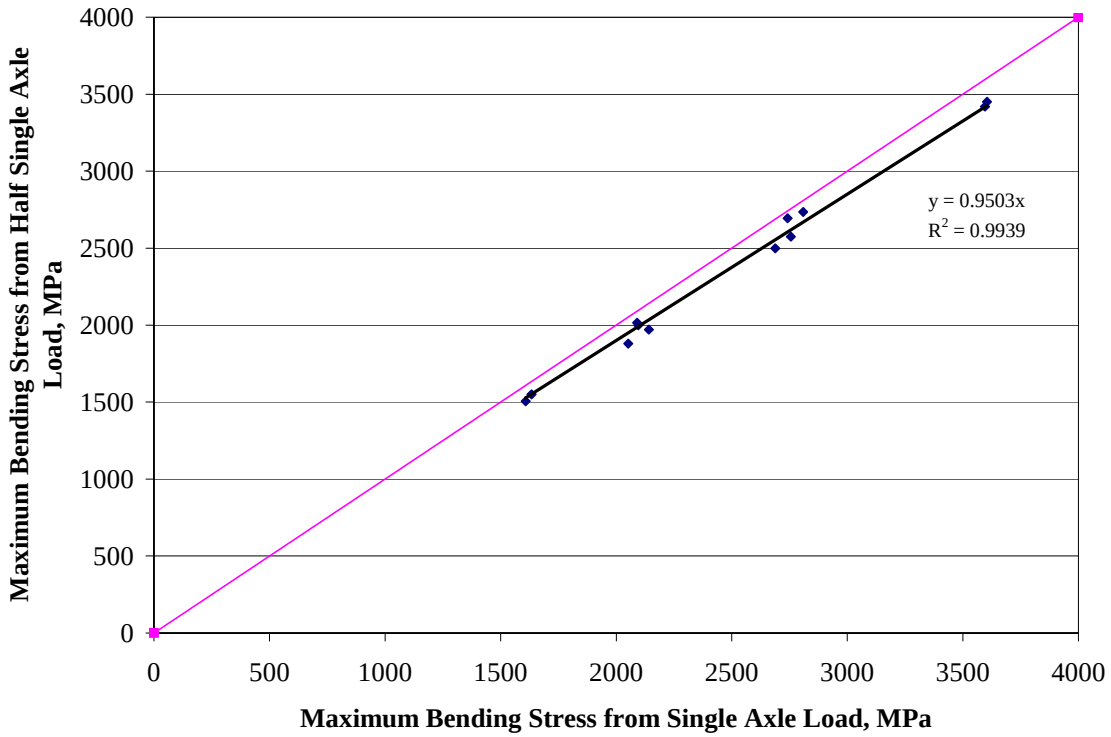

Figure 3.11. Effect of axle modeling on predicted maximum PCC bottom surface tensile stresses surface bending stresses.

Temperature Loading

Only a portion of positive temperature gradients should be considered. The magnitude of the temperature at 11 evenly spaced nodes in the PCC layer for every hour of the available climatic data should be obtained from the ICM program and adjusted for built-in curling and non-uniform shrinkage. For analysis, one may assume that the temperature distribution throughout the depth of each layer is linear. Although the temperature distribution may be nonlinear throughout the slab thickness (Thomlinson 1940, Choubane and Tia 1992), the stresses caused by the nonlinear part may be calculated analytically separately from the finite element model and superposed with the bending stresses obtained from the finite element model, as discussed in chapter 1 of this appendix. A zero temperature differential throughout the base layer may be assumed.

DEVELOPMENT OF RAPID SOLUTIONS FOR PREDICTION CRITICAL PCC BOTTOM SURFACE STRESSES

In spite of the simplifying assumptions presented in the previous section, the JPCP structural model still required up to 30 input parameters:

- PCC thickness
- PCC modulus of elasticity
- PCC Poisson's ratio
- PCC unit weight
- PCC coefficient of thermal expansion

- Base thickness
- Base modulus of elasticity
- Base unit weight
- Base Poisson's ratio
- PCC temperature at 11 evenly spaced nodes in the PCC layer
- Coefficient of subgrade reaction
- Joint spacing
- Load transfer efficiency of a PCC/shoulder joint
- Axle type
- Axle weight
- Tire pressure
- Wheel spacing

Although ISLAB2000 is much more computationally efficient than rival 3D finite element tools, it is not fast enough to allow a "brute force" approach to creating the database of finite element runs for the development of rapid solutions. Indeed, an attempt to run all combinations of all 30 input parameters would require analysis of more than $2x10^{14}$ cases if each parameter is allowed to have just 3 values. Therefore, the researchers explored more efficient approaches.

The most promising way to reduce the number of cases required is to use equivalency concepts. Simply put, these concepts allow the user to obtain solutions for a structural system if a solution for another equivalent structural system is known. This approach significantly reduces the dimension of the problem without introducing any additional error.

In this study, three available equivalent concepts were considered—equivalent thickness, equivalent temperature gradient, and equivalent slab. Based on these, a new concept—the Equivalent JPCP Structure—was developed.

Equivalency Concepts

Equivalent Single Layer Slab Concept

The equivalent single layer slab states that PCC stresses in the two-layered slab can be found from the corresponding stresses in the equivalent homogeneous plate that exhibits the same deflection profile as the in situ pavement (Ioannides et al. 1992). If no friction exists between the PCC and the base layers, and if the equivalent slab has the same modulus of elasticity and Poisson's ratio as the PCC layer, then the thickness of the equivalent slab is defined as follows:

$$h_{eff} = \sqrt[3]{h_{PCC}^3 + \frac{E_{base}}{E_{PCC}} h_{base}^3} \quad , , , , , , , , \quad (3.2)$$

where

h_{eff} = equivalent slab thickness
E_{PCC}= PCC modulus of elasticity
E_{base} = base modulus of elasticity
h_{PCC} = PCC thickness
h_{base} = base thickness

If full bond exists between the PCC and the base layers then the thickness of the equivalent slab is defined as follows:

$$h_{eff} = \sqrt[3]{h_{PCC}^3 + \frac{E_{base}}{E_{PCC}} h_{base}^3 + 12\left(h_{PCC}\left(x - \frac{h_{PCC}}{2} \right)^2 + \frac{E_{base}}{E_{PCC}}\left(h_{PCC} + \frac{h_{base}}{2} - x \right)^2 h_{base} \right)} \quad , (3.3)$$

where

h_{eff} = equivalent slab thickness
E_{PCC}= PCC modulus of elasticity
E_{base} = base modulus of elasticity
h_{PCC} = PCC thickness
h_{base} = base thickness
x = distance between the neutral plane and the top surface of the PCC layer which can be determined from the following equation:

$$x = \frac{\frac{h_{PCC}^2}{2} + \frac{E_{base}}{E_{PCC}} h_{base}\left(h_{PCC} + \frac{h_{base}}{2} \right)}{h_{PCC} + \frac{E_{base}}{E_{PCC}} h_{base}} \quad , , , , , , , , (3.4)$$

If a JPCP is subjected to an axle loading only (no curling), and if the stresses in the equivalent slab are known, then the corresponding PCC stresses at the bottom of the PCC slab can be found using the following relationship:

- Unbonded interface

$$\sigma_{PCC} = \frac{h_{pcc}}{h_e} \sigma_{eff} \quad , , , , , , , , (3.5)$$

- Bonded interface

$$\sigma_{PCC} = \frac{2\left(h_{PCC} - x\right)}{h_e} \sigma_{eff} \quad , , , , , , , , (3.6)$$

where

σ_{eff} = bottom surface stresses in the equivalent slab
σ_{PCC} = bottom surface PCC stresses
h_{PCC} = PCC thickness
h_{eff} = equivalent slab thickness
x = distance between the neural plane and the top surface of the PCC layer

Equivalent Linear Temperature Distribution Concept

The equivalent temperature gradient concept for a single-layer slab was introduced by Thomlinson (1940) and was further developed by other researchers (Choubane and Tia 1992, Mohamed and Hansen 1997). The concept was later generalized for a non-uniform, multi-layered slab (Khazanovich 1994, Ioannides and Khazanovich 1998). This concept states that if two slabs have the same plane-view geometry, flexural stiffness, self-weight, boundary conditions, and applied pressure, and rest on the same foundation, then these slabs have the same deflection and bending moments distributions if their through-the-thickness temperature distributions satisfy the following condition:

$$\int_{h_a} E_a(z)\alpha_a(z)(T_a(z)-T_{0,a})zdz = \int_{h_b} E_b(z)\alpha_b(z)(T_b(z)-T_{0,b})zdz \quad ,,,, (3.7)$$

where

a and b = subscripts denoting two slabs
z = distance from the neutral axis
T_0 = the temperatures at which theses slabs are assumed to be flat.
α = coefficient of thermal expansion
E = modulus of elasticity
h = slab thickness,

To apply this concept for the curling analysis of a two-layered system, the temperature distribution throughout the two-layered slab thickness should be split into its three components:

- The part that causes constant strain throughout-the-slab-thickness strain.
- The part that causes strain linear throughout-the-slab-thickness strain.
- The part that causes nonlinear strain.

The constant strain component has the following form:

- Unbonded interface

$$T_{c,PCC} = \frac{1}{h_{PCC}} \int_{-\frac{h_{PCC}}{2}}^{\frac{h_{PCC}}{2}} T(z)dz$$

$$T_{c,base} = \frac{1}{h_{base}} \int_{\frac{h_{PCC}}{2}}^{\frac{h_{PCC}}{2}+h_{base}} (T(z)zdz \quad ,,,, (3.8)$$

- Bonded interface

$$T_c(z) = T_0 + \frac{\int_{-x}^{h_{PCC}-x} \alpha_{PCC}E_{PCC}(T(z)-T_0)dz + \int_{h_{PCC}-x}^{h_{PCC}+h_{base}-x} \alpha_{base}E_{base}(T(z)-T_0)dz}{\alpha(z)\left(E_{PCC}h_{PCC} + E_{base}h_{base}\right)} \quad ,,, (3.9)$$

where

h_{PCC} = PCC slab thickness.
H_{base} = base thickness.
h_{eff} = Effective slab thickness computed.
T_0 = the temperatures at which theses slabs are assumed to be flat.
T_c = the constant strain temperature component
T(z) temperatures distribution through the PCC and base layers.
z = vertical coordinate measured downward from the neutral axis of the PCC slab (unbonded interface) or the composite slab (bonded interface)

The linear strain-causing component has the following form:

- Unbonded interface

$$T_{L,PCC}(z) = T_0 + 12S\frac{z}{\alpha_{PCC}}$$

$$T_{L,base}(z) = T_0 + 12S\frac{z - \frac{h_{PCC} + h_{base}}{2}}{\alpha_{base}}$$

$$S = \frac{\int_{-\frac{h_{PCC}}{2}}^{\frac{h_{PCC}}{2}} \alpha_{PCC} E_{PCC}(T(z) - T_0) z dz + \int_{-\frac{h_{base}}{2}}^{\frac{h_{base}}{2}} \alpha_{base} E_{base}(T(\frac{h_{PCC} + h_{base}}{2} + \zeta) - T_0)\zeta d\zeta}{E_{PCC} h_{PCC}^3 + E_{base} h_{base}^3} \quad (3.10)$$

- Bonded interface

$$T_L(z) = T_0 + \frac{12z}{\alpha(z)} \frac{\int_{-x}^{h_{PCC}-x} \alpha_{PCC} E_{PCC}(T(z) - T_0) z dz + \int_{h_{PCC}-x}^{h_{PCC}+h_{base}-x} \alpha_{base} E_{base}(T(z) - T_0) z dz}{E_{PCC} h_{PCC}^3 + E_{base} h_{base}^3 + 12\left(E_{PCC} h_{PCC}\left(x - \frac{h_{PCC}}{2}\right)^2 + E_{base}\left(h_{PCC} + \frac{h_{base}}{2} - x\right)^2 h_{base}\right)}$$

(3.11)

where

h_{PCC} = PCC slab thickness.
H_{base} = base thickness.
h_{eff} = effective slab thickness computed.
T_0 = the temperatures at which theses slabs are assumed to be flat.
T_L = the linear strain temperature component
T(z) temperatures distribution through the PCC and base layers.
z = vertical coordinate measured downward from the neutral axis of the PCC slab (unbonded interface) or the composite slab (bonded interface)

$$\zeta = z - \frac{h_{PCC} + h_{base}}{2}$$

Finally, the nonlinear strain-causing component of the temperature distribution is that portion that causes the reminder of the horizontal strains in the plate. Thus, it should satisfy the following equality:

$$T_{NL}(z) = T(z) - T_c(z) - T_L(z) - 2T_0 \text{, , , , } (3.12)$$

where

T_c = the linear strain temperature component
T_L = the constant strain temperature component
T_0 = the temperatures at which theses slabs are assumed to be flat.
T(z) temperatures distribution through the PCC and base layers.
z = vertical coordinate measured downward from the neutral axis of the PCC slab (unbonded interface) or the composite slab (bonded interface)

The constant strain temperature component does not cause any stresses in the PCC slab and the base layer if they are not restrained from the horizontal movement. The nonlinear strain component of the temperature distribution induces the following stresses:

$$\sigma_{NL}(z) = -\frac{E(z)}{1-\mu}\alpha(z)\left(T_N(z) - T_0\right), , , , , , , , (3.13)$$

where

σ_{NL} - stress caused by the nonlinear strain component of the temperature distribution.

The stresses in the two-layered slab caused by the linear strain temperature component and axle loadings can be found from the analysis of an equivalent single-layer slab. This equivalent slab should have the same geometry and self-weight, its thickness should is determined by equation 3.2 or 3.3, and the slab should be subjected to the same axle loading, the equivalent linear temperature distribution causing the same bending moment distributions in the equivalent and the original slabs.

To ensure equality of the self-weight of the original and equivalent slabs, the unit weight of the equivalent slab is defined as follows;

$$\gamma_{eff} = \frac{h_{PCC}\gamma_{PCC} + h_{base}\gamma_{base}}{h_{eff}} \qquad (3.14)$$

where

γ_{eff} = unit weight of the effective slab

γ_{PCC} = unit weight of the PCC slab

γ_{base} = unit weight of the base layer

h_{PCC} = PCC slab thickness.

H_{base} = base thickness.

h_{eff} = Effective slab thickness computed.

The following linear temperature distribution in the equivalent slab defined by the difference in temperatures at the top and bottom surfaces causes the same bending moment distributions in the equivalent single-layer slab and in the original composite slab:

- Unbonded interface

$$\Delta T_{eff} = \frac{12}{h_{eff}^2} * \left(\int_{-\frac{h_{PCC}}{2}}^{\frac{h_{PCC}}{2}} (T(z) - T_0) z dz + \frac{\alpha_{base}E_{base}}{\alpha_{PCC}E_{PCC}} \int_{-\frac{h_{base}}{2}}^{\frac{h_{base}}{2}} (T(\frac{h_{PCC} + h_{base}}{2} + \zeta) - T_0)\zeta d\zeta \right) \qquad (3.15)$$

- Bonded interface

$$\Delta T_{eff} = \frac{12}{h_{eff}^2} * \left(\int_{-x}^{h_{PCC}-x} (T(z) - T_0) z dz + \frac{\alpha_{base}E_{base}}{\alpha_{PCC}E_{PCC}} \int_{h_{PCC}-x}^{h_{PCC}+h_{base}-x} (T(z) - T_0) z dz \right) \qquad (3.16)$$

where

ΔT_{eff} = difference between temperatures at the top and bottom surfaces of the effective slab.

h_{PCC} = PCC slab thickness.

H_{base} = base thickness.

h_{eff} = effective slab thickness computed.

T(z) temperatures distribution through the PCC and base layers.

z = vertical coordinate measured downward from the neutral axis of the PCC slab (unbonded interface) or the composite slab (bonded interface)

Since it was assumed that the coefficient of thermal expansion of the PCC slab is equal to the coefficient of thermal expansion of the base layer, the value T_0 is unimportant. For simplicity of derivations, it was assumed equal to the temperature at the bottom surface of the PCC slab. Since it was also assumed that the temperature thought the base layer is equal to the temperature at the bottom surface of the PCC slab, equations 3.10 and 3.11 can be re-written in the following form:

- Unbonded interface

$$\Delta T_{eff} = \frac{12}{h_{eff}^2} * \int_{-\frac{h_{PCC}}{2}}^{\frac{h_{PCC}}{2}} (T(z) - T(\frac{h_{PCC}}{2}))zdz \qquad (3.17)$$

- Bonded interface

$$\Delta T_{eff} = \frac{12}{h_{eff}^2} * \int_{-x}^{h_{PCC}-x} (T(z) - T(h_{PCC} - x))zdz \qquad (3.18)$$

ΔT_{eff} = difference between temperatures at the top and bottom surfaces of the effective slab.
h_{PCC} = PCC slab thickness.
H_{base} = base thickness.
h_{eff} = Effective slab thickness computed.
T(z) temperatures distribution through the PCC and base layers.
z = vertical coordinate measured downward from the neutral axis of the PCC slab (unbonded interface) or the composite slab (bonded interface)

$$\zeta = z - h_1 - \frac{h_2}{2}$$

Since the temperature distribution is known in 11 points, integrals in equations 3.17 and 3.18 were evaluated numerically which resulted in the following expressions:

$$\Delta T_{eff} = \frac{12}{h_{eff}^2} * \frac{h_{PCC}}{60} \sum_{i=1}^{10} \left(T_i * \left((3*i-17) * \frac{h_{PCC}}{10} \right) + T_{i+1} \left((3*i-16) * \frac{h_{PCC}}{10} \right) \right) \qquad (3.19)$$

- Bonded interface

$$\Delta T_{eff} = \frac{12}{h_{eff}^2} * \frac{h_{PCC}}{60} \sum_{i=1}^{10} \left(T_i * \left((3*i-2) * \frac{h_{PCC}}{10} - 3*x \right) + T_{i+1} \left((3*i-1) * \frac{h_{PCC}}{10} - 3*x \right) \right) - \frac{T_{11}}{2} h_{PCC} * (h_{PCC} - 2x) \qquad (3.20)$$

where

$T_1, T_2, \ldots, T_{11}$ are PCC temperatures at equal spaced points. T_1 is PCC temperature at the top surface and T_{11} is PCC temperature at the bottom surface.
ΔT_{eff} = difference between temperatures at the top and bottom surfaces of the effective slab.
h_{PCC} = PCC slab thickness.
h_{eff} = Effective slab thickness computed.
x = distance between the neural plane and the top surface of the PCC layer

The bottom surface PCC stress caused by the linear strain temperature can be found from the stress in the equivalent slab using the following relationship:

- Unbonded interface

$$\sigma_{PCC,L} = \frac{h_{pcc}}{h_{eff}}\sigma_{eff} \qquad (3.21)$$

- Bonded interface

$$\sigma_{PCC,L} = \frac{2(h_{PCC} - x)}{h_{eff}}\sigma_{eff} \qquad (3.22)$$

where

σ_{eff} = bottom surface stresses in the equivalent slab

σ_{PCC} = bottom surface PCC stresses

h_{PCC} = PCC thickness

h_{eff} = equivalent slab thickness

x = distance between the neural plane and the top surface of the PCC layer

Stresses at the bottom of the PCC slab caused by the nonlinear strain component were evaluated numerically using the following expressions:

- Unbonded interface

$$\sigma_{PCC,NL} = -E_{PCC}\alpha_{PCC}\left(\frac{\Delta T_{eff}}{2h_{eff}}h_{PCC} - \frac{\sum_{i=1}^{10} T_i}{10} + \frac{T_1}{20} + \frac{21T_{11}}{20}\right) \qquad (3.23)$$

- Bonded interface

$$\sigma_{PCC,NL} = -\frac{E_{PCC}\alpha_{PCC}}{1-\mu_{PCC}}\left(\frac{\Delta T_{eff}}{h_{eff}}(h_{PCC} - x) - \frac{h_{PCC}}{h_{PCC} + \frac{E_{base}}{E_{PCC}}h_{base}}\left(\frac{\sum_{i=1}^{10} T_i}{10} - \frac{T_1}{20} - \frac{21T_{11}}{20}\right)\right) \qquad (3.24)$$

The single layer slab and equivalent linear temperature distribution concept relates solutions for the slabs with the same geometry and self-weight. Indeed, stresses from an arbitrary temperature distribution in a two-layered slab can be computed as a sum of the stresses caused by the non-linear strain component and a linear strain component. The latter can be computed from the stresses in the equivalent slab. Another concept utilized in this study is applicable to the slabs with different dimensions. This concept is presented next.

Korenev's Equivalent Slab Concept

Korenev and Chernigovskaya (1962) obtained the equivalency concept from analyzing the load and temperature curling stresses in a circular slab resting on a Winkler foundation. They found that, for a given geometry of the applied load, the combined load and curling stress at any point in the circular slab can be obtained from the following relationship:

$$\sigma_{comb}(\xi) = \frac{6\,\gamma\,\ell^2}{h} M^*\left(\frac{P}{Q}, \frac{L}{\ell}, \phi^*, \xi\right) \quad (3.25)$$

where

ξ = r/L

=, normalized radial distance

r = radial distance measured from the center of the slab

L = slab radius

γ = slab's unit self weight

h = plate thickness

ℓ = radius of relative stiffness of the plate-subgrade system for the dense liquid foundation

$= (D/k)^{1/4}$

$D = Eh3/(12(1-\mu^2))$

= flexural rigidity of the plate

E = plate elastic modulus

μ= plate Poisson's ratio

k = modulus of subgrade reaction

M* = nondimensional moment distribution

P = total applied load

Q = total self weight of the slab

φ = Korenev's nondimensional temperature gradient defined as

$$\phi = \frac{2\,\alpha\,(1+\mu)\,\ell^2}{h^2}\frac{k}{\gamma}\Delta T \quad (3.26)$$

α = coefficient of thermal expansion

ΔT = temperature difference through the slab

An important point to note is that Korenev's temperature gradient, ϕ^*, combines many factors that affect curling stresses into one parameter. Also, analysis of Korenev and Chernigovskaya's solution shows that the bending moment distribution and, therefore, stress in the slab, depends on the following three nondimensional parameters:

- Ratio of the total applied load to the slab self-weight, P/Q.
- Ratio of the slab characteristic dimension to the radius of relative stiffness, L/ℓ.
- Korenev's nondimensional temperature gradient, ϕ.

This leads to Korenev's equivalency concept that if two circular slabs with the same , L/ℓ ratio are subjected to the same Korenev's nondimensional gradient, and the ratios between the applied load and slab's self-weight (P/Q) are equal, then the stress distributions in these slabs are related as follows:

$$\sigma_{comb,2}(\xi) = \frac{h_1\,\gamma_2\,\ell_2^2}{h_2\,\gamma_1\,\ell_1^2}\sigma_{comb,1}(\xi) \quad (3.27)$$

where subscripts 1 and 2 denote the parameters of the first and second slab, respectively. This concept implies that the temperature stresses in a PCC slab of known dimensions, properties, and temperature gradient can be related to those in another slab, so long as the L/ℓ and P/Q ratios of

those slabs are the same and the slabs are subjected to the same Korenev's nondimensional temperature gradient.

Korenev's was modified for analysis of rectangular slab. It was found that bottom surface stresses in two single layer slab systems are directly related if the following conditions are satisfied:

$$\ell_1 = \ell_2 \qquad (3.28)$$

$$L_1 = L_2 \qquad (3.29)$$

$$\phi_1 = \phi_2 \qquad (3.30)$$

$$\frac{AGG_1}{k_1 \ell_1} = \frac{AGG_2}{k_2 \ell_2} \qquad (3.31)$$

$$\frac{P_1}{h_1 \gamma_1} = \frac{P_2}{h_2 \gamma_2} \qquad (3.32)$$

$$s_1 = s_2 \qquad (3.33)$$

where

ℓ = radius of relative stiffness, in.
L =joint spacing
ϕ = Korenev's nondimensional temperature gradient
AGG = aggregate interlock between the main lane and the shoulder
P =axle weight
γ =PCC slab unit weight
h = PCC thickness
s = distance between slab edge and outer wheel edge

and subscripts 1 and 2 denote slabs 1 and 2, respectively.

If conditions (3.28) through (3.33) are satisfied and tire footprint configurations are the same for both cases, then the stresses in a two-layered slab 1 can be found from the stress in a single layer slab 2 using the relationship in equation 3.27.

Model Simplification

To further simplify structural model, several series of ISLAB2000 runs were performed. A variety of pavement systems with different joint spacing, PCC slab thickness, coefficient of subgrade reaction, and so on were analyzed. For each pavement system, the following loading scenarios were considered:

- Axle loading only (no temperature curling). The axle load was applied at the mid-span of the slab near slab edge.
- Linear temperature distribution thought the slab thickness (no axle loading).
- Combined axle and temperature loading

The following observations were based on the results of the ISLAB2000 runs:

- There is an interaction between axle and temperature loadings so stresses from axle loading and temperature curling cannot be simply superimposed.

- Transverse joint spacing has a significant effect on PCC curling stresses and PCC stresses from combined axle and temperature loading but does not affect mid-slab edge stresses PCC stresses from axle loading only.
- The magnitude of LTE between the PCC slab and the shoulder does not affect PCC curling stresses, but affects PCC stresses from axle loading and from combined axle and temperature loading.
- Tire footprint geometry affects PCC stresses from axle loading and from combined axle and temperature loading, but does not affect the difference between the PCC stresses from combined axle and temperature loading and from axle loading.

Based on these observations, it was proposed to present stresses in the multi-slab system (figure 3.12-a) as a combination of stresses obtained from the analysis of the following two systems:

- A single slab (system A)
- A two-slab system (system B)

System A (see figure 3.12-b) is used for the slab curling analysis. It has the following characteristics:

- Slab length is equal to the transverse joint spacing in the original system.
- Slab width is equal to the slab width of the truck lane in the original system.
- Slab thickness is equal to the slab thickness of the original system.
- Slab modulus of elasticity, slab unit weight, and slab coefficient of thermal expansion are equal to the corresponding characteristics of thy slab thickness of the original system.
- Three regimes of loading are considered:
  - Temperature curling only.
  - Combined action of temperature curling and axle loading.
  - Axle loading only.

The axle loading has is of the same axle type and axle weight as the axle loading of the original system. The load is applied at the same location as the original system (at the center of the slab and the same distance form the longitudinal edge), however tire footprint geometry may be different. In system A, loading all tire footprints were squares 7 by 7 in.

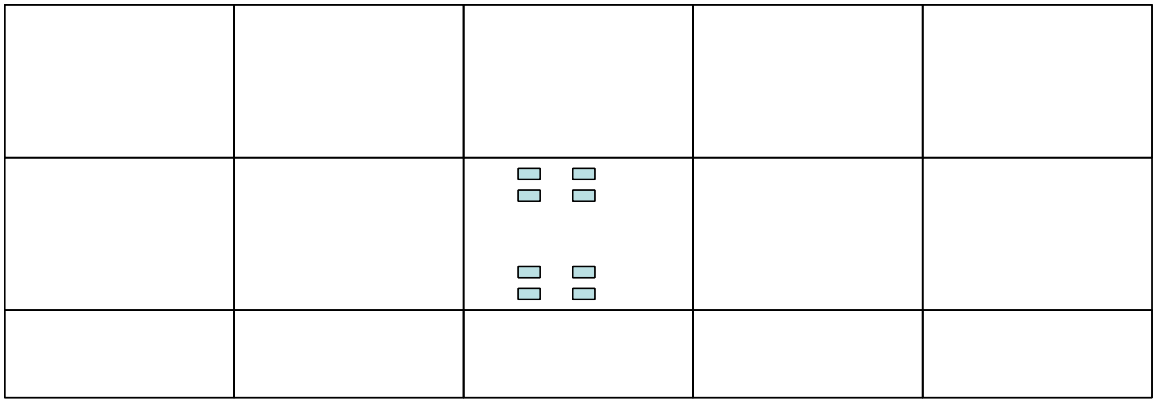

a. Original system

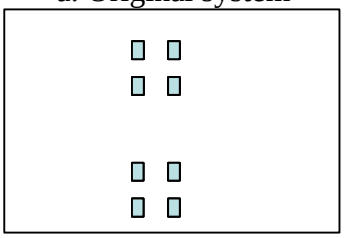

b. System A.

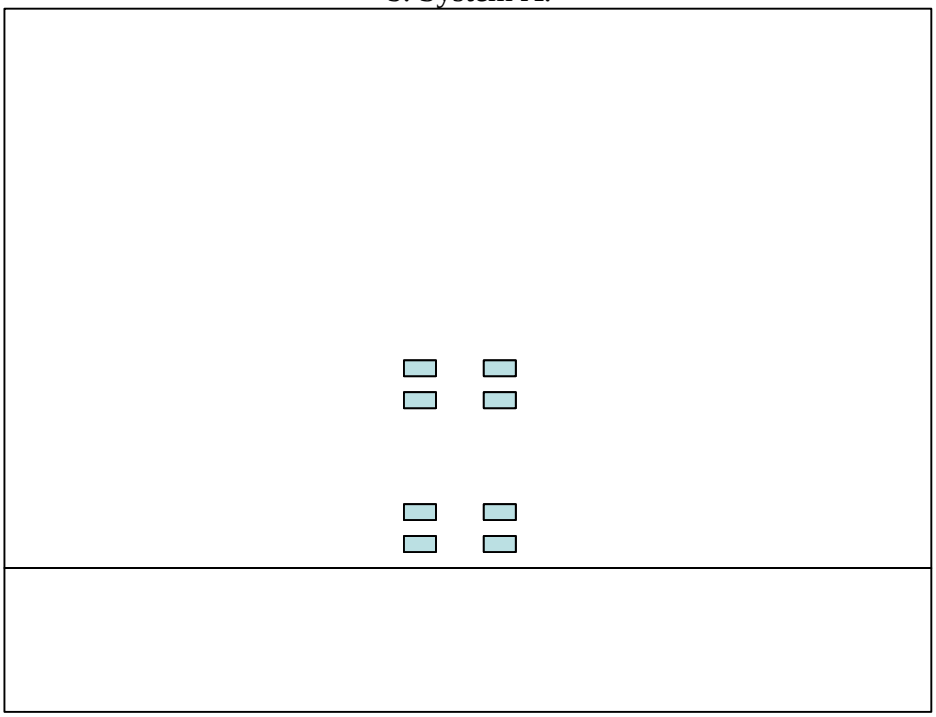

c. System B.

Figure 3.12. Substitution of the original multi-slab system by a combination of two simpler systems.

System B (see figure 3.12-c) is used for accounting for the effect of tire footprint geometry and the effect of shoulder support. It has the following characteristics:

- Slab length is sufficiently large to ignore the slab size effect.
- Slab width is equal to the slab width of the truck lane in the original system.

- Slab thickness is equal to the slab thickness of the original system.
- Slab modulus of elasticity, is equal to the corresponding characteristics of thy slab thickness of the original system.
- Two cases of the deflection LTE between the slabs are considered:
  - The deflection LTE is equal to 0.
  - The deflection LTE is equal to deflection load transfer efficiency between the PCC slab and the shoulder of the original system.
- Only axle loading (no temperature curling) is considered for this system. The axle loading has the same axle type, axle weight, and footprint geometry. The load is applied at the same form the longitudinal edge as the load in the original system.

Denote as $\sigma^A\ (P, \Delta T)$ stresses in the system A from the axle load P and temperature difference ΔT and denote $\sigma^B\ (LTE)$ stresses in the system B from the axle load P and with the deflection load transfer efficiency LTE. The following procedure was used to obtain stresses in the original system from stresses in the systems A and B:

Step 1. Find curling component of bending stresses. i.e. stress in the slab if no axle loading is present.

$$\sigma_{curl} = \sigma^A_{bot}\ (0, \Delta T) \quad (3.34)$$

Step 2. Find axle loading induced component of bending stresses (stress in the slab caused by the action of axle loading on top of the temperature curling) if the shoulder provides no edge support to the traffic lane slab.

$$\sigma_{load,no\,shoulder} = \sigma^A\ (P, \Delta T) - \sigma^A\ (0, \Delta T) - \sigma^A\ (P, 0) + \sigma^B\ (0) \quad (3.35)$$

Step 3. Find stress load transfer efficiency for the given axle load configuration and the axle load position.

$$LTE_{stress} = \sigma^B\ (LTE) \quad (3.36)$$

Step 4. Find axle loading induced component of bending stresses (stress in the slab caused by the action of axle loading on top of the temperature curling) accounting for the shoulder edge support to the traffic lane slab.

$$\sigma_{load,shoulder} = \sigma_{load,no\,shoulder} * LTE_{stress} \quad (3.37)$$

Step 5. Find combined stress in the original system.

$$\sigma_{comb} = \sigma_{load,shoulder} + \sigma_{curl} \quad (3.38)$$

To verify this approach, a factorial of finite element runs with different PCC slab parameters, axle weights, temperature gradients, and load transfer efficiency between the PCC slab and the shoulder was performed. The stresses calculated using the approach presented above were compared with stresses obtained from the finite element models accounting for a shoulder directly. The results of this analysis are shown on figure 3.13. An excellent correlation is observed between the two methods.

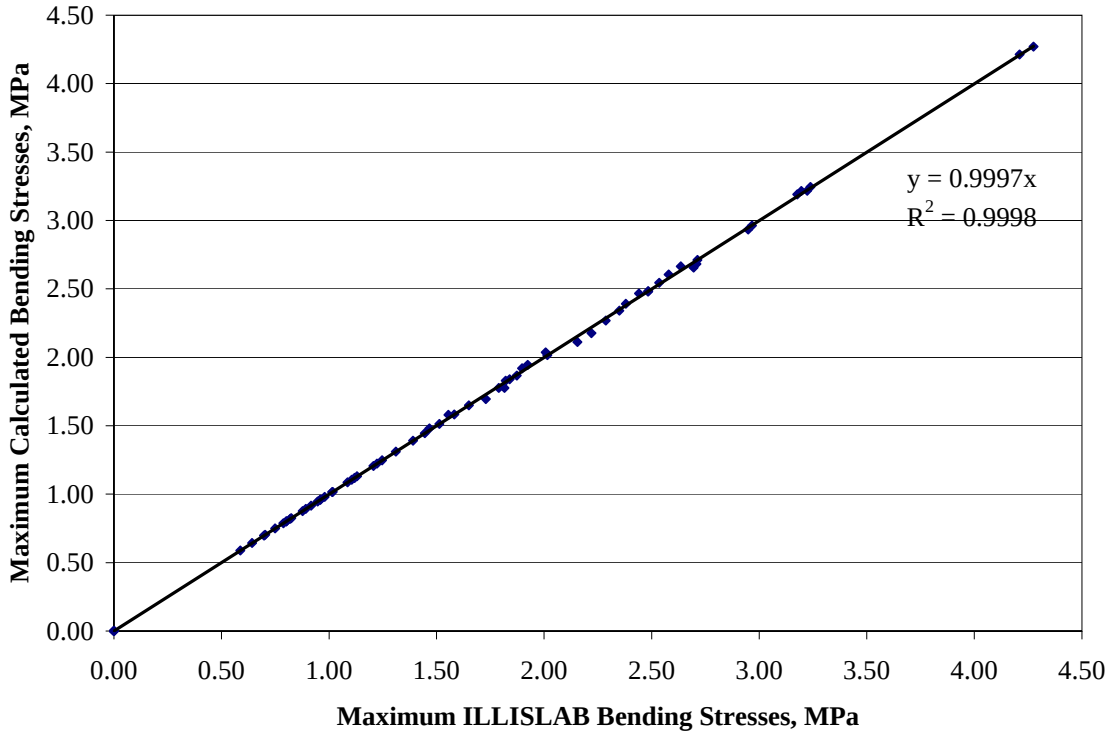

Figure 3.13. Verification of shoulder accounting procedure.

NN Development

The equivalency concepts and the model simplification procedure presented above allow the reduction of number of independent parameters and reduction of the number of cases needed to be considered for successful training of the neural networks for rapid prediction of critical PCC stresses at the bottom of the PCC slab. The following neural networks were developed in this study:

- NNA1 - for prediction of the maximum edge stresses at the bottom of a single slab subjected to a temperature curling and a single axle loading (see figure 3.14).
- NNA2 - for prediction of the maximum edge stresses at the bottom of a single slab subjected to a temperature curling and a tandem axle loading-NNA1 (see figure 3.15).
- NNB1 - for prediction of the maximum stresses at the bottom of a two-slab system (system B) subjected to a single axle single wheel loading (see figure 3.16).
- NNB2 - for prediction of the maximum stresses at the bottom of a two-slab system (system B) subjected to a single wheel loading (see figure 3.17).

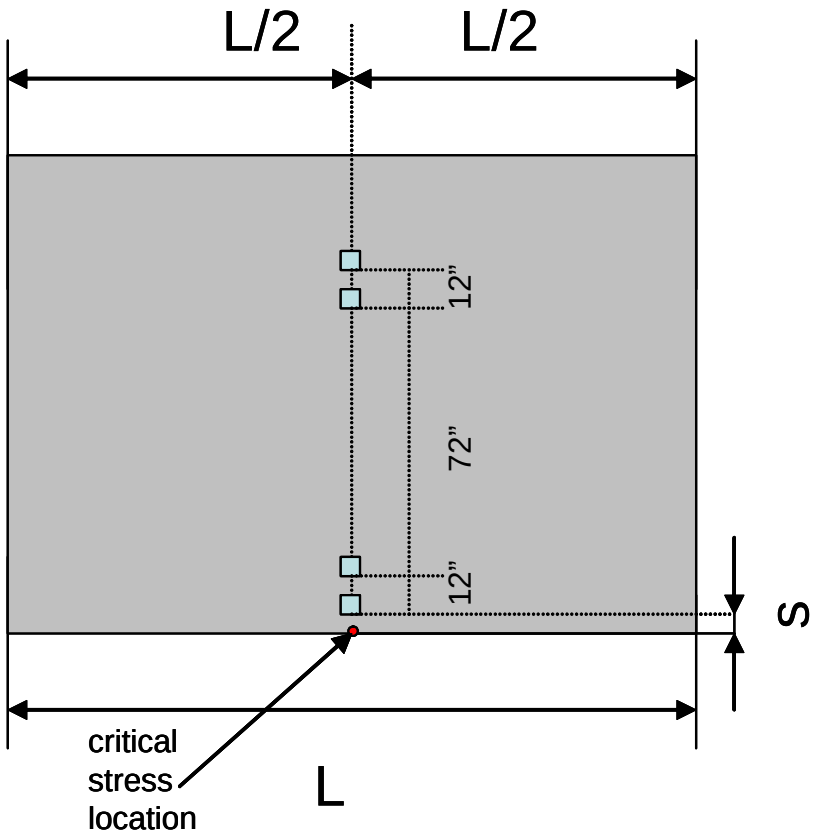

Figure 3.14. Structural model for the NNA1.

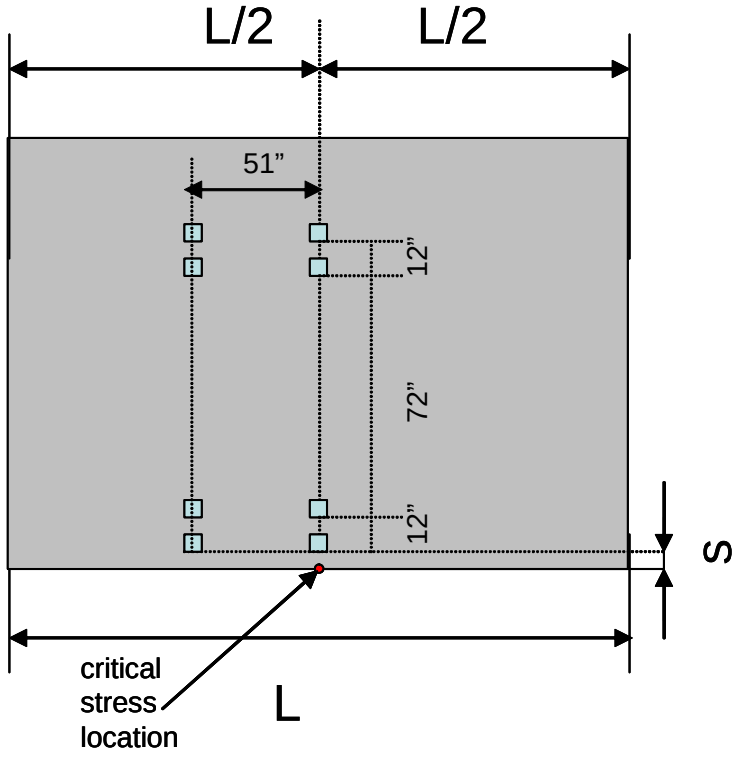

Figure 3.15. Structural model for the NNA2.

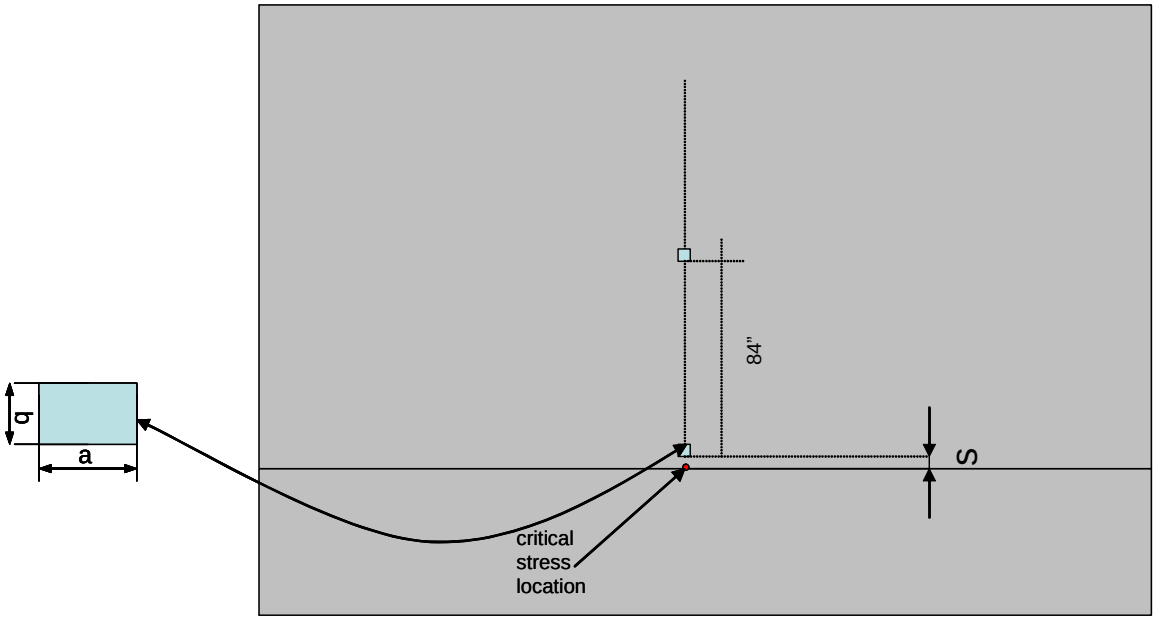

Figure 3.16. Structural model for the NNB1.

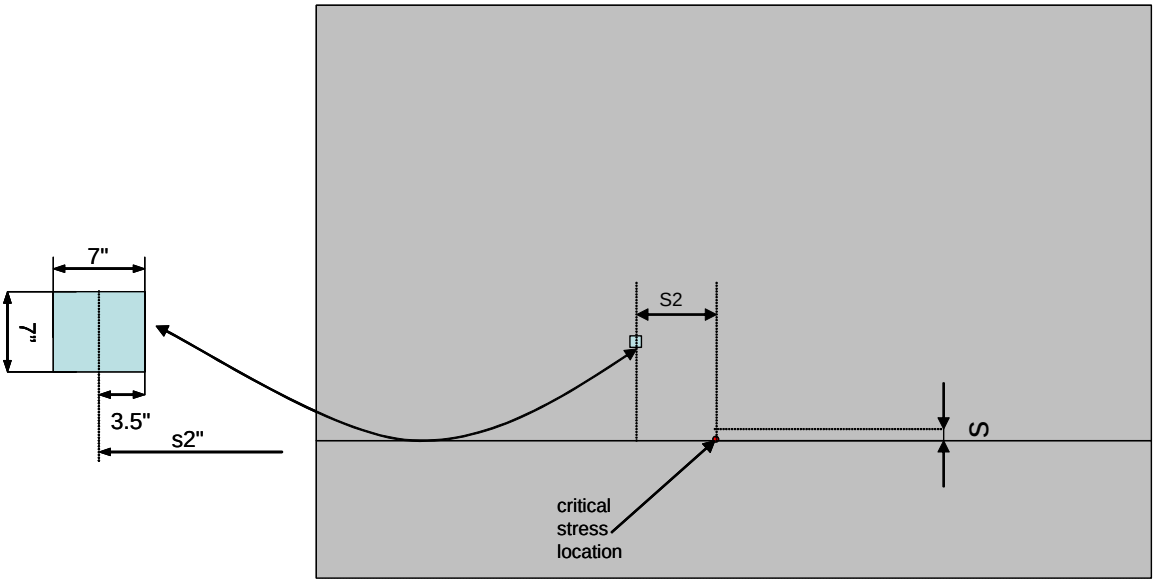

Figure 3.17. Structural model for the NNB2.

Two factorials of 14175 ISLAB2000 runs each were performed to create training databases for the NNA1 and NNA2. A single-layer slab was analyzed in all cases. The slab width, modulus of elasticity, Poisson's ratio, unit weight, and coefficient of thermal expansion were set equal to 12 ft, 4,000,000 psi, 0.15, 0.087 lb/in^3, and 5.5*10^{-6} 1/^{o}F, respectively. Each tire footprint was modeled using a square with a 7-in side. The coefficient of subgrade reaction was set equal to 100 psi/in. The following parameters were varied:

- Slab length. Slab lengths of 9, 15, 21, 27, and 33 ft were analyzed.
- L/ℓ ratios. L/ℓ ratios of 1.5, 3.5, 4.5, 5.5, 6.5, 7.5, 9.5, 12, and 14.5 were analyzed. To achieve it, the PCC slab thickness was varied 1 in to 112 in.
- Wheel offset was varied from 0 to 36 in (0, 2, 4, 6, 12, 24, and 36 in).

- Korenev's non-dimensional temperature gradient was varied from 0 to 200 (0, 5, 10, 15, 20, 25, 50, 100, and 200).
- Axle weight was varied to set the axle weight to slab weight ratio equal to 0, 1, 2, 3 or 4.

Since some of the ranges above are presented in terms of normalized or dimensionless parameters, it makes it somewhat difficult to understand the ranges of applicability of the database. To illustrate it in terms of real inputs, a baseline case was selected and one parameter at time was allowed to vary. Table 3.3 presents the baseline parameters and calculated ranges for those parameters.

Table 3.3. Ranges of NNA1 and NNA2 parameters if others are equal to the baseline values.

Variable	Baseline value	Min value	Max value
PCC thickness, in	9	5.1	27.7
PCC modulus of elasticity, psi	4,500,000	154,000	24,6170,950
Base , in	6	0	>30
Base modulus of elasticity, psi	40,000	0	>10,000,000
PCC coefficient of thermal expansion	5.50E-06	0	5.50E-05
PCC unit weight, lb/in^3	0.087	0	0.87
k-value, psi/in	200	7	1094
Temperature differential, ^{o}F	10	0	>100
Axle weight, lb	18,000-NNA1	0	>60,000
	34,000 – NNA2	0	>120,000

To train the third NN, NNB1, a factorial of 24300 ISLAB2000 runs was performed. A single-layer slab was analyzed in all cases. The slab width, modulus of elasticity, Poisson's ratio, unit weight, and coefficient of thermal expansion were set equal to 24 ft, 4,000,000 psi, 0.15, 0.087 lb/in^3, and 5.5*10^{-6} 1/^{o}F, respectively. An axle load consisted from two wheels with spacing equal to 84 in. The tire pressure was set to be equal to 100 psi. The coefficient of subgrade reaction was set equal to 100 psi/in. The following parameters were varied:

- Slab/shoulder deflection LTE. The deflection LTEs of 0.01, 25, 50, 75, and 90 percent were analyzed.
- Wheel offset was varied from 0 to 36 in (0, 2, 4, 6, 12, 18, 24, 36, and 60 in).
- A wheel width, b, was set to be equal to 3, 7, 9, 11, 13, or 15 in.
- A wheel width-to-length ratio was set to be equal to 0.1, 0.25, 0.4, 0.5, 1, or 2.
- The slab thickness was varied from 2.5 to 24 in (2.5, 3, 4, 4.5, 5, 5.5, 6, 7, 8, 10, 12, 14, 16, 20, and 24).

Table 3.4 presents the baseline parameters and calculated ranges for those parameters when a baseline case was selected and one parameter at time was allowed to vary.

Table 3.4. Ranges of NNB1 parameters if others are equal to the baseline values.

Variable	Baseline value	Min value	Max value
PCC thickness, in	9	5.1	27.7
PCC modulus of elasticity, psi	4,500,000	154,000	24,6170,950
Base , in	6	0	>30
Base modulus of elasticity, psi	40,000	0	>10,000,000
PCC coefficient of thermal expansion	5.50E-06	0	5.50E-05
PCC unit weight, lb/in^3	0.087	0	0.87
k-value, psi/in	200	7	1094
Axle weight, lb	18,000	0	>60,000

To train the fourth NN, NNB2, a factorial of 910 ISLAB2000 runs was performed. A single-layer slab was analyzed in all cases. The slab width, modulus of elasticity, and Poisson's ratio were set to be equal to 24 ft, 4,000,000 psi, 0.15, 0.087 lb/in^3, and $5.5*10^{-6}$ $1/^oF$, respectively. An axle load consisted from two wheels with spacing equal to 84 in. The tire pressure was set to be equal to 100 psi. The coefficient of subgrade reaction was set equal to 100 psi/in. The following parameters were varied:

- Slab/shoulder deflection LTE. The deflection LTEs of 0.01, 25, 50, 75, and 90 percent were analyzed.
- Wheel offset in transverse direction was varied from 0 to 168 in (0, 18, 30, 42, 54, 66, 78, 90, 102, 114, 126, 138, 150 and 168 in).
- Wheel offset in longitudinal direction was varied from 39.5 to 69.5 in (39.5, 48.5, 54.5, 60.5, and 69.5 in).
- The slab thickness was varied from 2.5 to 24 in (2.5, 3, 4, 4.5, 5, 5.5, 6, 7, 8, 10, 12, 14, 16, 20, and 24).

A modified MS-HARP neural network architecture was employed (Banan and Hjelmstad 1994, Khazanovich and Roesler 1997). Selection of this particular architecture was driven primarily by familiarity with this technique and convenience in the NN training. However, conventional backpropagation NNs could be implemented as well.

Step-By-Step Procedure for Determination of Critical Bottom Surface Stress in JPCP

Using the trained NN, JPCP stresses can be determined for a wide range of site conditions, design parameters, and axle loading. The detailed procedure is described below.

Step 1. Calculate the Equivalent Slab Thickness

If a PCC slab is not bonded with the base layer then the equivalent slab thickness is determined using equation 3.2; otherwise it is determined using equation 3.3.

Step 2. Calculate Unit Weight of the Equivalent Slab

$$\gamma_{eff} = \frac{\gamma_{PCC} h_{PCC}}{h_{eff}} \qquad (3.39)$$

where

γ_{eff} = effective unit weight
h_{PCC} = PCC slab thickness
$\gamma_{PCC.}$ = PCC unit weight
h_{eff} = effective thickness

Step 3. Calculate Radius of Relative Stiffness

$$\ell = \sqrt[4]{\frac{E_{PCC} h^3_{eff}}{12*(1-\mu^2_{eff})*k}} \qquad (3.40)$$

where

ℓ = radius of relative stiffness
h_{eff} = effective thickness
E_{PCC} = PCC elastic modulus
μ_{PCC} = PCC Poisson's ratio
k = coefficient of subgrade reaction

Step 4. Calculate Effective Temperature Differential

Equivalent temperature difference is determined from equation 3.17 if the interface between the PCC slab and the base is unbonded and from equation 3.18 if the interface between the PCC slab and the base is bonded.

Step 5. Compute Korenev's Nondimensional Temperature Gradient

$$\phi = \frac{2\alpha_{PCC}(1+\mu_{PCC})\ell^2}{h_{eff}^{\ 2}} \frac{k}{\gamma_{eff}} \Delta T_{eff} \qquad (3.41)$$

where

ϕ= nondimensional temperature gradient
h_{PCC} = PCC slab thickness
α_{PCC} = PCC coefficient of thermal expansion
μ_{PCC} = Poisson's ratio for PCC
γ_{eff} = effective unit weight
k = modulus of subgrade reaction (k-value)
ℓ = radius of relative stiffness
ΔT_{eff} = effective temperature gradient

Step 6. Compute Adjusted Load/Pavement Weigh Ratio (Normalized Load)

$$q^* = \frac{P}{LW\gamma_{eff}h_{eff}} \qquad (3.42)$$

where

q* = adjusted load/pavement weigh ratio
P = axle weight.
h_{PCC} = PCC slab thickness
γ_{PCC} = PCC unit weight
L = slab length
W = Slab width

Step 7. Calculate Effective Slab Thickness

The effective slab thickness is a thickness of the slab with the modulus of elasticity and Possion's ratio equal to 4,000,000 psi and 0.15, respectively, resting on the Winkler foundation with the coefficient of subgrade reaction equal to 100 psi/in, and having the same radius of relative stiffness as the equivalent slab. The effective slab is determined using the following equation:

$$h_{eq} = \sqrt[3]{\frac{\ell^4}{3410}} \qquad (3.43)$$

h_{eq} = equivalent slab thickness, in
ℓ = radius of relative thickness, in

Step 8. Compute Curling-Related Stresses in the Effective Slab

Using NNs, compute stresses in the effective plate which has the same ratio of radius of relative stiffness to joint spacing, joint spacing, traffic offset and appropriate Korenev's nondimensional temperature gradient, ϕ, and normalized load ratio q*. If the pavement is loaded by a single axle load, then use the neural network NNA1. For tandem or tridem loads use NNA2. The following cases should be considered:

- Case I – resulting stress $\sigma_{eff}^{A}(P,\Delta T)$: Korenev's nondimensional temperature gradient, ϕ, is equal to the nondimensional temperature gradient determined in Step 5; normalized load ratio q* is equal to normalized load ratio determined in Step 6.
- Case II – resulting stress $\sigma_{eff}^{A}(0,\Delta T)$: Korenev's nondimensional temperature gradient, ϕ, is equal to the nondimensional temperature gradient determined in Step 5; normalized load ratio q* is equal 0.
- Case III – resulting stress $\sigma_{eff}^{A}(P,0)$: Korenev's nondimensional temperature gradient, ϕ, is equal to 0; normalized load ratio q* is equal to normalized load ratio determined in Step 6.

Step 9. Compute Curling-Related Stresses in the Equivalent Structure

The stresses obtained in step 8 represent stresses in the slab with the modulus of elasticity and Possion's ratio equal to 4,000,000 psi and 0.15, respectively, resting on the Winkler foundation with the coefficient of subgrade reaction equal to 100 psi/in, and having the same radius of relative stiffness as the equivalent slab. The stresses in the equivalent slab are determined using the following equation:

$$\sigma^{A}(P,\Delta T)=\frac{h_{eff}\gamma_{eq}}{h_{eq}\gamma_{eff}}\sigma^{A}_{eff}(P,\Delta T) \qquad (3.44)$$

$$\sigma^{A}(0,\Delta T)=\frac{h_{eff}\gamma_{eq}}{h_{eq}\gamma_{eff}}\sigma^{A}_{eff}(0,\Delta T) \qquad (3.45)$$

$$\sigma^{A}(P,0)=\frac{h_{eff}\gamma_{eq}}{h_{eq}\gamma_{eff}}\sigma^{A}_{eff}(P,0) \qquad (3.46)$$

where

σ^{A} = stress in the equivalent structure

σ^{A}_{eff} = stress in the effective structure (obtained using NNs0

h_{eff} = effective slab thickness

h_{eq} = equivalent slab thickness

γ_{eff} = equivalent slab unit weight

γ_{eq} = effective slab unit weight

= 0.087 lb/in^2

Step 10. Using NB1, Compute Load-only Caused Stresses in the Effective Structure from the Wheels Located at the Mid-slab

In the case of a single axle loading, compute stresses from all wheels in the axle. In the case of tandem or tridem axle loading, ignore wheels located away from the slab mid-slab, as shown in figure 3.18.

Step 10.1 Compute stresses in the effective structure assuming that there is no load transfer between the slabs in the system B (LTE=0). If the axle consists from dual tires, subdivide it into two sub-axles as shown in figure 3.19. Calculate stresses separately from these sub-axles and superimpose the resulting stresses to obtain $\sigma^{B1}_{eff}(0)$.

Step 10.2 Compute stresses in the effective structure assuming that the load transfer efficiency between two slabs in the system B is equal to shoulder LTE. If the axle consists from dual tires, subdivide it into two sub-axles as shown in figure 3.xx. Calculate stresses separately from these sub-axles and superimpose the resulting stresses to obtain $\sigma^{B1}_{eff}(LTE_{sh})$.

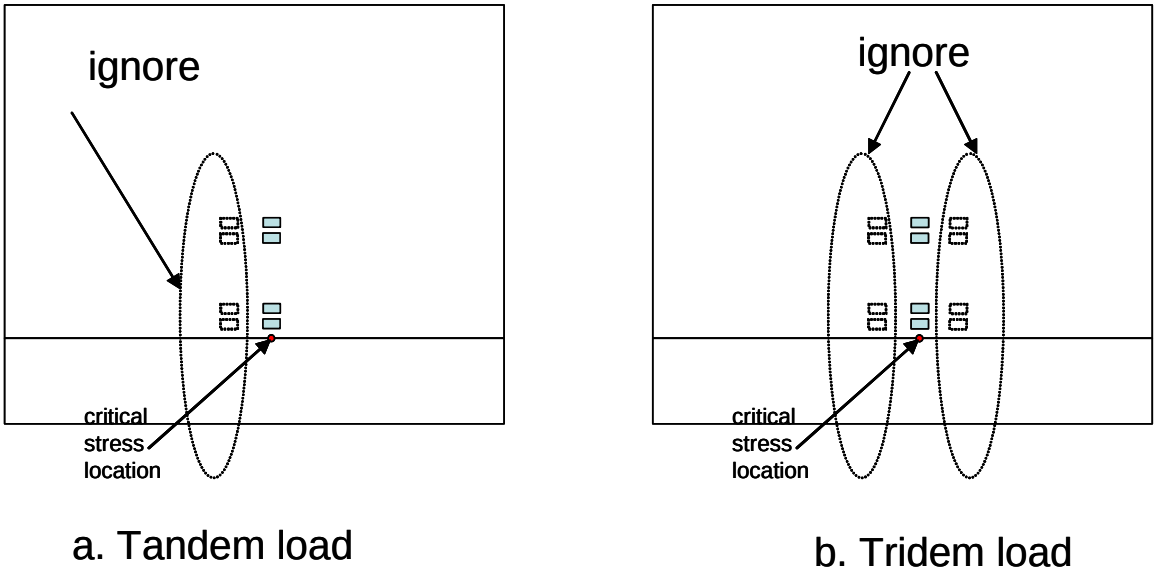

Figure 3.18. Analysis of tandem and tridem axle loading using NNB1.

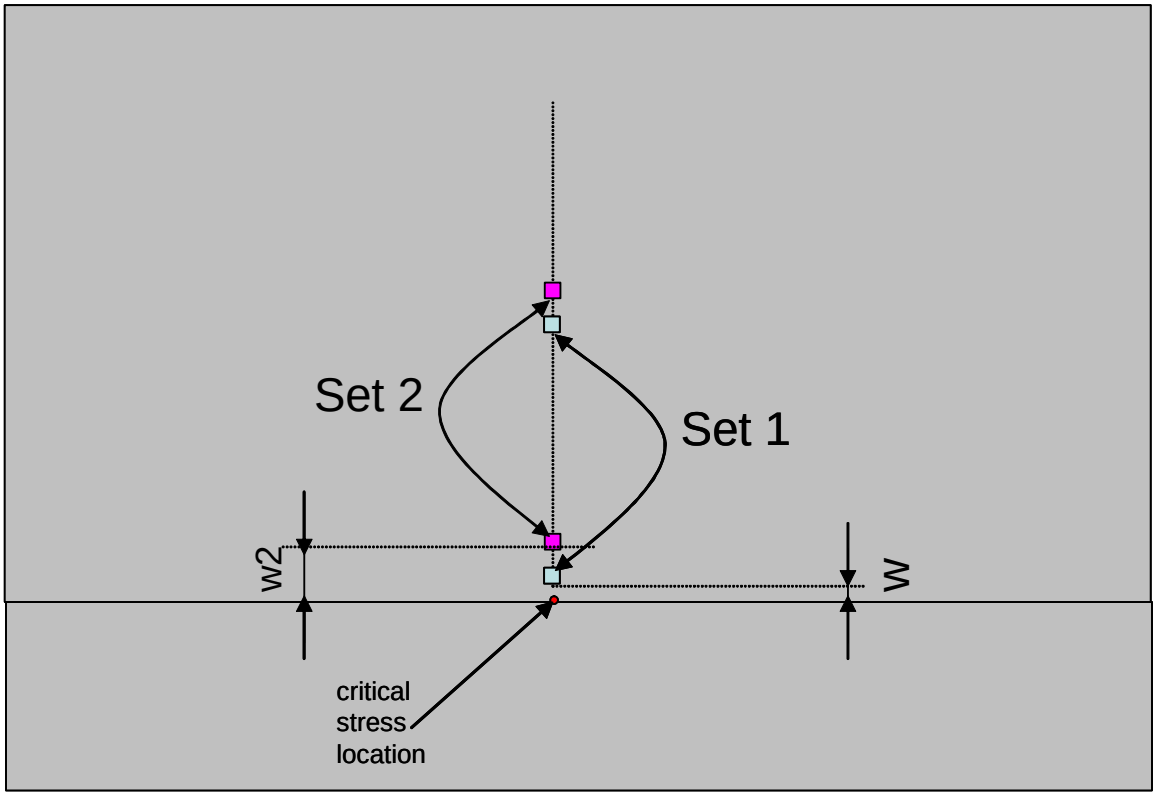

Figure 3.19. Analysis of a single axle load with dual tires using NNB1.

Step 11 (only if tandem or tridem). Compute Stresses from the Remaining Wheels in the Axle using NNB2

Step 11.1 Compute stresses in the effective structure assuming that there is no load transfer between the slabs in the system B (LTE=0). The stresses should be computed from the individual

wheels (four for a tandem axle and eight for a tridem). Superimpose these stresses to obtain $\sigma_{eff}^{B2}(0)$.

Step 11.2 Compute stresses in the effective structure assuming that the load transfer efficiency between two slabs in the system B is equal to shoulder LTE. The stresses should be computed from the individual wheels (four for a tandem axle and eight for a tridem). Superimpose these stresses to obtain $\sigma_{eff}^{B2}(LTE_{sh})$.

Step 12. Determine Load-only Caused Stresses in the Effective Structure from the Entire Axle

- Single axle loading

$$\sigma_{eff}^{B}(0) = \sigma_{eff}^{B1}(0)$$
$$\sigma_{eff}^{B}(LTE_{sh}) = \sigma_{eff}^{B1}(LTE_{sh}) \quad (3.47)$$

- Tandem or tridem laoding

$$\sigma_{eff}^{B}(0) = \sigma_{eff}^{B1}(0) + \sigma_{eff}^{B2}(0)$$
$$\sigma_{eff}^{B}(LTE_{sh}) = \sigma_{eff}^{B1}(LTE_{sh}) + \sigma_{eff}^{B2}(LTE_{sh}) \quad (3.48)$$

Step 13. Determine Load-only Caused Stresses in the Equivalent Structure

The load-only causing stresses in the equivalent structure can be determined using the following expression:

$$\sigma^{B}(0) = \frac{p}{p_{eff}} \frac{h_{eff}^2}{h_{eq}^2} \sigma_{eff}^{B}(0) \quad (3.49)$$

$$\sigma^{B}(LTE_{sh}) = \frac{p}{p_{eff}} \frac{h_{eff}^2}{h_{eq}^2} \sigma_{eff}^{B}(LTE_{sh}) \quad (3.50)$$

where

$\sigma_{eff}^{B}(0)$ = stresses in the effective structure if there is no load transfer between the slabs in the system B (LTE=0)

$\sigma_{eff}^{B}(LTE_{sh})$ = stresses in effective structure if the load transfer efficiency between two slabs in the system B is equal to shoulder LTE.

$\sigma^{B}(0)$ = stresses in the equivalent structure if there is no load transfer between the slabs in the system B (LTE=0)

$\sigma^{B}(LTE_{sh})$ = stresses in equivalent structure if the load transfer efficiency between two slabs in the system B is equal to shoulder LTE.

h_{eff} = effective slab thickness

h_{eq} = equivalent slab thickness

p_{eff} = wheel pressure in the effective system

=100 psi

p = actual wheel pressure

Step 14. Find Stress Load Transfer Efficiency for the Given Axle Load Configuration and the Axle Load Position

$$LTE_{stress} = \frac{\sigma^B\ (LTE_{sh})}{\sigma^B\ (0)} \qquad (3.51)$$

Step 15. Find Axle Loading Induced Component of Bending Stresses (stress in the slab caused by the action of axle loading on top of the temperature curling) in the Equivalent Structure if the Shoulder Provides no Edge Support to the Traffic Lane Slab

$$\sigma_{load,no\,shoulder} = \sigma^A\ (P, \Delta T) - \sigma^A\ (0, \Delta T) - \sigma^A\ (P, 0) + \sigma^B\ (0) \qquad (3.52)$$

Step 16. Find Axle Loading Induced Component of Bending Stresses (stress in the slab caused by the action of axle loading on top of the temperature curling) Accounting for the Shoulder Edge Support to the Traffic Lane Slab

$$\sigma_{load,shoulder} = \sigma_{load,no\,shoulder} * LTE_{stress} \qquad (3.53)$$

Step 17. Find Combined Stress in the Equivalent System

$$\sigma_{comb} = \sigma_{load,shoulder} + \sigma_{curl} \qquad (3.54)$$

Step 18. Find Bending PCC Stresses

Bending stresses (i.e., stresses caused by an axle load and a linear component of the temperature distribution) at the bottom of the PCC slab can be found using the following relationship:

- Unbonded interface

$$\sigma_{PCC,bend} = \frac{h_{pcc}}{h_e}\sigma_{comb} \qquad (3.55)$$

- Bonded interface

$$\sigma_{PCC,bend} = \frac{2(h_{PCC} - x)}{h_e}\sigma_{comb} \qquad (3.56)$$

where

σ_{curl} = curling stresses in the equivalent slab

$\sigma_{PCC,bend}$ = bottom surface PCC bending stresses

h_{PCC} = PCC thickness

h_{eff} = equivalent slab thickness

x = distance between the neural plane and the top surface of the PCC layer

Step 19. Find Total PCC Stresses

$$\sigma_{PCC} = \sigma_{PCC,bend} + \sigma_{NLT}$$

where

σ_{PCC} = total stress at the bottom of the PCC slab

$\sigma_{PCC} = \sigma_{PCC,bend} + \sigma_{NLT}$ = bending stress at the bottom of the PCC slab

$\sigma_{PCC} = \sigma_{PCC,bend} + \sigma_{PCC,NL}$ = stress at the bottom of the PCC layer caused by the nonlinear strain component of the temperature distribution, determined from equation 3.23 or 3.24 for unbonded and bonded interface, respectively.

NN Testing

A factorial of 2,100 independent ISLAB2000 runs was performed to verify the robustness of the NN. Since the purpose of this test was verification of not only the NN itself but rather the entire computation procedure, the following rules were followed:

- The finite element mesh for the testing cases was selected to be independent from the finite element meshes used for the model development.
- The input parameters were completely different from, but within the ranges of, those used for training of the NN model.
- Various tire footprints were used.

Figure 3.20 illustrates a comparison between the PCC stresses obtained from ISLAB2000 and those obtained using NN. A fairly good agreement is observed, with a mean standard error of 4.11 psi. At the same time, the NN require dramatically less computational time than the direct use of ISLAB2000 (several seconds versus 12 hours).

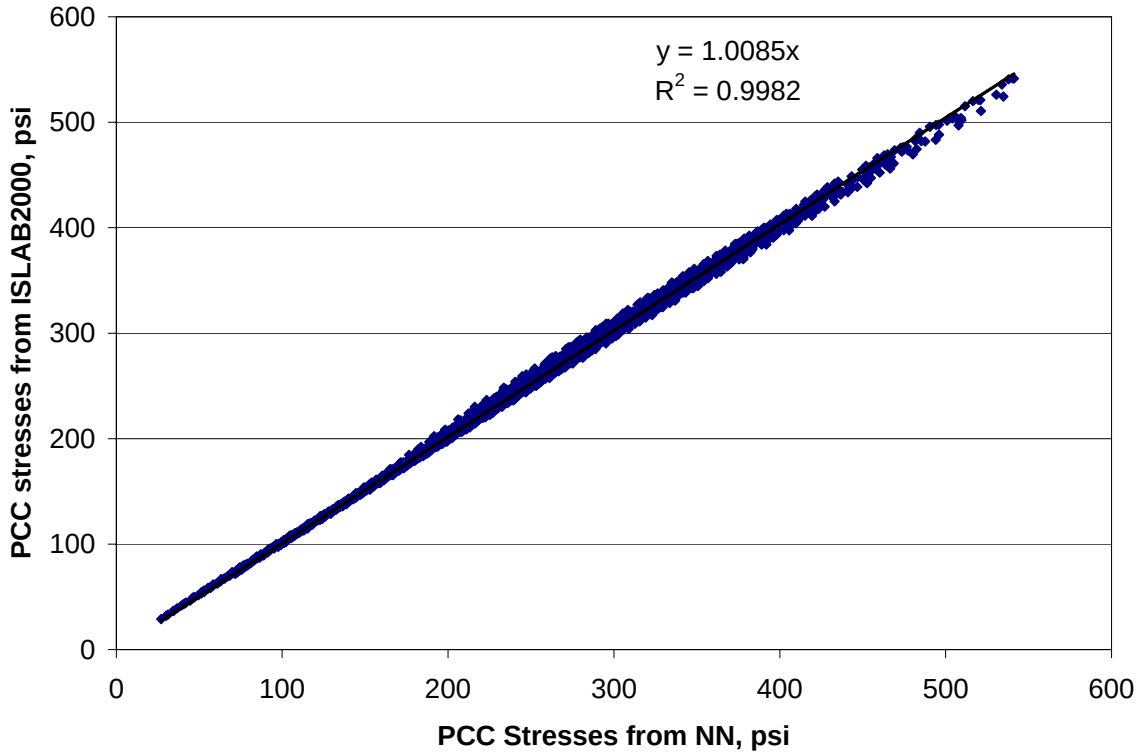

Figure 3.20 Comparison of critical JPCP bottom stresses predicted using ISLAB2000 and NN.

REFERENCES

Armaghani, J.M., T.J. Larsen, and L.L. Smith. (1987). Temperature Response of Concrete Pavements. *Transportation Research Record 1121*. Washington, DC: Transportation Research Board.

Barenberg, E.J., and M.R. Thompson. (1992). *Calibrated Mechanistic Design Procedure for Pavements*, Phase 2 NCHRP 1-26. Washington, DC: National Cooperative Highway Research Program/Transportation Research Board.

Ceylan, H., E. Tutumluer, and E.J. Barenberg. (1999). "Artificial Neural Network Analyses of Concrete Airfield Pavements Serving the Boeing B-777 Aircraft," In *Transportation Research Record 1684*, National Research Council, Washington, D.C., pp. 110-117.

Ceylan, H., E. Tutumluer, and E.J. Barenberg. (1998). "Artificial Neural Networks As Design Tools In Concrete Airfield Pavement Design", In *Proceedings of the 25th International Air Transportation Conference,* Austin, Texas, June 14-17, pp. 447-465.

Ceylan, H., E. Tutumluer, and E.J. Barenberg. (2000). "Effects of Combined Temperature and Gear Loading on the Response of Concrete Airfield Pavements Serving the Boeing B-777 Aircraft," *Proceedings of the International Air Transport Conference (IATC), 2020 Vision of Air Transportation*, San Francisco, California, June 18-21.

Choubane, B., and M. Tia. (1992). "Nonlinear Temperature Gradient Effect on Maximum Warping Stresses in Rigid Pavements," In *Transportation Research Record 1370,* National Research Council, Washington, D.C., pp. 11-19.

Crovetti, J.A. (1994*). Evaluation of Jointed Concrete Pavement Systems Incorporating Open-Graded Permeable Bases*. Ph.D. Dissertation, University of Illinois at Urbana-Champaign.

Darter, M.I. (1977). *Design of Zero-Maintenance Plain Jointed Concrete Pavement: Vol. I—Development of Design Procedures*. Federal Highway Administration, Report No. FHWA-RD-77-111, Washington, D.C

Haussmann, L.D., E. Tutumluer, and E.J. Barenberg. (1997). "Neural Network Algorithms for the Correction of Concrete Slab Stresses from Linear Elastic Layered Programs," In *Transportation Research Record 1568*, National Research Council, Washington D.C., pp. 44-51.

Ioannides, A.M. (1990). Extension of Westergaard Solutions Using Dimensional Analysis. *Proceedings*, Second International Workshop on the Theoretical Design of Concrete Pavements, Siguenza, Spain, pp. 357-388.

Ioannides, A.M., and L. Khazanovich. (1998). "Nonlinear Temperature Effects in Multi-Layered Concrete Pavements," *ASCE Journal of Transportation Engineering*, vol. 124, no. 2.

Ioannides, A.M., L. Khazanovich, and J.L. Becque. (1992). Structural Evaluation of Base Layers in Concrete Pavement Systems. *Transportation Research Record 1370*, Washington, DC: Transportation Research Board, National Research Council, pp. 20-28.

Khazanovich, L. (1994). "Structural Analysis of Multi-Layered Concrete Pavement Systems." Ph.D. Dissertation, University of Illinois, Urbana, Illinois.

Korenev, B.G., and E.I. Chernigovskaya. (1962). *Analysis of Plates on Elastic Foundation*. Gosstroiizdat, Moscow, (in Russian).

Meier, R.W., and G.J. Rix. (1994). "Backcalculation of Flexible Pavement Moduli Using Artificial Neural Networks," In *Transportation Research Record 1448*, National Research Council, Washington D.C.

Mirambell, E. (1990). Temperature and Stress Distributions in Plain Concrete Pavements Under Thermal and Mechanical Loads. *Proceedings,* Second International Workshop on the Design and Rehabilitation of Concrete Pavements, Sigüenza, Spain

Mohamed, A.R., and W. Hansen. (1997). "Effect of Nonlinear Temperature Gradient on Curling Stresses in Concrete Pavements," In *Transportation Research Record 1568*, National Academy Press, Washington, D.C., pp. 65-71.

Salsilli, R.A., E.J. Barenberg, and M.I. Darter. (1993). Calibrated Mechanistic Design Procedure to Prevent Transverse Cracking of Jointed Plain Concrete Pavements. *Proceedings of the 5th International Conference on Concrete Pavement Design and Rehabilitation*, Purdue University.

Smith, K.D., A.L. Mueller, M.I. Darter, and D.G. Peshkin. (1990). *Performance of Jointed Concrete Pavements, Volume IÎEvaluation and Modification of Concrete Pavement Design and Analysis Models.* FHWA-RD-89-137. Washington, DC: Federal Highway Administration.

Thomlinson, J. (1940). Temperature Variations and Consequent Stresses Produced by Daily and Seasonal Temperature Cycles in Concrete Slabs. *Concrete Constructional Engineering*, Vol. 36, No. 6, pp. 298-307; No. 7, pp. 352-360.

Yu, T. H., M. I. Darter, K. D. Smith, J. Jiang, and L. Khazanovich. (1997). *Performance of Concrete Pavements*: *Volume III-Improving Concrete Pavement Performance*, FHWA-RD-95-111, Federal Highway Administration.

CHAPTER 4. DETERMINATION OF CRITICAL BENDING STRESSES AT THE TOP SURFACE OF CRCP

INTRODUCTION

The performance of CRCP depends on critical stresses and deflections imposed by repeated traffic and environmental loading. These stresses depend in part on the deterioration of adjacent transverse cracks and loss of load transfer. This deterioration can be related to the crack width and the shear stresses in the reinforcement and at the crack surface. Punchout development is governed by the maximum tensile stresses at the top surface of the concrete slab that are highly dependent on loss of load transfer of cracks and erosion beneath the edge of the slab. Therefore, reliable predictions of pavement responses are essential for a mechanistic-empirical design procedure.

The structural model used for prediction of CRCP responses should adequately describe CRCP behavior under a variety of combinations of traffic and climatic loading, as well as account for crack spacing and load transfer effects and for void development under the slab edge. It would be extremely difficult, if not impossible, to develop a closed form analytical solution capable of accounting for all these effects. Over the past 30 years, the finite element method has been proven to be a flexible and accurate tool for predicting pavement response. However, FEM is quite inefficient for analyzing damage accumulation in the CRCP, which may require the prediction of PCC tensile stresses for a large number of loading and site condition combinations.

"Rapid solutions" based on factorials of finite element runs offer an attractive alternative to the direct use of finite element analysis for determining critical pavement responses in mechanistic-empirical design. This approach combines the convenience and computational efficiency of closed form solutions with the flexibility and power of the finite element analysis, and it has been used successfully in several major studies (Darter 1977, Barenberg and Thompson 1992).

Traditionally, rapid solutions for prediction of critical pavement responses can be obtained using nonlinear regression analysis. Several sophisticated nonlinear regression models have been developed for analyzing JPCP (Salsilli et al. 1993, Lee and Darter 1993). On the other hand, as the inference space of these models increases, the development process becomes more and more complex and time consuming. This prompted researchers to investigate alternative tools for development of rapid solutions.

In the last decade, artificial neural networks gained substantial popularity for solution of computationally efficient problems in pavement analysis, design, and evaluation (Meier and Rix 1994). Several NN models were proposed for predicting responses in airfield jointed concrete pavements (Haussmann et al. 1997, Ceylan et al. 1998, 1999, 2000). The most recent model can almost instantaneously predict responses for a variety of combinations of design and loading parameters. In spite of some limitations (single slab size and an inability to analyze the effect of the base layer), the model eliminates the need to use ILLI-SLAB for the most typical airport pavement analysis scenarios.

This chapter describes the development of NN for predicting critical top-of-slab tensile bending stresses in CRCP, which lead to punchouts. The development of the finite element model is presented first. Then, the Equivalent CRCP Structure concept is introduced. This concept is used

to reduce the number of independent input variables required for training the NN. Finally, this paper presents information about the training and testing of the NN, as well as a sensitivity study.

FACTORS AFFECTING CRCP STRESSES

Past research has shown that punchouts in CRCP are a result of accumulated fatigue damage caused by transverse stresses at the top surface of the slab (Zollinger Barenberg 1990). The higher the stresses induced by traffic and environmental loading, the more likely that punchouts develop. The magnitude of these stresses depends on a variety of factors, including the following:

- CRC surface and base layer parameters (thickness, modulus of elasticity, coefficient of thermal expansion, and unit weight).
- Interface condition between the CRCP and base layers.
- CRCP crack spacing.
- Crack load transfer efficiency.
- Lane width and load transfer efficiency between the lanes.
- Shoulder type.
- Subgrade properties (stiffness and presence of voids).
- Temperature distribution throughout the CRCP slab thickness.
- Axle type, weight, and position (distance from the slab edge).

Any finite element model used for analysis of stresses in CRCP should accurately account for all these factors.

Structural Model Selection

In this study, the selection of an appropriate analysis method was based on two types of evaluation criteria:

- Technical—The ability to predict the correct answer.
- Operational—The ability to implement the method in a practical environment. The development of rapid solutions requires that the analysis be performed several thousand times to develop a knowledge database to be used in NN training. Therefore, preference should be given to the method requiring less processor time.

ISLAB2000, a completely re-written version of an old finite element program, ILLI-SLAB, was selected as a primary tool for development of a structural response model (Tabatabae and Barenberg 1980, Khazanovich et al. 2000). ISLAB2000 can model the effects of all factors listed in the previous section but is more computationally efficient than rival 3D finite element tools.

FINITE ELEMENT MODEL DEVELOPMENT

For this study, CRCP was represented by a 10-slab assembly. Figure 4.1 shows the geometry and analysis conditions. A brief description of the model is presented, followed by a discussion on selection of certain parameters.

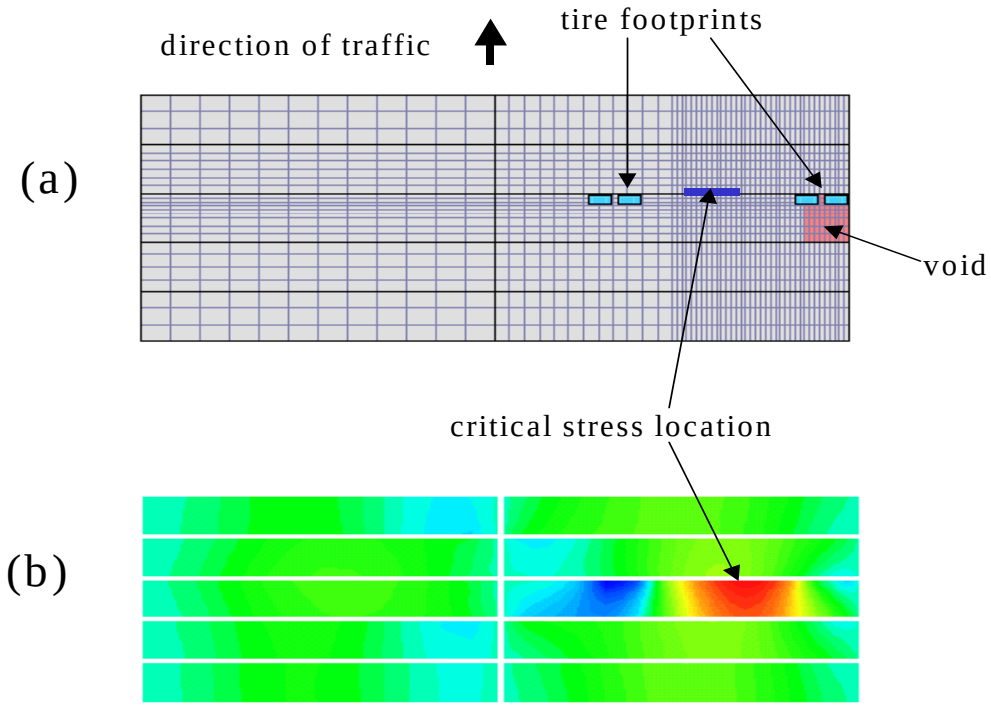

Figure 4.1. (a) Finite element model of a CRCP loaded by a dual tired single axle. (b) Distribution of transverse stresses at the top surface of CRCP.

- The constructed layers were modeled as a two-layer slab.
- The Poisson's ratio of the base layer was assumed to be equal to the PCC Poisson's ratio.
- It was assumed that the layers remain in full contact, but no friction exists on the interface between the layers.
- To avoid overestimation of the PCC curling stresses (caused by ignoring the ability of the PCC layer to separate from the base layer), the base layer was considered to be weightless.
- The subgrade was modeled using the Winkler (dense liquid) model.
- The cracks in CRCP are perpendicular to the direction of traffic, straight, and equally spaced.
- Permanent voids under a cracked panel are modeled using the dense liquid model with a very low stiffness. The void was assumed to occupy the entire length of the panel in the longitudinal direction and to be up to 36 in wide in the transverse direction.
- The effects of temperature curling, moisture warping, PCC shrinkage, and built-in (construction) curling are characterized by an equivalent temperature distribution that induces the same strain field in the CRCP.
- A zero temperature gradient throughout the base layer was assumed.
- An axle is placed near the transverse crack (all wheels are placed on the same side of the crack and the outer wheel is placed up to 18 in from the slab corner). An axle was characterized by its weight only. Thus, the effects of tire pressure and tire footprint geometry were ignored.
- Critical top surface PCC bending stresses were computed along the transverse crack edge from 3 to 5 ft from the slab edge.
- The effect of the AC shoulder on CRCP stresses was ignored.

The selection of this model was the result of a comprehensive study. Presented below are examples of the background analysis that supports the selection of these model features.

Model Geometry

An extensive parametric study was conducted to determine whether passing-lane slabs could be ignored in the analysis. Several finite element models were created and analyzed using different design parameters, including crack load transfer efficiency, temperature gradients, and loss of support conditions. The results of the analyses suggested that models with one traffic lane generally tend to overpredict critical stresses by up to 10 percent. Therefore, it was decided to use two lanes in the transverse direction to improve the accuracy of the finite element calculation of critical stresses.

To determine an appropriate number of cracked concrete panels in the longitudinal direction, several models were created using 1, 2, 3, 5, and 7 cracked panels. The models were analyzed using different material properties and environmental and loading conditions. Among the models with high load transfer efficiency and narrow crack spacing, those with 3 CRC panels overpredicted top tensile stresses by up to 20 percent (as compared to models with 7 cracked CRC panels); the models with 5 CRC panels overpredicted top tensile stresses by up to 3 percent (compared to the models with 7 cracked CRC panels). Although modeling only 5 cracked concrete panels in the longitudinal direction may result in a slight overestimation of stresses for the cases with high crack load transfer efficiency, this number of panels is adequate for modeling the top tensile stresses for punchout prediction.

Figure 4.2 illustrates the effect of the number of modeled cracked concrete panels on predicted top surface bending stresses for a model subjected to an 18-kip single axle load and –28 ºF temperature differential. The model is characterized by 3-ft crack spacing and has a loss of support extending 2 ft from the pavement edge. Two levels of crack load transfer efficiency (50 and 95 percent) are considered. For both cases, modeling of CRCP with 5 slabs in the direction of traffic provides sufficient accuracy.

Axle Loading

To assure accurate simulation of the tire–pavement contact area, the authors examined the sensitivity of critical stresses to the shape of the tire footprint. Tire footprints were modeled using rectangular and square shapes with equivalent contact areas. Since the top surface stresses critical for the development of edge punchout in CRCP occur at some distance away from the applied wheel load, the predicted stresses were found to be insensitive to the shape of the wheel loading. The model was analyzed using various concrete temperature differentials, various levels of load transfer efficiency, and various loss of support conditions. Based on analysis results, it was decided to ignore the effects of tire print.

Several axle loading positions in the direction of traffic were investigated for different crack spacing in order to determine the critical loading position. Figure 4.3 presents a comparison of the tensile stresses induced on the top surface of transverse cracks from axles placed near the crack or between the cracks. For all crack spacings, higher stresses were observed when the load was placed near the crack.

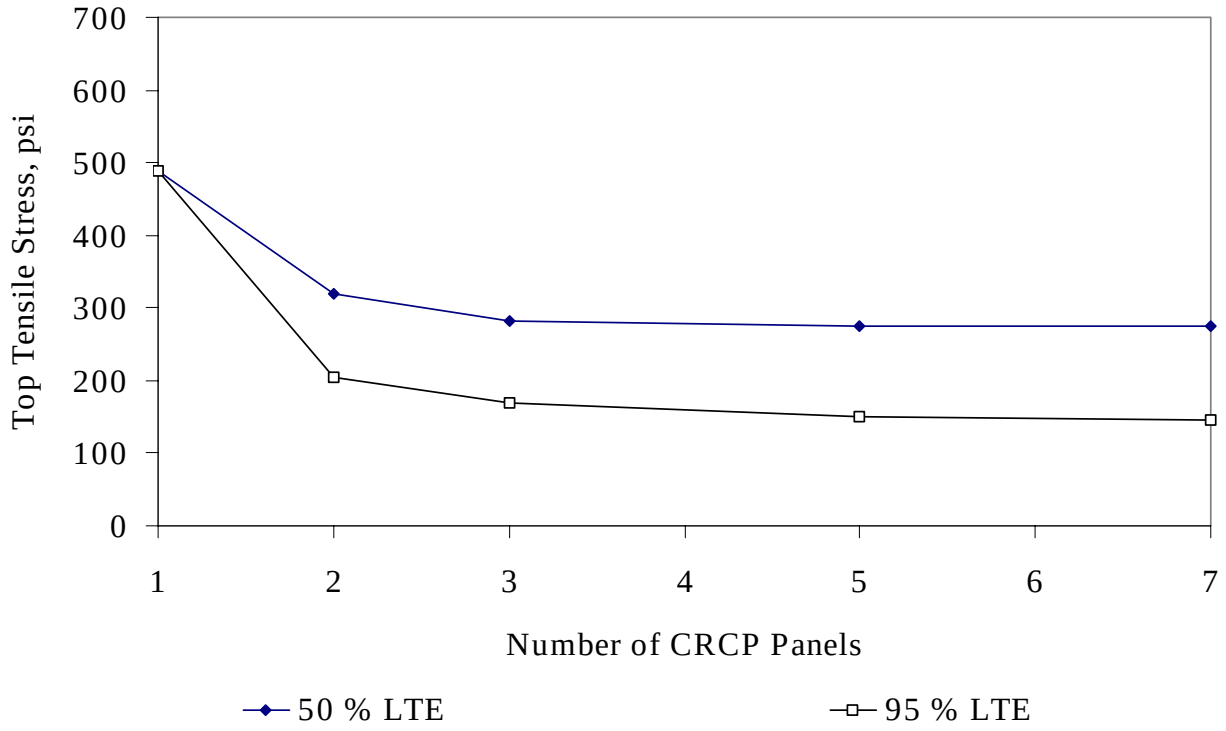

Figure 4.2. Effect of number of modeled cracked panels on predicted critical responses.

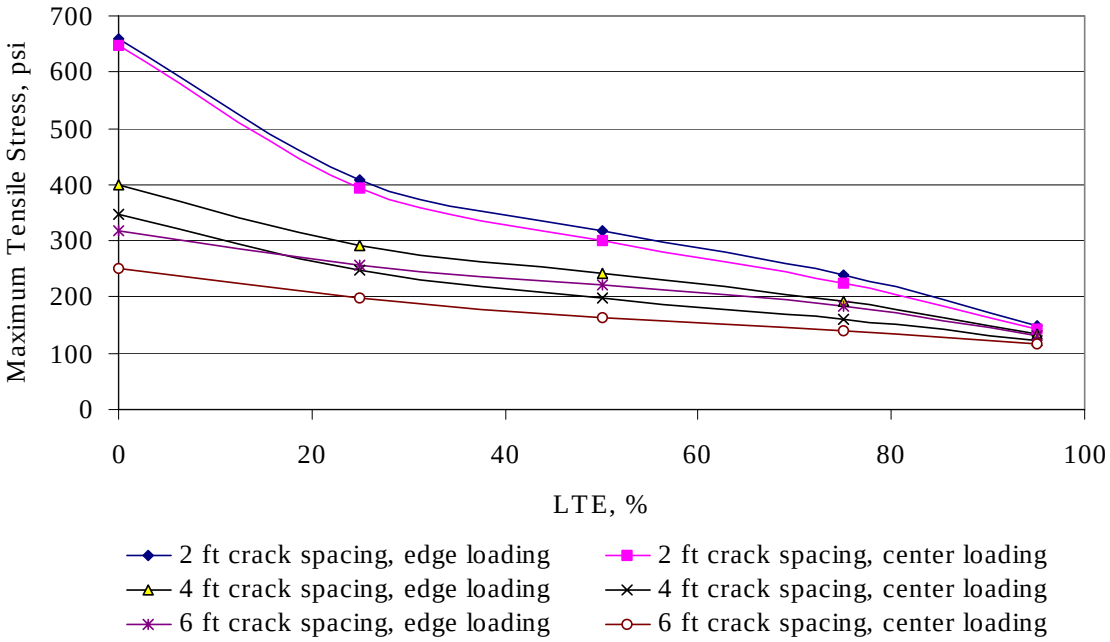

Figure 4.3. Comparison of critical CRCP tensile stresses (top of slab) for different crack spacing and axle location.

Finite Element Mesh

To find a compromise between acceptable computational efficiency and sufficient accuracy, a variety of finite element meshes were considered. It was found that a very fine mesh (2 by 2 in) is required near the loading area and the location of the critical stresses. At the same time, a relatively coarse mesh far from those places did not significantly affect the accuracy of the critical stress prediction. A maximum aspect ratio of 1 to 6 was also found to produce sufficient accuracy. Following these rules, it was possible to keep mesh-related error under 1 percent.

Equivalent Structural Model Concepts

In spite of the simplifying assumptions presented in the previous section, the CRCP structural model still required 17 input parameters (5 for the PCC layer, 3 for the base layer, 2 for load weight and position, 3 for temperature loading, and 1 each for subgrade stiffness, void size, crack spacing, and crack load transfer efficiency). Although ISLAB2000 is much more computationally efficient than rival 3D finite element tools, it is not fast enough to allow a "brute force" approach to creating the database of finite element runs for the development of rapid solutions. Indeed, an attempt to run all combinations of all 17 input parameters would require analysis of more than 125 million cases if each parameter is allowed to have just 3 values. Therefore, more efficient approaches were explored.

Like it was found for JPCP structures, the most promising way to reduce the number of cases required is to use equivalency concepts. This approach significantly reduces the dimension of the problem without introducing any additional error. Three available equivalent concepts were considered—equivalent thickness, equivalent temperature gradient, and equivalent slab. Based on these, a new concept—the Equivalent CRCP Structure—was developed.

Equivalent Single Layer Concept

As discussed in chapter 3, the equivalent slab thickness concept states that PCC stresses in the two-layered slab can be found from the corresponding stresses in the equivalent homogeneous plate which exhibits the same deflection profile as the in situ pavement If no friction exists between the PCC and the base layers, and if the equivalent slab has the same modulus of elasticity and Poisson's ratio as the PCC layer, then the thickness of the equivalent slab is defined as follows:

$$h_{eff} = \sqrt[3]{h_{PCC}^3 + \frac{E_{base}}{E_{PCC}} h_{base}^3} \quad (4.1)$$

where

h_{eff} = equivalent slab thickness
E_{PCC}= PCC modulus of elasticity
E_{base} = base modulus of elasticity
h_{PCC} = PCC thickness
h_{base} = base thickness

If a CRCP is subjected to an axle loading only (no curling), and if the stresses in the equivalent slab are known, then the corresponding PCC stresses can be found using the following relationship:

$$\sigma_{PCC} = \frac{h_{pcc}}{h_{eff}} \sigma_{eff} \qquad (4.2)$$

where

σ_{eff} = top surface stresses in the equivalent slab

σ_{PCC} = top PCC stresses

h_{PCC} = PCC thickness

h_{eff} = equivalent slab thickness

Equivalent Linear Temperature Distribution Concept

To apply this concept for the curling analysis of a two-layered system, the temperature distribution throughout the two-layered slab thickness should be split into its three components:

- The part that causes constant strain throughout-the-slab-thickness strain.
- The part that causes strain linear throughout-the-slab-thickness strain.
- The part that causes nonlinear strain.

Since the interface between the CRCP and the base is assumed to be unbonded and the temperature distribution throughout the base layer is assumed to be constant, the constant strain, linear strain, and nonlinear strain temperature components of the temperature distribution in the PCC layer have the following forms:

$$T_{c,PCC} = \frac{1}{h_{PCC}} \int_{-\frac{h_{PCC}}{2}}^{\frac{h_{PCC}}{2}} T(z)dz \qquad (4.3)$$

$$T_{L,PCC}(z) = T_0 + 12\frac{z}{\alpha_{PCC}} \int_{-\frac{h_{PCC}}{2}}^{\frac{h_{PCC}}{2}} (T(z) - T_0)zdz \qquad (4.4)$$

$$T_{NL,PCC}(z) = T(z) - T_{c,PCC}(z) - T_{L,PCC}(z) - 2T_0 \qquad (4.5)$$

where

h_{PCC} = PCC slab thickness.

H_{base} = base thickness.

h_{eff} = effective slab thickness computed.

T_0 = the temperatures at which theses slabs are assumed to be flat.

T(z) temperatures distribution through the PCC and base layers.

$T_{c,PCC}$ = the constant strain temperature component in the PCC layer

$T_{L,PCC}$ = the linear strain temperature component in the PCC layer

$T_{NL,PCC}$ = the non-linear strain temperature component in the PCC layer

The constant strain temperature component does not cause any stresses in the PCC slab and the base layer if they are not restrained from the horizontal movement. The nonlinear strain component of the temperature distribution induces the following stresses:

$$\sigma_{NL,PCC}(z) = -\frac{E(z)}{1-\mu}\alpha(z)\left(T_{NL,PCC}(z) - T_0\right) \qquad (4.6)$$

where

σ_{NL} - stress caused by the nonlinear strain component of the temperature distribution.

The stresses in the two-layered slab caused by the linear strain temperature component and axle loadings can be found from the analysis of an equivalent single-layer slab. This equivalent slab should have the same geometry and self-weight, its thickness should is determined by equation 4.1, and the slab should be subjected to the same axle loading, the equivalent linear temperature distribution causing the same bending moment distributions in the equivalent and the original slabs.

To ensure equality of the self-weight of the original and equivalent slabs, and accounting for the assumption that the base layer is assumed to be weightless, the unit weight of the equivalent slab is defined as follows:

$$\gamma_{eff} = \frac{h_{PCC}\gamma_{PCC}}{h_{eff}} \qquad (4.7)$$

where

γ_{eff} = unit weight of the effective slab.

γ_{PCC} = unit weight of the PCC slab.

h_{PCC} = PCC slab thickness.

h_{eff} = effective slab thickness computed.

The following linear temperature distribution in the equivalent slab defined by the difference in temperatures at the top and bottom surfaces causes the same bending moment distributions in the equivalent single-layer slab and in the original composite slab:

$$\Delta T_{eff} = \frac{12}{h_{eff}^2} * \int_{-\frac{h_{PCC}}{2}}^{\frac{h_{PCC}}{2}} (T(z) - T(\frac{h_{PCC}}{2}))zdz \qquad (4.8)$$

where

ΔT_{eff} = difference between temperatures at the top and bottom surfaces of the effective slab.

h_{PCC} = PCC slab thickness.

h_{eff} = Effective slab thickness computed using equation 4.1.

T(z) temperatures distribution throught the PCC and base layers.

z = vertical coordinate measured downward from the neutral axis of the PCC slab (unbonded interface)

Since the temperature distribution is known in 11 points, the integral in equations 4.8 was evaluated numerically which resulted in the following expressions:

$$\Delta T_{eff} = \frac{12}{h_{eff}^2} * \frac{h_{PCC}}{60} \sum_{i=1}^{10} \left(T_i * \left((3*i-17) * \frac{h_{PCC}}{10} \right) + T_{i+1} \left((3*i-16) * \frac{h_{PCC}}{10} \right) \right) \qquad (4.9)$$

where

$T_1, T_2, \ldots, T_{11}$ are PCC temperatures at equal spaced points. T_1 is PCC temperature at the top surface and T_{11} is PCC temperature at the bottom surface.

ΔT_{eff} = difference between temperatures at the top and bottom surfaces of the effective slab.
h_{PCC} = PCC slab thickness.
h_{eff} = effective slab thickness computed.

The top surface PCC stress caused by the linear strain temperature can be found from the stress in the equivalent slab using the following relationship:

$$\sigma_{PCC,L} = \frac{h_{pcc}}{h_{eff}} \sigma_{eff} \qquad (4.10)$$

where

σ_{eff} = bottom surface stresses in the equivalent slab
σ_{PCC} = bottom surface PCC stresses
h_{PCC} = PCC thickness
h_{eff} = equivalent slab thickness

Stresses at the bottom of the PCC slab caused by the nonlinear strain component were evaluated numerically using the following expressions:

$$\sigma_{PCC,NL} = -E_{PCC}\alpha_{PCC}\left(\frac{\Delta T_{eff}}{2h_{eff}} h_{PCC} - \frac{\sum_{i=1}^{10} T_i}{10} + \frac{T_1}{20} + \frac{21T_{11}}{20}\right) \qquad (4.11)$$

Equivalent CRCP Structure Concept

The Equivalent CRCP Structure concept developed for this study states that top surface stresses in two pavement systems are directly related if the following conditions are satisfied:

$$\ell_1 = \ell_2 \qquad (4.12)$$
$$L_1 = L_2 \qquad (4.13)$$
$$V_1 = V_2 \qquad (4.14)$$
$$\phi_1 = \phi_2 \qquad (4.15)$$
$$\frac{AGG_1}{k_1\ell_1} = \frac{AGG_2}{k_2\ell_2} \qquad (4.16)$$
$$\frac{P_1}{h_1\gamma_1} = \frac{P_2}{h_2\gamma_2} \qquad (4.17)$$
$$s_1 = s_2 \qquad (4.18)$$

where

ℓ = radius of relative stiffness, in.
V =void width
L =crack spacing
ϕ = Korenev's nondimensional temperature gradient (Korenev and Chernikhovskaya 1962)
AGG = aggregate interlock factor of cracks
P =axle weight

γ =PCC slab unit weight
h = PCC thickness
s = distance between slab edge and outer wheel edge

and subscripts 1 and 2 denote slabs 1 and 2, respectively.

If conditions (4.12) through (4.18) are satisfied and tire footprint configurations are the same for both cases, then the stresses in a two-layered slab 1 can be found from the stress in a single layer slab 2 using the following relationship:

$$\sigma_{PCC,1} = \frac{h_1^2 h_2 \ \gamma_1}{h_{eff}^3 \gamma_2} \sigma_{PCC,2} \qquad (4.19)$$

where

h_{eff} = effective thickness for slab 1 computed from equation (4.1).

This equivalency concept was derived using rigorous mathematical principles and is valid for any combination of input parameters. However, to verify the procedure, a factorial of analysis was performed. For each set of input parameters, stresses were calculated using two approaches:

- Directly using ISLAB2000.
- An equivalent system was determined, critical stresses were determined for that system, and later those stresses were adjusted using equation (4.19).

Figure 4.4 presents a comparison of the analysis results. As expected, a near perfect correspondence was obtained.

Although the equivalency concept guarantees the exact correspondence only for axle loading with the same tire footprint, since the tire footprint does not significantly affect stresses at some distance from the applied load, equation (4.19) can be used to relate stresses from a given axle type.

NN Development

The Equivalent CRCP Structure concept allows the reduction of number of independent parameters to seven: radius of relative stiffness, crack spacing, Korenev's nondimensional temperature gradient, traffic offset, normalized axle weight, and nondimensional aggregate interlock factor.

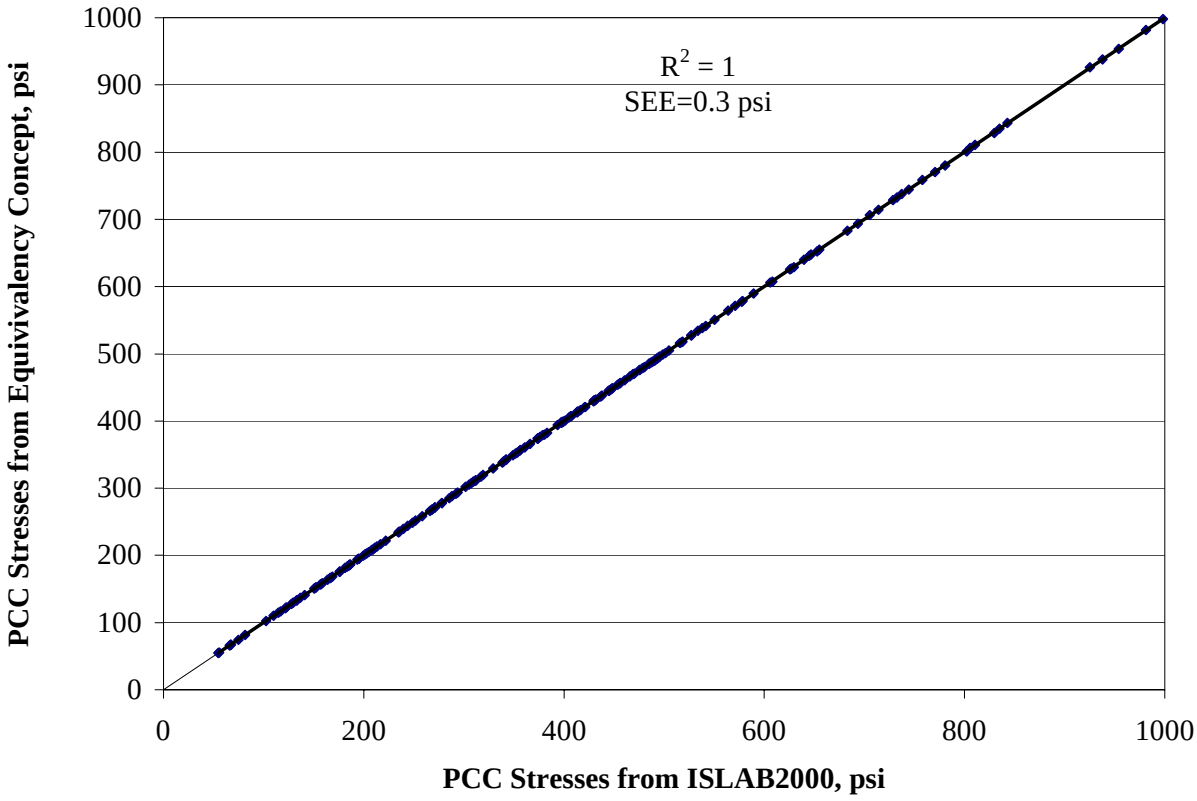

Figure 4.4. Comparison of CRCP top surface stresses determined directly from ISLAB2000 and those obtained using the Equivalent CRCP Structure concept.

A factorial of 46,800 ISLAB2000 runs was performed to create a training database. A single-layer slab was analyzed in all cases. The thickness of the slab, modulus of elasticity, Poisson's ratio, unit weight, and coefficient of thermal expansion were set equal to 10 in, 4,000,000 psi, 0.15, 0.087 lb/in^3, and 5.5*10^{-6} 1/^{o}F, respectively. The following parameters were varied:

- Crack spacing. Spacings of 1, 2, 3, 5, 7, and 9 ft were analyzed.
- Coefficient of subgrade reaction. A wide range of the coefficients was considered to cover the range of radii of relative stiffness from 22.5 to 80 in.
- Temperature gradients were varied to cover range in Korenev' s temperature gradient from 0 to 50.

The aggregate interlock factor, AGG, was varied to provide the load transfer efficiency for flat slab conditions and FWD type loading from 0 to 95 percent. The load transfer efficiency of the crack was estimated using an approximate equation developed by Crovetti (1994):

$$LTE = \frac{1}{0.01 + 0.012 * \left(\frac{AGG}{k\,\ell} \right)^{-0.849}} \qquad (4.20)$$

where LTE is deflection load transfer efficiency of a crack from as measured by a FWD-type loading device.

- Axle weight was varied from 0 to 67650 lb, which covers normalized ratio from 0 to 77760 in^2.
- Wheel offset was varied from 0 to 18 in.
- Void width was varied from 0 to 36 in.

Since some of the ranges above are presented in terms of normalized or dimensionless parameters, it makes it somewhat difficult to understand the ranges of applicability of the database. To illustrate it in terms of real inputs, a baseline case was selected and one parameter at time was allowed to vary. Table 4.1 presents the baseline parameters and calculated ranges for those parameters.

Table 4.1. Ranges of NN parameters if others are equal to the baseline values.

Variable	Baseline value	Min value	Max value
PCC thickness, in	9	5.1	27.7
PCC modulus of elasticity, psi	4,500,000	154,000	24,6170,950
Base , in	6	0	>30
Base modulus of elasticity, psi	40,000	0	>10,000,000
PCC coefficient of thermal expansion	5.50E-06	0	5.50E-05
PCC unit weight, lb/in^3	0.087	0	0.87
k-value, psi/in	200	7	1094
Temperature differential, ^oF	-10	0	<-100
Axle weight, lb	18,000	0	>60,000

A modified MS-HARP neural network architecture was employed (Banan and Hjelmstad 1994, Khazanovich and Roesler 1997). Selection of this particular architecture was driven primarily by familiarity with this technique and convenience in the NN training. However, conventional backpropagation NNs could be implemented as well.

STEP-BY-STEP PROCEDURE FOR DETERMINATION OF TOP SURFACE STRESSES IN CRCP

Using the trained NN, CRCP stresses can be determined for a wide range of site conditions, design parameters, and axle loading. The detailed procedure is described below.

Step 1. Calculate the Effective Slab Thickness

The equivalent slab thickness is determined using equation 4.1.

Step 2. Calculate Unit Weight of the Equivalent Slab

Unit weight of the equivalent slab thickness is determined using equation 4.7.

Step 3. Calculate Radius of Relative Stiffness

$$\ell = \sqrt[4]{\frac{E_{PCC} h^3_{eff}}{12*(1-\mu^2_{eff})*k}} \qquad (4.21)$$

where

h_{eff} = effective thickness
E_{PCC} = PCC elastic modulus
μ_{PCC} = PCC Poisson's ratio
k = coefficient of subgrade reaction

Step 4. Calculate Effective Temperature Differential

Equivalent temperature differential is determined from equation 4.9.

Step 5. Compute Korenev's Nondimensional Temperature Gradient

$$\phi = \frac{2\alpha_{PCC}(1+\mu_{PCC})\ell^2}{h_e^2}\frac{k}{\gamma_{eff}}\Delta T_{eff} \qquad (4.22)$$

where

ϕ= nondimensional temperature gradient
h_{PCC} = PCC slab thickness
α_{PCC} = PCC coefficient of thermal expansion
μ_{PCC} = Poisson's ratio for PCC
γ_{eff} = effective unit weight
k = modulus of subgrade reaction (k-value)
ℓ = radius of relative stiffness
ΔT_{eff} = effective temperature gradient

Step 6. Compute Adjusted Load/Pavement Weigh Ratio (Normalized Load)

$$q^* = \frac{P}{\gamma_{eff} h_{eff}} \tag{4.23}$$

where

q* = adjusted load/pavement weigh ratio
P = axle weight
h_{PCC} = PCC slab thickness
γ_{PCC} = PCC unit weight

Step 7. Compute Stresses in the Equivalent Structure

Using NN, compute stresses in the equivalent structure which has the same radius of relative stiffness, crack spacing, Korenev's nondimensional temperature gradient, traffic offset, normalized load ratio, and crack load transfer efficiency. Using equation (4.19), convert stresses in the equivalent CRCP structure into stresses in the equivalent single layer system.

Step 8. Compute Bending Stresses in the Original Structure

Using equation (4.2), convert stresses in the equivalent single layer structure into bending stresses in the original CRCP structure.

Step 9. Compute Non-Linear Temperature Stresses at the top Surface of the CRCP Pavement

Using equation (4.11), compute non-linear temperature stresses at the top surface of the CRCP.

Step 10. Superimpose Non-Linear Temperature and Bending Stresses

Add stresses obtained in step 8 and 9 to obtain critical stresses at the top surface of CRCP pavement.

NN TESTING

A factorial of 2,400 independent ISLAB2000 runs was performed to verify the robustness of the NN. Since the purpose of this test was verification of not only the NN itself but rather the entire computation procedure, the following rules were followed:

- The finite element mesh for the testing cases was selected to be independent from the finite element meshes used for the model development.
- The input parameters were completely different from, but within the ranges of, those used for training of the NN model.
- Various tire footprints were used.

Figure 4.5 illustrates a comparison between the PCC stresses obtained from ISLAB2000 and those obtained using NN. A fairly good agreement is observed, with a mean standard error of 3.24 psi.

At the same time, the NN require dramatically less computational time than the direct use of ISLAB2000 (several seconds versus 12 hours).

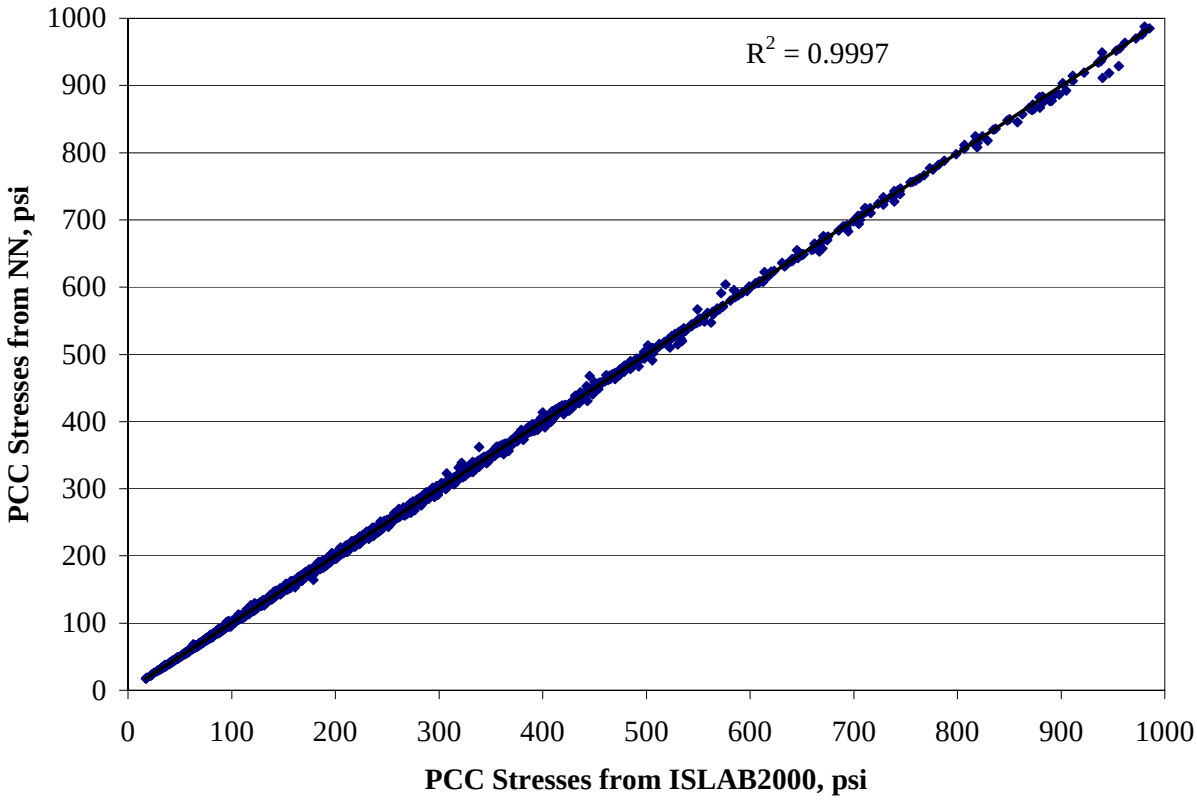

Figure 4.5. Comparison of critical CRCP stresses predicted using ISLAB2000 and NN.

Sensitivity Studies

By varying the input parameters, one can see the effect of each parameter on predicted critical CRCP stresses. For some input parameters, the results were compared with ISLAB2000 results. Figure 4.6 shows that critical stresses decrease when CRCP thickness increases. Figure 4.7 demonstrates that a decrease in crack load transfer efficiency and creation of voids under the CRCP edge lead to significant increases in CRCP top surface stresses.

These results agree with the results of past research and field observation. Also, for all cases considered, good correspondence between NN and ISLAB2000 was observed. Therefore, although more comprehensive verification/validation of the rapid solution is underway, one can conclude that the proposed procedure is an efficient tool for predicting critical CRCP tensile stresses.

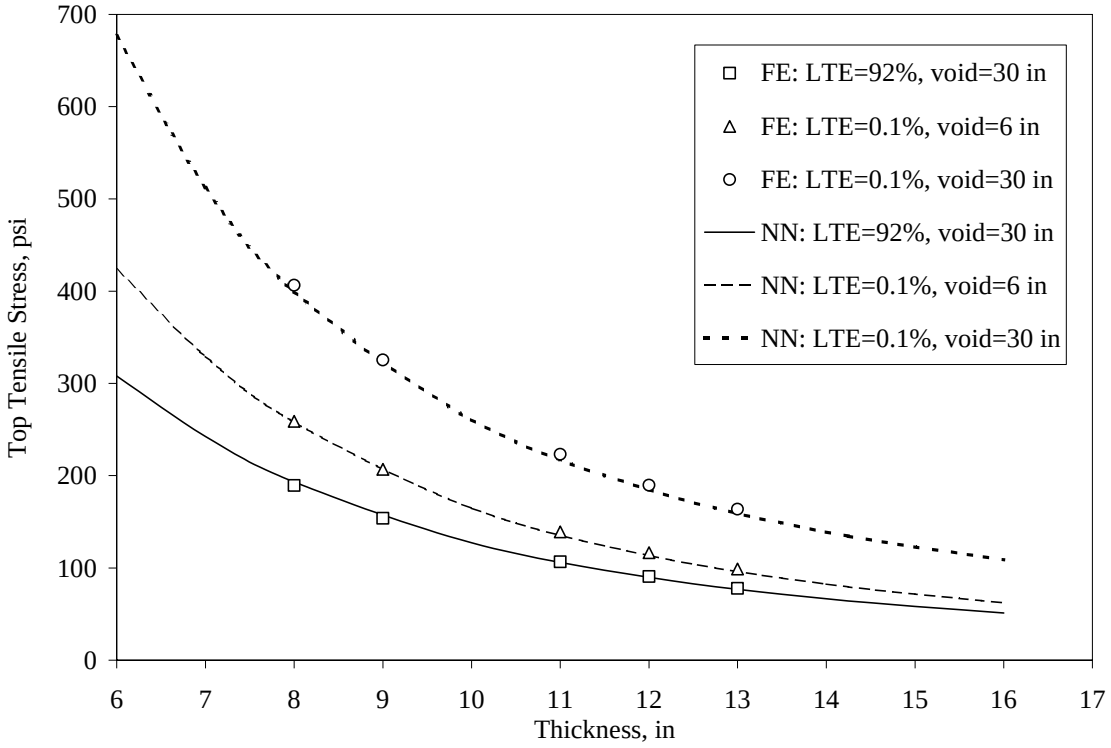

Figure 4.6. Effect of CRCP thickness on critical CRCP stresses for 6 feet crack spacing model with k=100 pci, T_{top}-T_{bot}=-30°F, Axle weight = 12,000 lb.

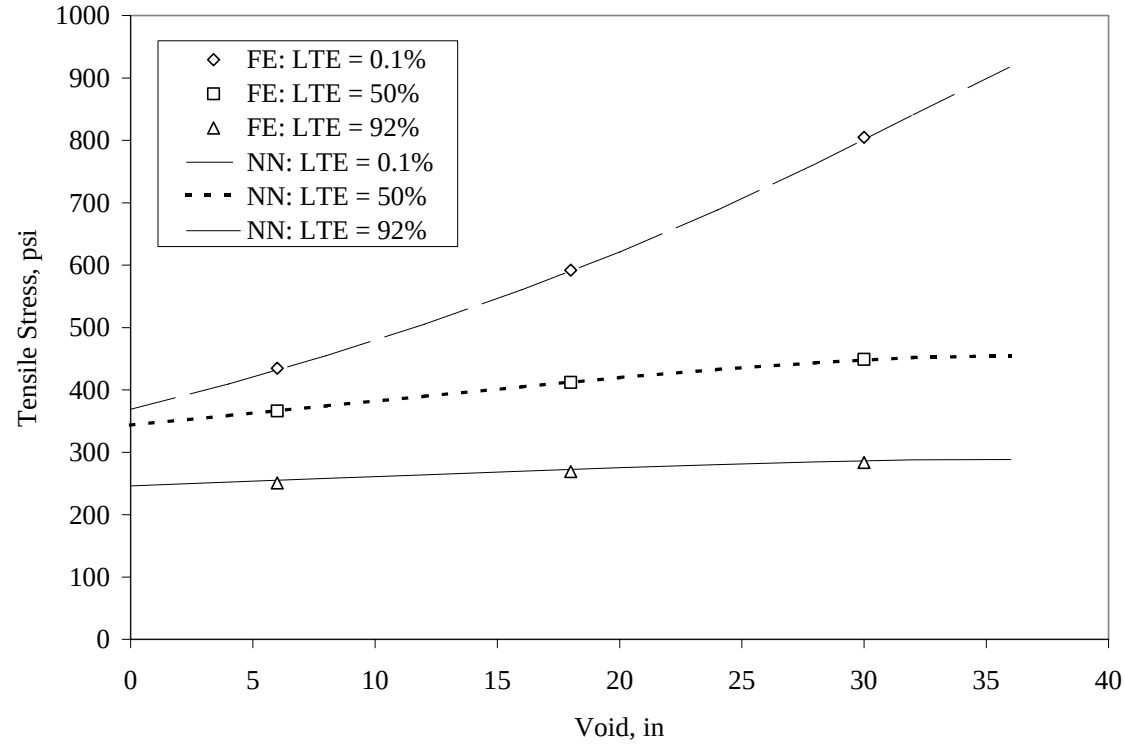

Figure 4.7. Effect of void width on critical CRCP stresses for 5 feet crack spacing model with k=100 pci, T_{top}-T_{bot}=-30°F, Axle weight = 24,000 lb, PCC thickness=8 in.

REFERENCES

Banan, M., and Hjelmstad. (1994). *Data-Based Mathematical Modeling: Development and Application*, SRS No. 590, Civil Engineering Studies, University of Illinois, Urbana, Illinois.

Barenberg, E.J., and M.R. Thompson. (1992). *Calibrated Mechanistic Design Procedure for Pavements*, Phase 2 NCHRP 1-26. National Cooperative Highway Research Program/Transportation Research Board, Washington, D.C.

Ceylan, H., E. Tutumluer, and E.J. Barenberg. (1998). "Artificial Neural Networks As Design Tools In Concrete Airfield Pavement Design", In *Proceedings of the 25th International Air Transportation Conference,* Austin, Texas, June 14-17, pp. 447-465.

Ceylan, H., E. Tutumluer, and E.J. Barenberg. (1999). "Artificial Neural Network Analyses of Concrete Airfield Pavements Serving the Boeing B-777 Aircraft," In *Transportation Research Record 1684*, National Research Council, Washington, D.C., pp. 110-117.

Ceylan, H., E. Tutumluer, and E.J. Barenberg. (2000). "Effects of Combined Temperature and Gear Loading on the Response of Concrete Airfield Pavements Serving the Boeing B-777 Aircraft," *Proceedings of the International Air Transport Conference (IATC), 2020 Vision of Air Transportation*, San Francisco, California, June 18-21.

Choubane, B., and M. Tia. (1992). "Nonlinear Temperature Gradient Effect on Maximum Warping Stresses in Rigid Pavements," In *Transportation Research Record 1370,* National Research Council, Washington, D.C., pp. 11-19.

Crovetti, J.A. (1994). "Evaluation of Jointed Concrete Pavement Systems Incorporating Open-Graded Permeable Bases." Ph.D. Dissertation, University of Illinois, Urbana, Illinois.

Darter, M.I. (1977). *Design of Zero-Maintenance Plain Jointed Concrete Pavement: Vol. I—Development of Design Procedures*. Federal Highway Administration, Report No. FHWA-RD-77-111, Washington, D.C.

Haussmann, L.D., E. Tutumluer, and E.J. Barenberg. (1997). "Neural Network Algorithms for the Correction of Concrete Slab Stresses from Linear Elastic Layered Programs," In *Transportation Research Record 1568*, National Research Council, Washington D.C., pp. 44-51.

Ioannides, A.M., and L. Khazanovich. (1998). "Nonlinear Temperature Effects in Multi-Layered Concrete Pavements," *ASCE Journal of Transportation Engineering*, vol. 124, no. 2.

Ioannides, A.M., L. Khazanovich, and J.L. Becque. (1992). "Structural Evaluation of Base Layers in Concrete Pavement Systems," In *Transportation Research Record 1370*, National Research Council, Washington, D.C., pp. 20-28.

Khazanovich, L. (1994). "Structural Analysis of Multi-Layered Concrete Pavement Systems." Ph.D. Dissertation, University of Illinois, Urbana, Illinois.

Khazanovich, L., and J. Roessler. (1997). "DIPLOBACK: a Neural Networks-Based Backcalculation Program for Composite Pavements," In *Transportation Research Record 1570,* National Academy Press.

Khazanovich, L., H.T. Yu, S. Rao, K. Galasova, E. Shats, and R. Jones. (2000). "ISLAB2000—Finite Element Analysis Program for Rigid and Composite Pavements. User's Guide." ERES Consultants, Champaign, Illinois.

Korenev, B.G., and E.I. Chernigovskaya. (1962). *Analysis of Plates on Elastic Foundation*. Gosstroiizdat, Moscow (in Russian).

Lee, Y.H., and M.I. Darter. (1993). "Mechanistic Design Models of Loading and Curling in Concrete Pavements," *Proceedings, ASCE Specialty Conference Airport Pavement Innovations—Theory to Practice.* Waterways Experiment Station, Vicksburg, Mississippi, pp. 1-15.

Meier, R.W., and G.J. Rix. (1994). "Backcalculation of Flexible Pavement Moduli Using Artificial Neural Networks," In *Transportation Research Record 1448*, National Research Council, Washington D.C.

Mohamed, A.R., and W. Hansen. (1997). "Effect of Nonlinear Temperature Gradient on Curling Stresses in Concrete Pavements," In *Transportation Research Record 1568*, National Academy Press, Washington, D.C., pp. 65-71.

Salsilli, R.A., E.J. Barenberg, and M.I. Darter. (1993). "Calibrated Mechanistic Design Procedure to Prevent Transverse Cracking of Jointed Plain Concrete Pavements," *Proceedings of the 5th International Conference on Concrete Pavement Design and Rehabilitation*, Purdue University, West Lafayette, Indiana.

Tabatabaie, A.M., and E.J. Barenberg. (1980). "Structural Analysis of Concrete Pavement Systems," *ASCE, Transportation Engineering Journal.* vol. 106, no. 5, pp. 493-506.

Thomlinson, J. (1940). "Temperature Variations and Consequent Stresses Produced by Daily and Seasonal Temperature Cycles in Concrete Slabs," *Concrete Constructional Engineering*, vol. 36, no. 6, pp. 298-307 and vol 36, no. 7, pp. 352-360.

Zollinger, D.G., and E.J. Barenberg. (1990). *Continuously Reinforced Pavements: Punchouts and Other Distresses and Implications for Design*, Project IHR - 518, Illinois Cooperative Highway Research Program, University of Illinois, Urbana, Illinois.